The identification of novel *Staphylococcus aureus* protein arginine kinase McsB ligands

by

Ryan Chetty

Submitted in the fulfilment of the academic requirements of

Doctor of Philosophy

in Biochemistry

School of Life Sciences

College of Agriculture, Engineering and Science

University of KwaZulu-Natal

Pietermaritzburg

South Africa

2025

PREFACE

The research contained in this dissertation was completed by the candidate while based in the Discipline of Biochemistry, School of Life Sciences of the College of Agriculture, Engineering and Science, University of KwaZulu-Natal, South Africa. The research was financially supported by the National Research Foundation UID: 150279.

The contents of this work have not been submitted in any form to another university and, except where the work of others is acknowledged in the text, the results are due to investigations by the candidate.

Signed: Ryan Chetty

Date: 06 February 2025

As the Supervisor I agree to the submission of this dissertation

Signed: Professor Raymond Hewer

Date: 06 February 2025

As the Supervisor I agree to the submission of this dissertation

Signed: Professor Clinton Veale

Date: 06 February 2025

DECLARATION 1 – PLAGIARISM

I, Ryan Chetty, declare that

1. The research reported in this dissertation, except where otherwise indicated, is my original research.

2. This dissertation has not been submitted for any degree or examination at any other university.

3. This dissertation does not contain other persons" data, pictures, graphs or other information, unless specifically acknowledged as being sourced from other persons.

4. This dissertation does not contain other persons' writing, unless specifically acknowledged as being sourced from other researchers. Where other written sources have been quoted, then:

a. Their words have been re-written, but the general information attributed to them has been referenced

b. Where their exact words have been used, then their writing has been placed in italics and inside quotation marks and referenced.

5. This dissertation does not contain text, graphics or tables copied and pasted from the Internet, unless specifically acknowledged, and the source being detailed in the dissertation and in the References section.

Signed: Ryan Chetty

Date: 06 February 2025

DECLARATION 2 – PUBLICATIONS

My role in each paper is indicated. The * indicates corresponding author.

Journal Article (research)

Chetty R, Delport A, Mthembu S, Veale C*, Hewer R*. Screening the Pandemic Response Box identifies novel ligands of the *Staphylococcus aureus* protein arginine kinase, McsB. Article submitted to Molecular Biology Reports

All experiments were conducted by the candidate and the paper was written by the candidate Chetty R.

Signed: Ryan Chetty

Date of submission: 06 February 2025

ABSTRACT

The protein arginine kinase McsB plays a pivotal role in the ClpCP stress-response system in gram-positive bacteria and has been evaluated as a potential target for combating gram-positive pathogens. There are currently no recorded ligands or inhibitors reported for McsB. We aimed to discover novel ligands for the *Staphylococcus aureus* protein arginine kinase ($McsB_{SA}$) through screening of the Medicines for Malaria Venture (MMV) and Drugs for Neglected Diseases initiative (DNDi) Pandemic Response Box of compounds. The recombinant expression and purification of $McsB_{SA}$ in *Escherichia coli* was successfully optimized to yield soluble protein. The first thermal stability measure, the melting temperature (T_m), of $McsB_{SA}$ was optimized though implementation of a buffer screen conducted utilising the thermal shift assay (TSA) and the highest T_m obtained was 49.73 ± 0.21℃ when evaluated with sodium phosphate, pH 7.4. The second stability measure, the aggregation temperature (T_{agg}) of $McsB_{SA}$ was delineated through cellular thermal shift assay (CETSA) analysis to be 48.28 ± 0.18℃ and to our knowledge is the first reported aggregation temperature for any McsB orthologue. The Pandemic Response Box was screened against $McsB_{SA}$ through utilization of thermal stability assays, and six compounds were identified as novel $McsB_{SA}$ ligands. These compounds were observed to cause positive shifts in the T_m and T_{agg} of the protein. The identified ligands demonstrated no inhibitory effect or toxicity as determined by minimum inhibitory concentration assays measuring the growth of *S. aureus*. This is the first description of novel $McsB_{SA}$ ligands being delineated. Compound MMV1593539 and MMV1782355 induced the greatest stability of $McsB_{SA}$ with increases in T_m of 1.19℃ ($p<0.001$) and 0.68℃ ($p<0.05$) respectively and increases in T_{agg} of 1.30℃ ($p<0.001$) and 0.95℃ ($p<0.01$) respectively. These findings were corroborated through molecular docking and molecular dynamic studies which suggested that compounds MMV1593539 and MMV1782355 bind to the ATP site of $McsB_{SA}$ with favourable docking scores of -7.095 and -7.873 respectively. The findings from thermal stability assays conducted in combination with in silico studies thus validate the identification of at least six novel $McsB_{SA}$ ligands from the Pandemic Response Box of compounds and signify these ligands as promising candidates for future drug discovery studies aimed at exploiting or inhibiting the protein arginine kinase $McsB_{SA}$.

ACKNOWLEDGEMENTS

I would like to express my gratitude and thanks to the following individuals who were instrumental in the completion of this PhD. First and foremost, I wish to thank my supervisor, Professor Raymond Hewer. There are truly no words to exemplify the impact you have had on my academic career and on myself as an individual. You surpass all expectations and go above and beyond your duties. Your kindness and support have made all the difference in completing this project under very difficult circumstances. You have shown patience and understanding in times where I have felt as if I did not deserve it. Thank you for being the best supervisor one could ask for and most importantly for being an exceptional human being. You are an exemplary role model to everyone under your supervision. Thank you for never giving up on me Prof. I will forever be grateful for the support and compassion you bestowed upon me when my mother passed away, for allowing me time to grieve and time to assist my visually impaired sister complete her matric year and navigate university life, you helped me survive during this traumatic time and I truly cannot thank you enough Prof.

To my supervisor Professor Veale, thank you for your support, patience time and understanding throughout this study. It has been a pleasure to have worked with you. This study would not have been possible without your contributions.

To Professor Fernando Albericio and Professor Beatriz Garcia De la Torre of the Discipline of Chemistry, UKZN, Durban. Thank you for synthesising the Ac-KRGGGGYIKIIKV-OH peptide used in this study.

To the academics of the School of Life Sciences, UKZN, Pietermaritzburg. To my honours supervisor Dr Pillay and Masters co-supervisor Prof. Coetzer, thank you for the significant impact you both have had on my academic career. To my colleagues in Lab 46, I would like to extend a huge thank you for making this experience one to remember and for creating a friendly environment to work in, specifically to Alex, Shantal and Sandile, thank you for all of your support and guidance. I appreciate all of your time and kindness.

I would like to thank the following institutes for their contributions. The National Research Foundation (NRF) for their partial funding of this project. The South African Medical Research Council (MRC) for funding of this project. The Centre for High Performance Computing (CHPC) of South Africa for providing access to the Schrödinger drug discovering suite software. I would also like to thank the University of Kwazulu-Natal for providing the space to work, excel and complete this study.

I would like to dedicate this thesis to my parents, to my mother who suddenly passed away in 2021 due to the pandemic outbreak, I can only hope and pray that you are smiling down from heaven and that I have made you proud, these past few years have been an incredibly tough journey without your love, guidance and support. I miss and love you dearly, and this one is for you mums. To my father, who has been my rock in recent years and has had to deal with incredible loss and yet still be a pillar to everyone around him, thank you for your continued support and belief in my success. I will never be able to repay you for all that you have done. You are the man I strive to become one day. To my sister, Amy, thank you for constantly showing me what bravery is and giving me the strength to face every day. You are a blessing and inspiration to everyone around you. To every other family member who has held me up, encouraged me, and believed in me, I say thank you.

Lastly and most importantly, I would like to thank the Lord Jesus Christ for keeping me and guiding me through a very difficult time in my life and for seeing me through to the end of this PhD. It has been a journey with many trials and tribulations but with God, all things are possible. “I can do all things through Christ who strengthens me.” Philippians 4:13

TABLE OF CONTENTS

LIST OF FIGURES

LIST OF TABLES

LIST OF ABBREVIATIONS

2xYT	2 x yeast tryptone
3D	Three-dimensional
ADP	Adenosine diphosphate
BIM2	Bisindolyl maleimide
BSA	Bovine serum albumin
CETSA	Cellular thermal shift assay
CHAPS	3-[(3-cholamidopropyl)dimethylammonium]-1-propanesulfonate
Clp	Caseinolytic protease
ClpCP	ClpC – ClpP complex
DD	Dimerization domain
DMSO	dimethyl sulfoxide
DNDi	Drugs for Neglected Diseases initiative
DSC	Differential scanning calorimetry
DSF	Differential scanning fluorimetry
ESKAPE	*Enterococcus faecium, Staphylococcus aureus, Klebsiella pneumoniae, Acinetobacter baumannii, Pseudomonas aeruginosa,* and *Enterobacter spp.*
ExPASy	Expert protein analysis system
FDA	Food and drug association
Glide	Grid-based ligand docking with energetics
HEPES	4-(2-hydroxyethyl)-1-piperazineethanesulfonic
IPTG	Isopropyl ß-D-1-thiogalactopyranoside
IUPAC	International Union of Pure and Applied Chemistry nomenclature
LOC	Ligand only control
$McsB_{BS}$	*Bacillus subtilis* protein arginine kinase McsB
$McsB_{GS}$	*Geobacillus stearothermophilus* protein arginine kinase McsB
$McsB_{SA}$	*Staphylococcus aureus* protein arginine kinase McsB
MD	Molecular dynamics
MDR	Multidrug resistant
MES	4-Morpholineethanesulfonic acid
MIC	Minimum inhibitory concentration
MLS	Multiangle light scattering
MMV	Medicines for Malaria Venture
MRSA	Methicillin resistant *Staphylococcus aureus*

MS	Mass spectrometry
MWM	Molecular weight marker
NNRTI	Nonnucleoside reverse transcriptase inhibitor
NPC	No protein control
NTD	N-Terminal domain
OD	Optical density
PAINS	Pan assay interference structures
pArg	Phosphorylated arginine
PBS	Phosphate buffered saline
PD	Phosphotransferase domain
PhKs	Phosphagen kinases
pI	Isoelectric point
PK	Pyruvate kinase
PMSF	Phenylmethylsulfonyl fluoride
PNP	Purine nucleoside phosphorylase
PTMs	Post translational modifications
RCSB PDB	Research Collaboratory for structural bioinformatics protein data bank
RMSD	Root mean square deviation
RMSF	Root mean square fluctuation
RoG	Radius of gyration
RPM	Revolutions per minute
RT	Room Temperature
RT-PCR	Real time polymerase chain reaction
Sarkosyl	N- Lauroylsarcosine
SD	Standard deviation
SDS	Sodium dodecyl sulphate
SDS-PAGE	Sodium dodecyl sulphate- polyacrylamide gel electrophoresis
SEC	Size-exclusion chromatography
T_{agg}	Aggregation temperature
TBS	Tris buffered saline
TCEP	Tris(2-carboxyethyl)phosphine
TM	Template modelling
T_m	Melting temperature
TSA	Thermal shift assay
XDR	Extensively drug resistant

CHAPTER 1: LITERATURE REVIEW

1.1. Introduction

Antimicrobial resistance has risen to one of the top 10 global health threats as of 2019 and continues to present a major global healthcare crisis. The persistent use of antibiotics has resulted in the accelerated spread of multidrug-resistant (MDR) bacteria and extensively drug-resistant (XDR) bacteria (Mulani *et al.*, 2019 , De Oliveira *et al.*, 2020, Avci, 2024). The "ESKAPE" pathogens: *Enterococcus faecium, Staphylococcus aureus, Klebsiella pneumoniae, Acinetobacter baumannii, Pseudomonas aeruginosa*, and *Enterobacter spp* are known to display multidrug resistance and virulence *(Rice, 2008, Mulani et al., 2019 , De Oliveira et al., 2020)*. *Enterococcus faecium* and *Staphylococcus aureus* are Gram-positive, while the remaining pathogens are Gram-negative. Mutations resulting in the development of antimicrobial resistance genes by ESKAPE pathogens has limited the selection of treatments available for serious infections and results in increased death rates due to treatment failure. These antimicrobial resistance genes have been detected on the bacterial chromosome, plasmid, and transposons (Santajit and Indrawattana, 2016).

Undergoing stress is common for all living organisms and the ESKAPE pathogens are no exception (Bonilla, 2020). The ability to sense and adapt in a timely manner to changes in environment is vital for their survival and virulence (Bonilla, 2020). Bacteria have an array of tools which allow them to overcome environmental stresses which make them resilient (Bonilla, 2020). These tools / responses include regulation of gene expression, post-translational protein regulation and toxin remediation (Bonilla, 2020). The stress responses demonstrated by the pathogens cause existing treatments to become obsolete leading to the urgent need of new treatments. The general antimicrobial approach to treat infections involves the use of either a single antibiotic or a combination of antibiotics. Continuous use of these antibiotic treatments consequently results in many of them becoming ineffective against the ESKAPE pathogens as this triggers bacterial stress responses which induce resistance mechanisms resulting in MDR and XDR strains (Avci, 2024). The mechanisms of antibiotic resistance have been divided into the following categories: drug inactivation/alteration, modification of drug binding site/targets, changes in cell permeability (decreases the accumulation of drugs intracellularly) and biofilm formation (Santajit and Indrawattana, 2016).

Staphylococcus aureus is one of the ESKAPE pathogens and is known to cause a wide range of infections including sepsis, wound infections, pneumonia, and catheter related infections. The occurrence of these infections is also attributed to *S. aureus's* ability to adhere to inert

surfaces of medical implanted devices and to colonize biological substrates such as heart valves (Chatterjee *et al.*, 2005). Penicillin was used for treatment as it had proven to be effective against infections caused by *Staphylococcus* species, however by 1948 , the excessive use of the antibiotic had led to the development of β-lactamase producing strains capable of breaking down the beta-lactam ring of beta-lactam antibiotics such as penicillin, rendering the antibiotic ineffective as a treatment option (Santajit and Indrawattana, 2016). Methicillin (a semi-synthetic penicillin) was developed in response to the emergence of these penicillin resistant strains, however, within a short time period of exposure (~ 2 years), methicillin resistant *S. aureus* (MRSA) was identified (Fuda *et al.*, 2005). The pathogen continues to adapt, evolve and gain new resistance mechanisms as there have been reports of MRSA variants emerging, for example, the MRSA variant which is resistant to vancomycin. *S. aureus* is also known to survive under stresses such as oxidative stress, changes in pH, osmotic pressure and heavy metal exposure (Wozniak *et al.*, 2012). The pathogen can survive these stresses by employing mechanisms which include heavy metal efflux pumps, superoxide dismutases, and most importantly, misfolded protein responses that trigger protein degradation (Wozniak *et al*., 2012). The pathogen can degrade misfolded/unfolded proteins (caused by environmental stress) prior to aggregation and precipitation (Wozniak *et al*., 2012). This protein degradation response is mediated by specific bacterial proteases (Wozniak *et al*., 2012, Culp and Wright, 2017).

Bacterial proteases have several key roles in bacterial physiology, biochemistry and pathogenicity (Culp and Wright, 2017). Caseinolytic protease (Clp) belongs to the AAA+ family of proteases (Culp and Wright, 2017). The Clp proteolytic complex is responsible for cellular protein control and pathogen intracellular viability in hosts for both Gram-positive and Gram-negative bacteria. Clp proteases are well conserved in most bacterial species and have been shown to be essential for the full expression of virulence traits in *S. aureus*. These Clp proteins are encoded by five genes in *S. aureus*: *clpC*, *clpP*, *clpB*, *clpX* and *clp L* (Chatterjee *et al.*, 2005, Wozniak *et al.*, 2012, Culp and Wright, 2017).

1.2. The ClpCP system

The ClpC-ClpP complex (ClpCP) is composed of a self-compartmentalizing serine protease (ClpP) which associates with the Clp ATPase, a AAA+ unfoldase (ClpC) as detailed in Figure 1.1. The ClpP proteolytic chamber is composed of fourteen subunits that typically assemble into a stack of two heptameric rings, creating a hollow barrel-like structure (Frees *et al.*, 2014, Aljghami *et al.*, 2022, Queralto *et al.*, 2023). Each protomer contains a Ser-His-Asp catalytic

triad that faces the interior of the complex resulting in the formation of the catalytic degradation chamber. Each ClpP subunit is composed of three subdomains: the N-terminal loops, the head domain and the handle region. The N-terminal loops line the surface of the axial pore and protrude from the apical surface of ClpP, the head domain forms the main body of the degradation chamber, and the handle region facilitates the interaction between the two heptameric rings. N-terminal regions are typically disordered and partially block the entrance to the degradation chamber when ClpP is not in complex with ClpC (Chatterjee *et al.*, 2005, Aljghami *et al.*, 2022, Queralto *et al.*, 2023). The ClpP tetradecamer can degrade short peptides which are capable of passing through the axial pores and thus partial blocking of the degradation chamber is crucial in protecting cellular proteins from uncontrolled proteolysis by the catalytic residues within the ClpP degradation chamber. This allows for ClpP to have strict selection of protein substrates. The ClpCP complex is required for proteolysis of larger proteins (Aljghami *et al.*, 2022).

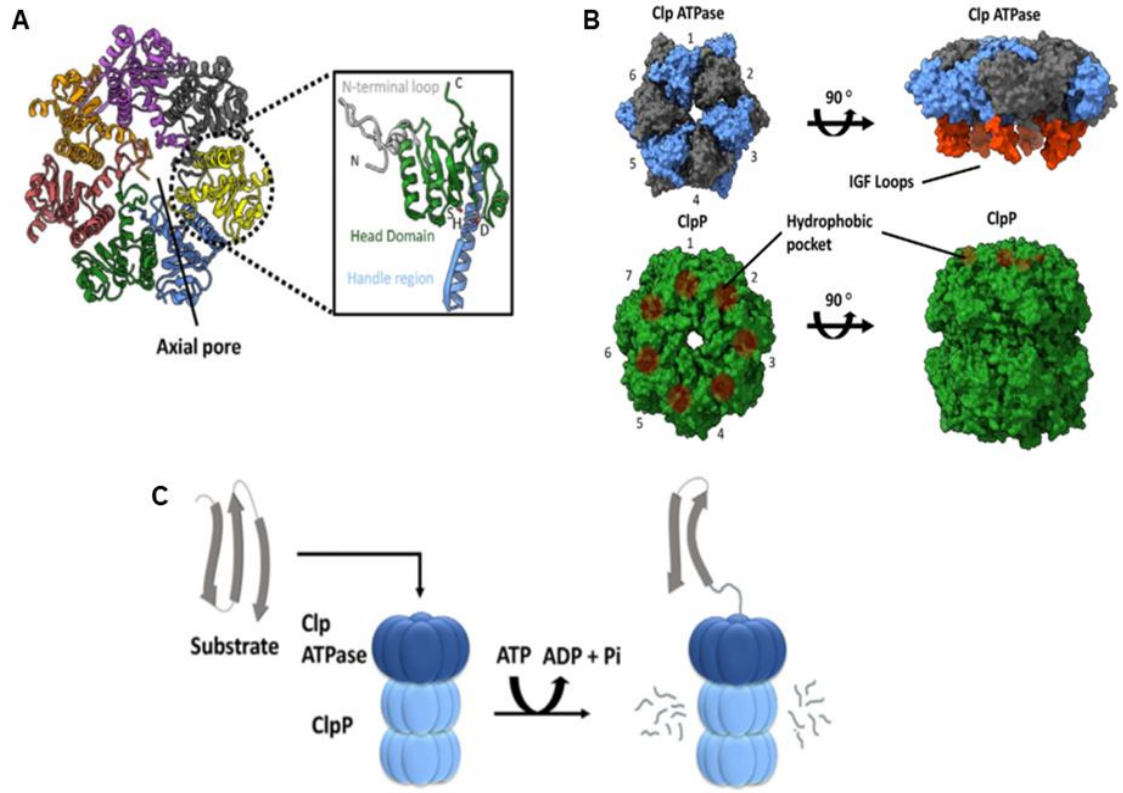

Figure 1.1. ClpP and ClpC (Clp ATPase) general architecture. (A) Top view of the *E. coli* ClpP chamber (PDB ID: 1YG6). In the insert to the right, the N-terminal loop (silver), head domain (green), handle region (blue) and catalytic triad of the ClpP monomer are indicated (PDB ID 1YG6). (B) The association of a Clp ATPase hexamer (PDB ID 6SFW) with a ClpP tetradecamer (PDB ID 6SFX). Clp ATPase subunits (blue and grey) with their corresponding IGF loops (orange) are shown. ClpP subunits (green) with their hydrophobic pockets represented as brown circles. (C) A schematic of the substrate degradation process facilitated by the Clp ATPase- ClpP complex. Substrates are unfolded by the Clp ATPase and then translocated in an ATP-dependent manner into the ClpP degradation chamber for degradation. Adapted from Aljghami *et al.*, 2022.

The ClpC operon comprises of four genes: *ctsR, mcsA, mcsB* and *clpC* (Kruger *et al.*, 2001). ClpC is an ATP dependant protease which has substrate-specific chaperone functions such as refolding and reactivation of proteins (Frees *et al.*, 2004, Frees *et al.*, 2007, Frees *et al.*, 2014, Trentini *et al.*, 2016). Monomeric and dimeric forms of CtsR bind to heptamer repeat sequences within promoter regions resulting in the expression of the *clpC* operon being negatively regulated. ClpC plays a role in regulating the expression of genes and/or proteins of gluconeogenesis, the pentose phosphate pathway, pyruvate metabolism, the electron transport chain, nucleotide metabolism, oxidative stress, metal ion homeostasis, stringent response and programmed cell death (Chatterjee *et al.*, 2009).

The ClpCP system is one of the main quality control systems in gram-positive bacterial physiology as it degrades misfolded proteins and aids in the adaptation of the bacteria during environmental stress (Kruger *et al.*, 2001). The N-terminal domain of ClpC recognises a specific degradation motif which is generally located at the N- or C- terminal ends of target proteins and these degradation motifs fundamentally tag the protein for degradation. The ClpC ATPase was observed to have a phosphorylated arginine (pArg)-binding site which recognises pArg with high propensity and was defined as a unique property of ClpC which inferred that pArg was the degradation motif recognised by ClpC (Trentini *et al.*, 2016). This unique pArg tagging recognition by the ClpC ATPase is displayed in Figure 1.2. The identified pArg site was suggested to have two possible functions, both of which are crucial for protein degradation. The first, was to serve as a docking site for the protein arginine kinase McsB which is capable of autophosphorylation and more significantly, arginine phosphorylation, and alternatively, was suggested to directly recognise substrates containing pArg and this implied that the ClpCP complex is controlled by the protein arginine kinase McsB (Trentini *et al.*, 2016). Interestingly, this specific substrate recruitment required for ClpC ATPase activity which in-turn promotes the assembly of an active ClpCP complex, is similar to the eukaryotic ubiquitin-proteasome degradation system where the protein arginine kinase McsB plays a similar role that of E3 ubiquitin ligase. (Trentini *et al.*, 2016, Hajdusits *et al.*, 2021, Arifuzzaman *et al.*, 2024).

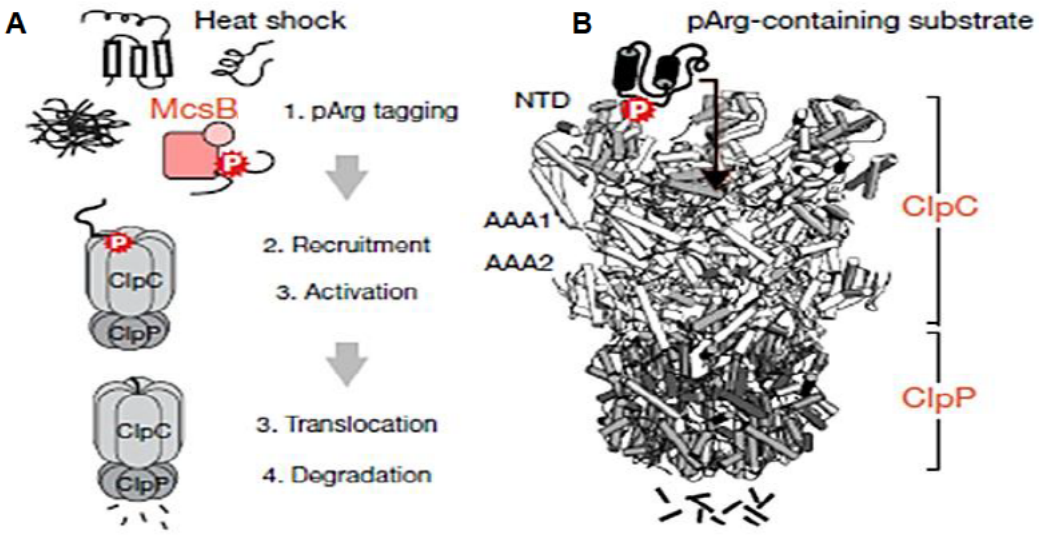

Figure 1.2. The recognition of phosphorylated arginine (pArg) residues within a substrate by the ClpC ATPase. (A) A cartoon representation displaying the protein degradation pathway which is initiated by the arginine kinase McsB tagging unfolded/denatured proteins (represented by the black coiled lines) through arginine phosphorylation (where pArg is represented by a white P enclosed in a red star) and the recognition of pArg by the ClpC ATPase. (B) A model displaying the binding of a pArg protein to one of the N-terminal domains (NTD) of the ClpC ATPase (displayed in grey) which in-turn leads to the ClpC activity and the translocation of the pArg-containing substrate (displayed in black) into the degradation chamber of ClpP (displayed in dark grey) thus resulting in protein degradation. Adapted from Trentini *et al*, 2016.

1.3. The protein arginine kinase McsB

Cellular proteins undergo numerous alterations, which include phosphorylation, methylation, glycosylation, lipidation, carboxylation, oxidation and acetylation. These post translational modifications (PTMs) are ubiquitously established amongst eukaryotes, archaea, and bacteria, and cause changes to protein folding and stability which in-turn affects protein function as well as ligand binding and activity (Fuhrmann *et al.*, 2009, Mijakovic *et al.*, 2016, Suskiewicz *et al.*, 2019, Arifuzzaman *et al.*, 2024).

Protein phosphorylation was the first PTM discovered to alter protein function and is the most common and most documented of these modifications. In eukaryotic organisms, approximately 30% of all cellular proteins are phosphorylated which affects all cellular processes. Protein post-translational phosphorylation plays a fundamental role in how signals are transmitted intracellularly. Residue specific kinases and phosphatases ensure that protein phosphorylation is regulated within the cell. Residues with reactive side chains (hydroxyl, amino, carboxyl, or thiol groups) are targets for phosphorylation (Arifuzzaman *et al.*, 2024). Gram-positive bacteria such as *S. aureus* specifically phosphorylate arginine residues. Phosphoproteomics studies have identified hundreds of arginine specific phosphorylation

sites in *Bacillus subtilis* and *S. aureus*. The precise role of arginine phosphorylation has not yet been fully elucidated however it has been implicated in important roles such as motility, protein homeostasis and more importantly, stress response pathways (Boggon, 2019). McsB is the founding member of an arginine specific class of protein kinases and is responsible for protein-arginine phosphorylation. McsB serves as an integral component in the stress response operon of gram-positive pathogens, along with the repressor CtsR, the activator McsA (enhances McsB activity), the phosphatase YwlE and the protease ClpCP (Kirstein *et al.*, 2007, Fuhrmann *et al.*, 2009, Elsholz *et al.*, 2012, Trentini *et al.*, 2016, Suskiewicz *et al.*, 2019, Arifuzzaman *et al.*, 2024).

1.3.1. Structure and Function

Structure-function studies have previously been conducted with the *Geobacillus stearothermophilus* protein arginine kinase McsB ($McsB_{GS}$), the prevalent model for protein arginine kinases (Fuhrmann *et al.*, 2009, Suskiewicz *et al.*, 2019, Hajdusits *et al.*, 2021) and the *S. aureus* protein arginine kinase McsB ($McsB_{SA}$) (Lu *et al.*, 2024). For $McsB_{GS}$, studies showed that dimer formation is required for attaining full kinase activity (Suskiewicz *et al.*, 2019, Hajdusits *et al.*, 2021). As such, the McsB dimer represents the basic functional unit of the protein arginine kinase, although, various oligomeric states have been reported which range from monomers to higher-order oligomers. It is still unclear, however, if these higher-order oligomers contribute to the pivotal role of McsB in the bacterial heat shock response (Hajdusits *et al.*, 2021).

The determined crystal structure of $McsB_{GS}$ in the apo state and in complex with an adenosine diphosphate (ADP) analogue (AMP-PN) revealed that the McsB dimer adopts a flat ‘domino tile’ shape, with the two active sites opening on the same side (Figure 1.3). McsB subunits are composed of the N-terminal catalytic domain [the ATP: guanido phosphotransferase domain (PD)] and the C-terminal dimerization domain (DD). These domains are organized linearly in a PD-DD-DD-PD manner (Figure 1.3). The PD consists of an antiparallel, nine-stranded β-sheet surrounded by seven α-helices. The centre of the PD contains the active site which is comprised of adjacent binding pockets for Mg-ATP and the guanidino group of the targeted arginine side chain. The DD is a four-helix bundle which is tightly associated with the PD.

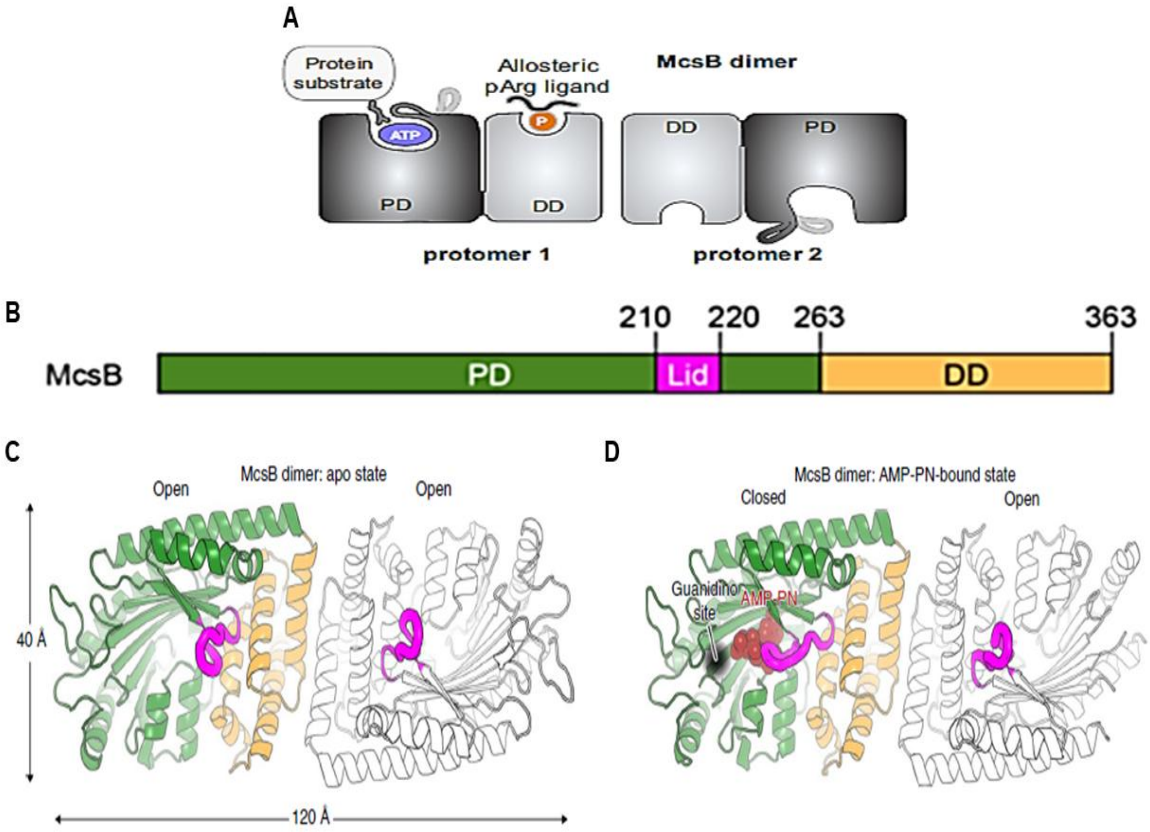

Figure 1.3. Structure of the protein arginine kinase McsB. (A) A simplified schematic image of the McsB dimer highlighting linear domain organization [phosphotransferase domain (PD) and dimerization domain (DD), catalytic site and allosteric site. (B) The domain organization of the *Geobacillus stearothermophilus* McsB monomer. (C) Ribbon diagram of an McsB dimer in the apo state revealing the two open active sites on the same side. (D) Ribbon diagram of an McsB dimer in complex with an *adenosine diphosphate (*ADP*)* analog, AMP-PN state. Adapted from Suskiewicz *et al*., 2019 and Hajdusits *et al*, 2021.

McsB co-ordinates stress signalling and protein degradation pathways as part of the pathogens' stress response system. McsB co-ordinates stress signalling by uniquely phosphorylating arginine residues, specifically within the binding domains of the central heat shock repressors, CtsR and HrcA (Fuhrmann *et al.*, 2009, Suskiewicz *et al.*, 2019). Subsequently, the heat shock repressor is released from its cognate promoter and recruited by the ClpCP proteasome for degradation which induces the expression of genes on the Clp operon (stress response genes) and includes the induction of McsB expression amongst other quality control factors (Suskiewicz *et al.*, 2019, Arifuzzaman *et al.*, 2024, Lu *et al.*, 2024). The induction of McsB expression results in the formation of higher order oligomers of McsB with enhanced phosphorylation activity (Hajdusits *et al.*, 2021).

The protein degradation pathway is also co-ordinated by McsB as the protein arginine kinase serves as a degron labeller, specifically tagging misfolded or unfolded proteins for degradation (Kirstein *et al.*, 2007, Trentini *et al.*, 2016, Lu *et al.*, 2024). McsB labels a specific protein through the post-translational phosphorylation of arginine residues. These pArg residues (degradation motif or degron) are recognised by ClpC and recruited to the ClpCP proteasome, thus initiating the degradation process. The significance of arginine phosphorylation elucidates the pivotal role of McsB as a virulence factor which enables *S. aureus* to cope with the hostile conditions created by the host immune system (Wozniak *et al.*, 2012).

1.3.2. Catalytic domain

Sequence analysis identified low homology between McsB and other protein kinases and structural studies on $McsB_{GS}$ corroborated this through the identification of a catalytic domain which displayed similarities to phosphagen kinases (PhKs) as opposed to other protein kinases. Phosphagen kinases are distributed in the animal kingdom and thus the similarity observed was unexpected due to the evident evolutionary distance between the two classified kingdoms (Ellington, 2001, Arifuzzaman *et al.*, 2024). Phosphagen kinases phosphorylate small guanidino substrates such as arginine and thus a similar catalytic domain elucidates McsB's propensity for arginine (Fuhrmann *et al.*, 2009, Suskiewicz *et al.*, 2019, Arifuzzaman *et al.*, 2024). The active core of the catalytic domain is conserved between McsB and PhKs (Arifuzzaman *et al.*, 2024). The McsB active site consists of a large binding pocket for the substrate, the NEEDH motif and the catalytic cysteine which are covered by two loops (Figure 1.4).

There are eight key residues (five arginine residues, two glutamate residues and one cysteine residue) recognised to be crucial for the catalytic activity of PhKs that are conserved in McsB and are essential for the protein phosphorylation activity of McsB *in vivo* (Suskiewicz *et al.*, 2019). The identification of these eight residues also highlighted the difference between McsB and other protein kinases (serine, threonine and tyrosine kinases) as McsB requires three negatively charged residues (two glutamate and one cysteine) for the positioning of the guanidino group for substrate phosphorylation whereas other protein kinases typically interact with the substrate through a single negatively charge residue (either aspartate or glutamate) which is represented in Figure 1.5 (Suskiewicz *et al.*, 2019).

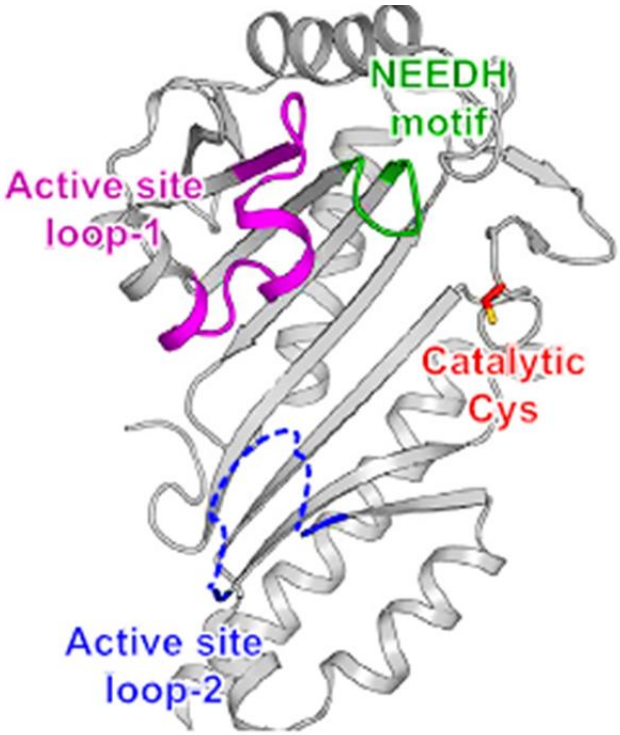

Figure 1.4. Crystal structure of the McsB phosphotransferase domain highlighting the components of the active site. The catalytic cysteine is displayed in red (Cys167), the two active site loops are displayed in magenta and blue (active site loop one and two respectively), and the NEEDH motif is displayed in green. Adapted from Arifuzzaman *et al*., 2024.

The active site of PhKs and McsB share a high degree of structural homology however their substrate specificity differs in size and complexity as McsB phosphorylates proteins whereas PhKs phosphorylates small guanidino compounds which indicated that there was an underlying structural difference between the two kinases (Suskiewicz *et al*., 2019). This difference was found in the auxiliary domain of both kinases as McsB has a C-terminal dimerization domain whilst PhKs contain an N-terminal small domain which accounts for PhKs specificity for small molecules (Suskiewicz *et al*., 2019). The DD of McsB does not contain a small domain and has a loop-helix-loop segment similar to that found in PhKs however is distinctly shorter (by 10 residues) and these structural differences create a larger area for McsB to accommodate larger and more complex substrates as opposed to PhKs (Suskiewicz *et al.*, 2019).

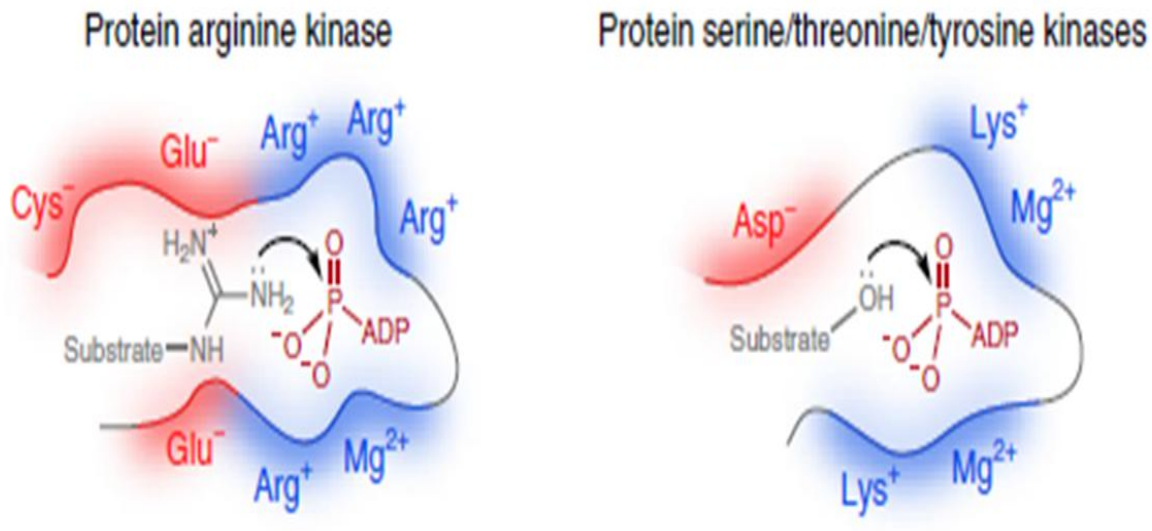

Figure 1.5. Schematic representations of the active site mechanisms of the protein arginine kinase McsB compared to protein serine/threonine/tyrosine kinases. The negatively charged residues involved in substrate phosphorylation are represented in red (two glutamates and one cysteine for McsB and one aspartate residue for canonical protein kinases). Adapted from Suskiewicz *et al*, 2019.

1.3.3. The pArg-binding domain

The C-terminal DD is unique to McsB, and structural analysis revealed similarities to the C-terminal region of the CtsR transcription factor, conversely, the overall sequence identity between $McsB_{GS}$ and CtsR was only 15% (Suskiewicz *et al*., 2019). However, a shared RDXXRA region was confirmed through structure-guided sequence alignments. This shared region forms a surface pocket which consists of both a positively and negatively charged area and resembled the identified pArg-recognition sites of ClpC (Suskiewicz *et al*., 2019). This surface pocket was demonstrated to specifically bind pArg and thus recognised as a pArg binding domain (Suskiewicz *et al.*, 2019). The C-terminal DD plays a role in enzyme regulation by facilitating both dimerization and recognition of pArg residues. This unique pArg binding pocket of the C-terminal DD effectively turns the kinase into an allosteric enzyme and allows pArg-carrying proteins to allosterically enhance McsB kinase activity (Suskiewicz *et al*., 2019).

1.3.4. Higher order oligomer formation of McsB

Initial claims based on size-exclusion chromatography identified McsB as a monomer (Kirstein *et al.*, 2005) however crystallography efforts combined with native mass spectrometry (MS) and size exclusion chromatography (SEC) coupled with multiangle light scattering (MLS) characterised the dimer as the active form of the kinase and as the primary oligomeric form of McsB whilst also describing the formation of higher order oligomers, specifically for $McsB_{GS}$ in solution (Suskiewicz *et al.*, 2019). This higher order oligomer formation was further examined

for the protein arginine kinase McsB in *Bacillus subtilis* ($McsB_{BS}$) by Hajdusits and coworkers. They observed higher peaks for the large higher order oligomers (250-450 kDa) and lower peaks for the dimer (80 kDa) through SEC and determined that $McsB_{BS}$ was recombinantly expressed predominantly as large higher order oligomers (Hajdusits *et al.*, 2021).

The significance of the observed higher oligomer formation of $McsB_{BS}$ on kinase activity were elucidated through the attained crystal structure of octameric $McsB_{BS}$ (Hajdusits *et al.*, 2021). It was observed that the $McsB_{BS}$ octamer was composed of fours $McsB_{BS}$ dimers which form an octameric cage (phosphorylation chamber) with narrow entrance gates (Hajdusits *et al.*, 2021). The formation of the octameric chamber is dependent on the autophosphorylation of Arg194 (R194). The pArg194 (pR194) is buried deep within the octameric cage and is essential for the stability of the cage whilst also preventing dephosphorylation of pR194 by the YwlE phosphatase (Hajdusits *et al.*, 2021). The pR194 of one dimer is housed in the complimentary charged pocket of a neighbouring dimer (pArg receptor site) which corresponds to the previously identified pArg binding pocket of $McsB_{GS}$ (Suskiewicz *et al.*, 2019, Hajdusits *et al.*, 2021).

The octameric cage like orientation buries the active sites of McsB within the cage and thus potential substrates must enter the cage through the narrow entrance gates to gain access to the active sites. The eight key residues identified for substrate binding are not involved in the octamer formation which suggested that the buried active sites remained functional. The formation of the cage (phosphorylation chamber) is essential under stress conditions as the narrow entry gate ensure that native folded proteins cannot enter the cage and thus increases the specificity of the $McsB_{BS}$ octamer to phosphorylate unfolded/misfolded proteins (Hajdusits *et al.*, 2021).

1.3.5. McsA enhances McsB activity

McsA is expressed within the same ClpC operon as McsB and plays a key role in modulating McsB kinase activity (Arifuzzaman *et al.*, 2024). The precise role of McsA has been controversial as it was initially described as an inhibitor/repressor of kinase activity (Kruger *et al.*, 2001, Elsholz *et al.*, 2011), however recent studies proposed that McsB required McsA binding to enhance its kinase activity thus suggesting McsA to be an McsB activator as opposed to a repressor (Kirstein *et al.*, 2005, Trentini *et al.*, 2016, Arifuzzaman *et al.*, 2024). McsA has two zinc-coordinating domains (a C-terminal zinc domain and an N-terminal zinc domain) which were implicated in McsA functioning as a stress response sensor and inducing

CtsR expression under oxidative stress (Trentini *et al.*, 2016, Arifuzzaman *et al.*, 2024). Each zinc-coordinating domain contain a Cys2-Cys2 zinc finger motif containing two CXXC motifs. (Sitthisak *et al.*, 2012). These CXXC motifs can undergo oxidation resulting in disulphide cysteine bonds which leads to protein stress. The CXXC motifs have also been delineated to play a role in the binding of McsA to CtsR and more importantly, to McsB (Sitthisak *et al.*, 2012).

Crystallography efforts directed at elucidating the binding mechanism of McsA to McsB revealed that binding of McsA to McsB created a wider groove for binding of the substrate as compared to the groove observed in the crystal structures of the octameric and dimeric forms of McsB alone (Figure 1.6). The active site loop one was also observed to be less flexible and more stable when compared to the dimeric and octameric forms of McsB as observed in Figure 1.6 (Arifuzzaman *et al.*, 2024, Lu *et al.*, 2024). The binding of McsA to McsB was found to prevent higher oligomer (octameric McsB) formation as the C-terminal zinc domain of McsA was delineated to bind to McsB and consequently occupied the same space as the binding interface of the octamer (Arifuzzaman *et al.*, 2024). McsA was determined to expand the active site of McsB thus promoting substrate binding and increased McsB kinase activity through the reduced flexibility of the active site loop one whilst also preventing uncontrolled McsB self-assembly (higher order oligomer formation) (Arifuzzaman *et al.*, 2024, Lu *et al.*, 2024).

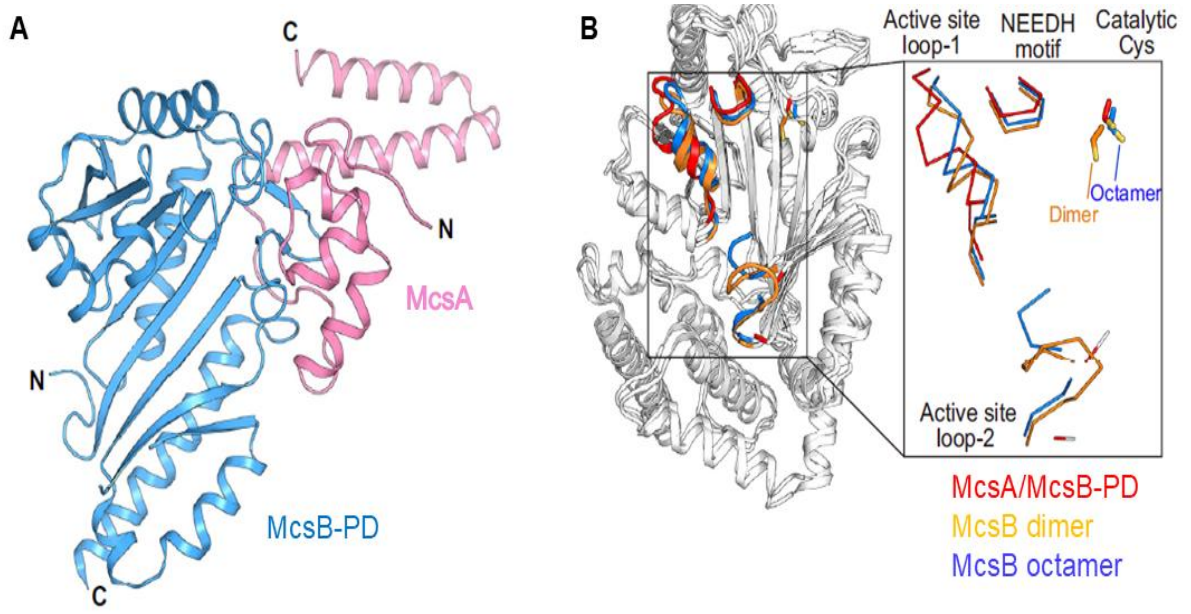

Figure 1.6. Crystal Structure of McsB-phosphotransferase domain (PD*)* /McsA. (A) The crystal structure of the McsB-PD/McsA heterodimer. McsB-PD is displayed as a blue cartoon model and McsA is displayed as a pink cartoon model. (B) A structural comparison of McsB-PD in the crystal structures of McsB-PD/McsA, McsB dimer (PDB ID: 6FH1) and McsB octamer (PDB ID: 6TV6). The active site motifs are shown in different *colours,* and the motifs are emphasized within the black rectangle on the right. Adapted from Arifuzzaman *et al*., 2024.

The protein arginine kinase McsB serves as a crucial constituent of the bacterial proteostasis network due to the protein's unique arginine phosphorylation activity which allows McsB to tag unfolded/misfolded proteins for degradation. The arginine phosphorylation power of McsB is vital for pathogen virulence and survival under stress conditions and this has led to McsB being delineated as a potential target for antimicrobial drug discovery, however, the lack of identified ligands or inhibitors which interact with McsB have hampered drug discovery efforts aimed to pharmacologically validate the protein as a potential druggable target.

1.4. Drug discovery and ligand screening

Drug discovery is a process which aims at discovering a compound / ligand that is therapeutically useful in treating disease symptoms (Deore *et al.*, 2019, Berdigaliyev and Aljofan, 2020). The process involves candidate / target identification, synthesis, characterization, validation, optimization, screening and assays for therapeutic efficacy. The process is costly and, on average, takes more than a decade from the discovery of a drug-candidate to obtaining drug approval (as outlined in Figure 1.7).

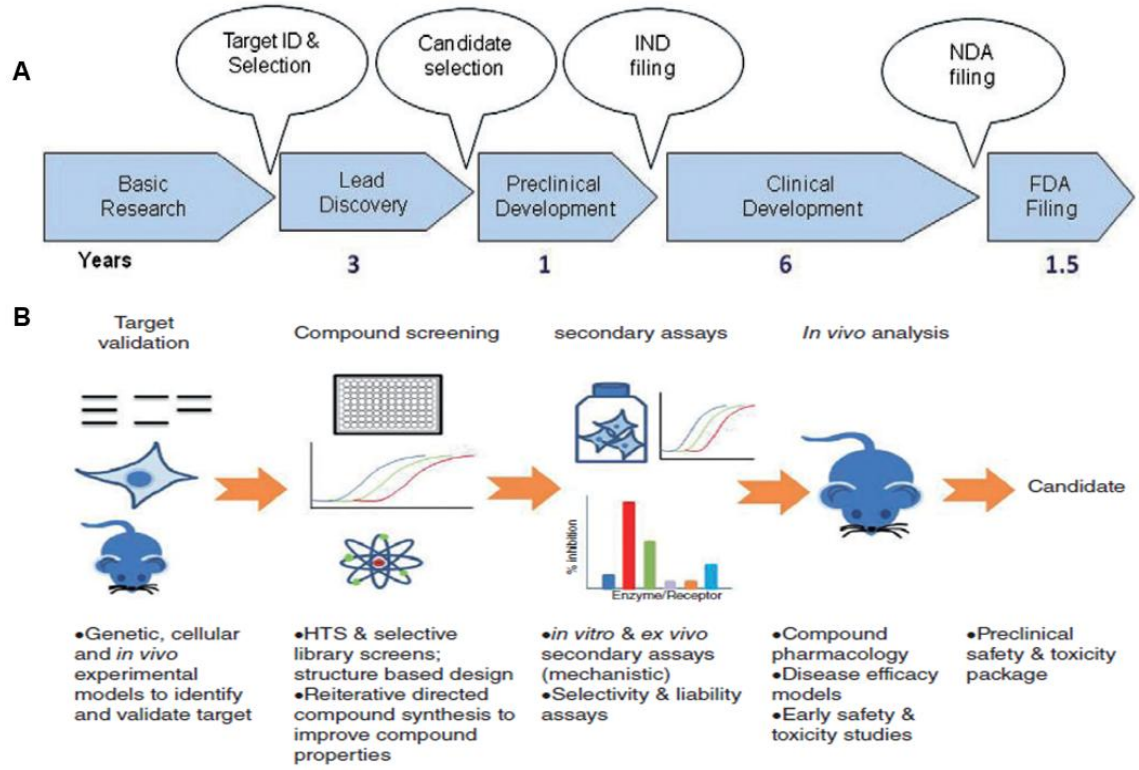

Figure 1.7. Drug discovery pipeline overview. (A) An overview of the drug discovery process in the USA, highlighted from initial research leading to target identification, followed by lead discovery and candidate selection, followed by preclinical testing and development leading to Investigational New Drug filing (IND), followed by clinical trials and development and New Drug Application (NDA) filing which culminates in Food and Drug Administration (FDA) filing and approval. (B). An overview of a drug discovery high throughput screening (HTS) assay highlighting target validation, compound screening, secondary assays and *in vivo* analysis. Adapted from Hughes *et al*., 2011.

The associated cost and approval time differs depending on the disease targeted and the urgency required for a new drug. Initial research generates data to develop a hypothesis that the inhibition or activation of a pathway or protein will have a therapeutic effect on a targeted disease (Hughes *et al*., 2011). The outcome of this activity may require further validation prior to progression into the lead discovery phase (Hughes *et al*., 2011). During the lead discovery phase, the discovery of drug-like small molecules is pursued to ultimately enter into clinical development and lead to a marketed drug (Deore *et al.*, 2019). Traditionally the process relied on natural products as the main source of new drug compounds but now also includes high-throughput synthesis, chemistry-based development and drug repurposing (Hughes *et al.*, 2011, Deore *et al.*, 2019, Pushpakom *et al.*, 2019, Berdigaliyev and Aljofan, 2020). New technologies are continually being developed for high throughput screening of compounds to identify novel ligands for targets of interest.

1.4.1. Drug repurposing

Drug repurposing, also known as drug repositioning, reprofiling or re-tasking has become an increasingly attractive strategy in the drug discovery process as it utilises compounds which have already been approved or are further ahead in the drug discovery pipeline and investigates these compounds outside of their original intended target (Pushpakom *et al.*, 2019). There are numerous instances where drug repurposing has led to the discovery of novel therapies, some examples include, the use of thalidomide which was initially approved as a sedative and thereafter repurposed for treatment of leprosy and has since been licensed for treatment of multiple myeloma (Azvolinsky, 2017, Sinha and Vohora, 2018), the use of sildenafil was initially directed towards cardiovascular disease and reached phase one trials but was repurposed as a treatment for erectile disfunction and has been sold as Viagra since 2005 (Azvolinsky, 2017, Pushpakom *et al.*, 2019), and raloxifene which was initially selected to target osteoporosis was repurposed to treat breast cancer and was approved by the U.S Food and Drug Association (FDA) for invasive breast cancer and worldwide sales reached $237 million for 2015 (Pushpakom *et al.*, 2019). The main advantages of implementing a drug repurposing approach as a drug discovery strategy are reduced time frames and a reduced risk, in terms of safety, as the existing compound would have already been deemed safe if most of the preclinical testing has been performed (Berdigaliyev and Aljofan, 2020, Huang *et al.*, 2024).

1.4.1.1. Compound libraries

The success of drug repurposing efforts has led to the design and construction of numerous compound libraries which comprise of compounds that are generally currently under development. The design and assembly of these compound libraries aid in possible drug repurposing efforts by minimizing the time taken to collect compounds individually whilst also increasing the availability of these compounds (Ayon, 2023). Product development partnerships between Medicines for Malaria Venture (MMV), Drugs for Neglected Diseases initiative (DNDi) and Global Alliance for Tuberculosis (TB Alliance) have partnered with pharmaceutical companies and academic groups and have developed compound libraries (compound boxes) to aid in the discovery of new drug therapies (Samby *et al.*, 2021). To date, they have designed four open access compound boxes, which are, the Malaria Box (2013-1015), the Pathogen Box (2016-2020), the COVID Box (2020-present) and the Pandemic Response Box (2019-present) (Samby *et al.*, 2021).

The Pandemic Response Box was designed as a collaboration between MMV and DNDi to increase the rate of discovery of novel treatments for life-threatening pandemic diseases (Samby *et al.*, 2022, Boonyalai *et al.*, 2024). The collection of 400 structurally diverse compounds comprises 201 antibacterial, 153 antiviral and 46 antifungal compounds. Each of the compounds selected are currently under early development and have been described to have useful biological activities (Samby *et al.*, 2022, Boonyalai *et al.*, 2024). The box serves as a source for potential novel antimicrobial agents and ligands. The Pandemic Response Box has been utilized in numerous drug discovery efforts since released and has led to the advancement in research directed towards combatting parasitic nematode diseases (haemonchosis) (Shanley *et al.*, 2022), malaria (Reader *et al.*, 2021, Singh *et al.*, 2023, Reghunandanan *et al.*, 2024), microsporidiosis (Huang *et al.*, 2023), *Mycobacterium abscessus* infection (Kim *et al.*, 2021), mucormycosis fungal infection (Xisto *et al.*, 2023), sporotrichosis (Borba-Santos *et al.*, 2022), *Klebsiella pneumoniae* infection (Sivasanker *et al.*, 2023) and more.

1.4.2. Screening techniques

Fluorescence based methods such as the thermal shift assay (TSA) and the cellular thermal shift assay (CETSA) have been employed previously to screen and detect potential ligands (Pantoliano *et al.*, 2001, Niesen *et al.*, 2007). These methods rely on monitoring the melting temperature (T_m) and aggregation temperature (T_{agg}) of a protein respectively. An increase

observed in the T_m/T_{agg} of the protein of interest is associated with the successful binding of a ligand. In silico screening has become a popular approach for the screening of compound libraries due to the availability of numerous protein crystal structures and molecular docking tools/programmes.

1.4.2.1. Thermal shift assay

The TSA, also referred to as differential scanning fluorimetry (DSF) (Niesen *et al.*, 2007) and high-throughput thermal scanning (HTTS) (Lavinder *et al.*, 2009) was first described as a screening assay to aid in drug discovery by Pantoliano and co-workers (Pantoliano *et al.*, 2001) and is considered an improvement over the differential scanning calorimetry (DSC) technique (Reinhard *et al.*, 2013, Bruce *et al.*, 2019). The assay is a rapid and inexpensive tool to screen and identify low-molecular weight ligands that bind and stabilize purified proteins (Niesen *et al.*, 2007). The assay exploits protein denaturation, where heat is used to expose the hydrophobic regions of a protein as it unfolds and the use of environmentally safe (non-toxic) dye which must have an affinity for hydrophobic residues and a real-time polymerase chain reaction (RT-PCR) machine that is used to create a temperature profile and monitor the fluorescence of the dye in real time (Figure 1.8). The dyes most commonly used for the assay are highly fluorescent in non-polar environments (the hydrophobic regions of an unfolded protein) and are quenched when exposed to aqueous solutions. The RT-PCR machine measures the fluorescence of the dye as it binds to the hydrophobic regions of the protein as the protein denatures when exposed to the temperature profile.

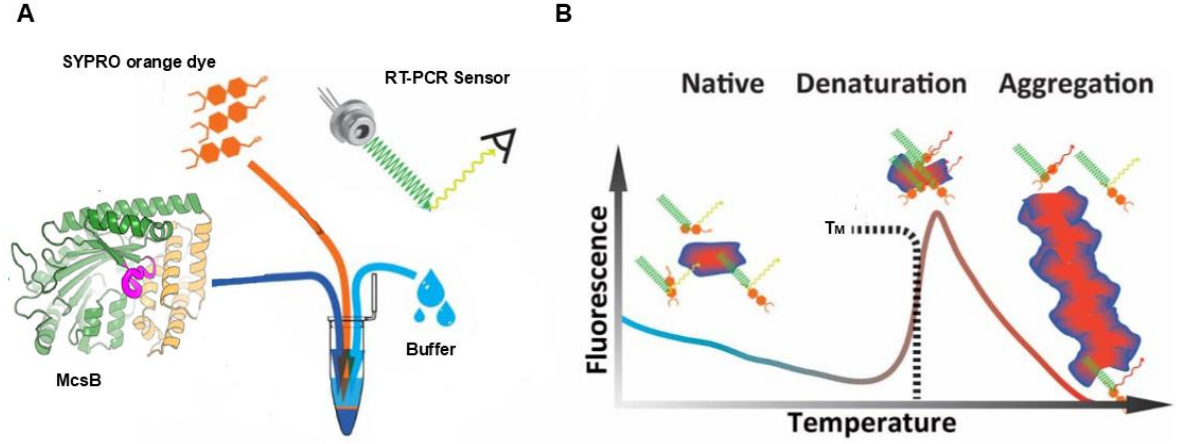

Figure 1.8. Thermal shift assay (TSA) schematic diagram. (A) An illustration showing the elements required for the TSA including the protein of interest, McsB, SYPRO orange dye and buffer of choice all dispensed into in a clear PCR tube or plate. The RT-PCR sensor then records the fluorescence obtained as SYPRO orange dye binds to the protein. (B) A standard fluorescence vs temperature curve obtained for a TSA experiment, where the dye cannot bind to the protein in its native state but begins binding to the hydrophobic regions of the protein as denaturation occurs, the fluorescence finally decreases as the protein begins to aggregate at very high temperatures and the dye dissociates. Adapted from Vollrath *et al*., 2014 and Suskiewicz *et al*., 2019.

The data obtained from a TSA experiment is presented as a graph of fluorescence vs temperature. The assay is used to calculate the point at which the ΔG_U of the protein reaches zero. The temperature at which this occurs reflects the melting point of the protein. For the example represented in Figure 1.9 A, the point at which the ΔG_U of hen egg-white lysozyme reaches zero can be observed for two different concentrations of the protein. Both samples exhibit the same melting point regardless of the increase in fluorescence obtained for the sample with the higher concentration. The melting point represented in Figure 1.9 A is calculated by determining the temperature at which there are equal quantities of folded and unfolded protein. This point is referred to as the inflection point and is represented by the midpoint of the slope. This point is not easily extrapolated from the raw data obtained. There are two methodologies to calculate the melting point using the raw data obtained from a TSA experiment.

The first method utilizes the Boltzmann equation, and the melting point determined is referred to as the Boltzmann T_m:

$$y = \mathrm{LL} + \frac{(\mathrm{UL} - \mathrm{LL})}{1 + \exp\left(\frac{Tm - x}{a}\right)}$$, where

y is the fluorescence intensity at temperature *x,*

LL is the minimum fluorescence intensity observed

UL is the maximum fluorescence intensity observed, and
α denotes the slope of the curve within the T_m (Ericsson *et al.*, 2006)

The second method is simpler and faster to carry out and is performed by normalizing the data through calculation of the first derivative (Niesen *et al*., 2007). The first derivative is then plotted against the temperature and the melting point is now identified as the maximum first derivative obtained which is represented by the peak of the sigmoidal curve (Figure 1.9 B). The melting point attained through this method is defined as the derivative T_m (Niesen *et al*., 2007).

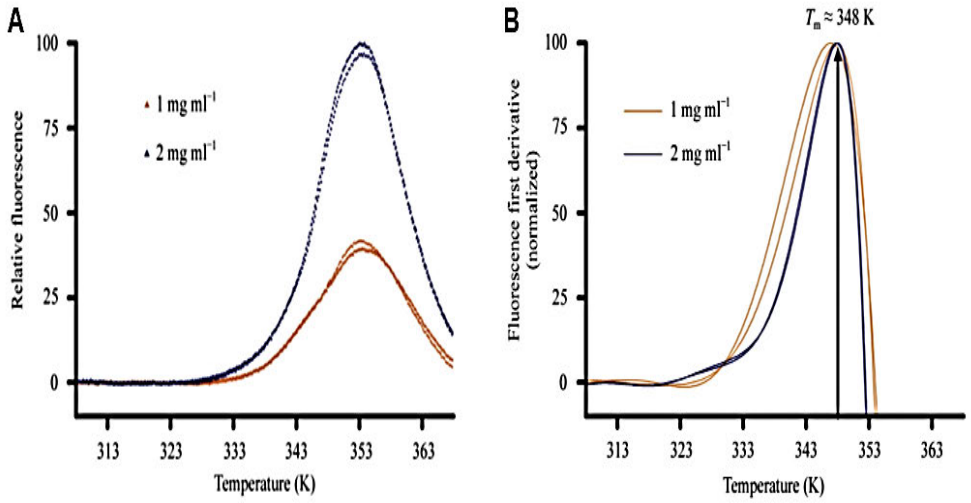

Figure 1.9. Melting curves of hen egg white lysozyme at two different concentrations in 100 mM Bis-Tris propane buffer pH 8. (A) A graph of the raw fluorescence obtained against temperature where the melting point is identified as the midpoint of the slope. (B) The first derivative calculated from the date in (A), where the melting point is identified as the peak of the slope. Taken from Yeh *et al*., 2006.

1.4.2.2. Cellular thermal shift assay

The CETSA was developed by Molina and co-workers to monitor and quantify the efficacy of a compound reaching its protein target and binding in a cellular environment (Molina *et al.*, 2013, Jafari *et al.*, 2014). The TSA requires purified protein samples for melting point determination whilst the CETSA measures the T_{agg} (the temperature point at which 50% of the protein remains soluble) of the protein of interest from whole cell lysates. This proves invaluable when working with a protein which is difficult to solubilise and purify. The CETSA, as its name suggests, essentially measures the stability of the protein of interest in the cellular environment. The assay is performed by first growing cells and expressing the protein of interest, the cells are lysed, and the soluble fraction is obtained. These soluble fractions are exposed to different temperatures for a specific period. The exposure to different temperatures results in different degrees of denaturation and aggregation. The samples are centrifuged to obtain the soluble protein that is remaining. These soluble fractions are quantified by means of western blot and melt curves are generated which are used to determine the T_{agg} of the protein of interest (Molina *et al.*, 2013, Jafari *et al.*, 2014, Delport and Hewer, 2022). The assay is used to detect ligand binding in the same manner as the TSA whereby an increase in T_{agg} indicates successful ligand binding and decreased protein aggregation (Martinez *et al.*, 2018). The CETSA offers a unique advantage when detecting novel ligands for a target protein as compared to other protein stability and ligand screening assays, as it not only confirms ligand binding, but it also offers valuable information pertaining to cell membrane permeability of the

tested ligands (Molina *et al.*, 2013, Jafari *et al.*, 2014, Martinez *et al.*, 2018, Delport and Hewer, 2019, Delport and Hewer, 2022). The CETSA is however not amenable for screening of large compound libraries as compared to the TSA.

1.4.2.3. Isothermal dose-response fingerprint cellular thermal shift assay

The $ITDRF_{CETSA}$ is a variation of the standard CETSA and results in an isothermal dose-response curve being generated which allows for the stability of the target protein to be monitored as a function of increasing ligand concentration (Jafari *et al.*, 2014, Tolvanen, 2022). The assay allows for the establishment of the relevant binding affinities of previously identified ligands (identified through CETSA / TSA) and determine the concentration that these ligands are required to exert their effects (Jafari *et al.*, 2014, Du *et al.*, 2024). The CETSA experiment tests a variable temperature profile in conjunction with a constant ligand concentration to detect the binding of ligands through a shift in T_{agg} whereas the $ITDRF_{CETSA}$ conversely tests a standard temperature in conjunction with increasing ligand concentrations in order to attain information about the ligands binding affinity (Jafari *et al.*, 2014, Tolvanen, 2022, Du *et al.*, 2024). The standard temperature is selected based on the T_{agg} of the protein of interest without any ligand present and thus it is crucial to have identified the temperature at which the unliganded protein denatures and aggregates prior to performing the $ITDRF_{CETSA}$ (Molina *et al.*, 2013, Jafari *et al.*, 2014, Martinez *et al.*, 2018). The $ITDRF_{CETSA}$ has been employed successfully to demonstrate binding and ranking between ligands for a broad range of different target proteins(Molina *et al.*, 2013, Jafari *et al.*, 2014, Molina and Nordlund, 2016, Guo *et al.*, 2020, Du *et al.*, 2024). The thermal stability assays described are invaluable in screening for ligands of a target protein.

1.4.2.4. Molecular docking

Molecular docking has become a popular tool used for in silico screening of ligand libraries. The crystal structure of the target protein which was generally obtained through X-ray crystallography or nuclear magnetic resonance (NMR) was a prerequisite for molecular docking. However, the development of AlphaFold has now allowed for the prediction of a proteins' three-dimensional (3D) structure based on its amino acid sequence (Friesner *et al.*, 2004, Pagadala *et al.*, 2017). Specifically, virtual libraries containing a large number of molecules are computationally screened against the target protein using software which predicts the binding of the compounds to the target proteins 3D structure. Currently, there are more than sixty different docking tools and programmes available for academic and commercial use and are generally categorised into three different types of software which are

rigid docking, flexible-rigid docking and flexible (soft docking) (Pagadala *et al.*, 2017, Fan *et al.*, 2019).

One of the most widely used molecular docking software is Schrodinger's Glide (grid-based ligand docking with energetics) and is characterised as a flexible docking software (Friesner *et al.*, 2004, Pagadala *et al.*, 2017, Fan *et al.*, 2019). The software implements a series of hierarchical filters (Figure 1.10) to search for possible sites for the ligand to bind to the active site of the target protein (Friesner *et al.*, 2004). The docking is initialised by first finding the best fit of the ligand/compound to the receptor site of the target protein which is attained through Glides' exhaustive systematic search of the conformational, orientational and positional space of the docked compound with the Optimized Potentials for Liquid Simulations-All Atoms (OPLS-AA) force field (Friesner *et al.*, 2004, Pagadala *et al.*, 2017). The best fit obtained is thereafter subjected to Monte-Carlo simulations for further refinement. Finally, Glide scores are assigned to the simulated binding interaction between the compound and the receptor. The glide scores indicate how tightly bound the ligand is to the receptor site, where a lower glide score is indicative of stronger binding to the receptor (Friesner *et al.*, 2004).

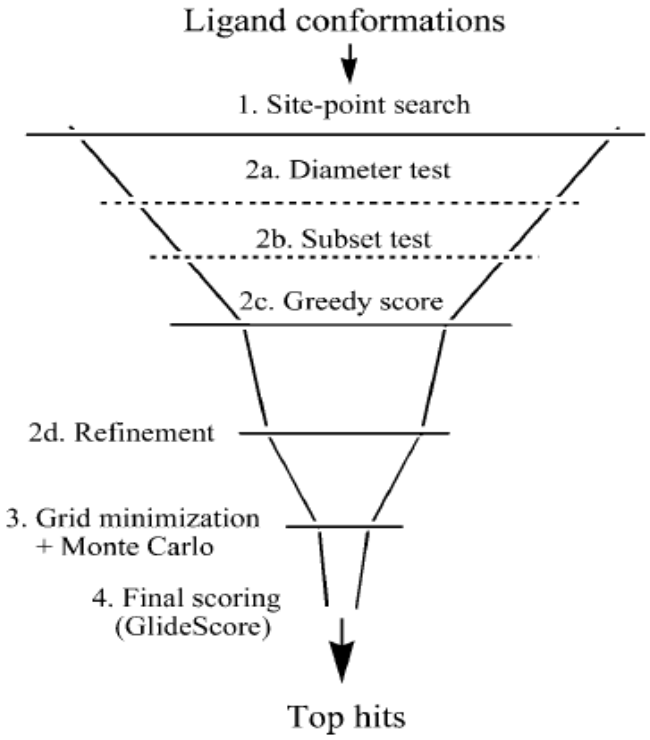

Figure 1.10. Glide docking schematic, highlighting the glide docking hierarchy. The hierarchy outlines the funnel approach the glide docking software employs where a large exhaustive systematic search is performed to find the best fit of ligand to the receptor site (from 1 to 2c), which is followed by Optimized Potentials for Liquid Simulations-All Atoms (OPLS-AA) force field refinement (2d), and further refined through grid minimization using Monte Carlo simulation (3) and finally a glide score is assigned to the predicted ligand-receptor interaction. Taken from Friesner *et al*, 2004.

Molecular dynamic (MD) simulations are often performed in conjunction with molecular docking simulations (Durrant and McCammon, 2011, Arcon *et al*., 2017) . Molecular docking predictions identify the orientation and binding affinity of a ligand whilst MD simulations also provide insights on protein-ligand interaction through computational models which track the physical movements and capture conformational changes between protein and ligand over time (Durrant and McCammon, 2011, Arcon *et al*., 2017). Integration of MD simulations with molecular docking studies allow for a more comprehensive understanding of the binding mechanisms involved and the dynamics of ligand-protein complexes (Deng and Roux, 2009, Durrant and McCammon, 2011, Arcon *et al*., 2017).

1.4.3. Inhibition assay: Minimum inhibitory concentration

The most used technique to determine whether a ligand has any bactericidal or bacteriostatic activity is to perform an agar dilution and/or broth dilution and calculate the minimum inhibitory concentration (MIC) of the ligand. The agar dilution method utilises bacterial culture solutions which have a distinct number of bacterial cells (Wiegand *et al.*, 2008). These cells are spotted directly onto nutrient agar plates which have different concentrations of antibiotic/ligand incorporated in them. The plates are incubated for a defined time period at temperature conditions which favour cell growth. The plates are checked for presence of bacterial colonies and the lowest concentration of antibiotic or ligand tested which shows no bacterial growth is defined as the MIC (Stubbings *et al.*, 2004, Wiegand *et al.*, 2008).

The broth dilution method utilises liquid growth medium containing increasing concentrations of ligand / antimicrobial reagent (usually in a twofold dilution series) which is inoculated with a defined number of cells (Stubbings *et al.*, 2004, Wiegand *et al.*, 2008, Parvekar *et al.*, 2020). The final volume of the experiment determines whether it is a macrodilution (total volume = 2 ml) or a microdilution (total volume ≤ 500 µl per well) (Wiegand *et al.*, 2008, Pereira *et al.*, 2012). The broth is incubated using optimum growth conditions (temperature, RPM). The broth is checked for turbidity and/or sediment which is indicative of bacterial growth. The lowest concentration of the antimicrobial agent / ligand for which no growth is observed is classified as the MIC. In clinical practices, the MIC parameter is used to classify the tested microorganism as either clinically susceptible, intermediate or resistant to the tested ligand / drug (Stubbings *et al.*, 2004, Wiegand *et al.*, 2008, Pereira *et al.*, 2012).

1.5. Hypothesis, aims and objectives of the study

The identified pArg-binding domain of McsB extends the spectrum of known bacterial phospho-binding domains. The McsB from *S. aureus* ($McsB_{SA}$) plays a pivotal role in the pArg signalling and virulence of this bacterial species and has been recognized as a potential drug target to specifically combat Gram-positive pathogens. To the best of our knowledge there are currently no known inhibitors or ligands for the protein arginine kinase $McsB_{SA}$. Our study aimed to discover novel $McsB_{SA}$ ligands/inhibitors through screening of the Pandemic Response Box. The discovery of novel $McsB_{SA}$ ligands will expand the knowledge of the structural properties required for a ligand to interact with McsB and thus contribute towards drug discovery efforts through facilitating the development of $McsB_{SA}$ specific inhibitors and assist in exploitation of the ClpCP proteasome. This Aim was accomplished through the following objectives:

1. Assessment of the suitability of recombinantly expressed $McsB_{SA}$ for use with thermal stability assays.
2. Determination of the melting temperature and the first reported aggregation temperature of recombinantly expressed $McsB_{SA}$.
3. Screening of the Pandemic Response Box and detection of $McsB_{SA}$ ligands.
4. Prediction of protein-ligand interactions through molecular docking and molecular dynamic studies.
5. Evaluation of novel $McsB_{SA}$ ligand activity against the ESKAPE pathogen *S. aureus*.

CHAPTER 2: MATERIALS AND METHODS

2.1. Sequence analysis for $McsB_{SA}$

The amino acid sequences for $McsB_{SA}$ (accession number: Q2G0P6) and $McsB_{GS}$ (accession number: P0DMM5) were attained from the UniProt database (https://www.uniprot.org/). The sequences obtained were used for comparative analysis and hydrophobicity analysis of $McsB_{SA}$.

2.1.1. Comparative sequence alignment for $McsB_{SA}$ and $McsB_{GS}$

The SIM - Alignment Tool for Protein Sequences available from the Expert Protein Analysis System (ExPASy) Swiss Bioinformatics Resource portal (www.expasy.org) was accessed to analyse the sequence similarity between the two amino acid sequences. The parameters were set to default and are as follows: the number of alignments to be computed were 20, the gap open penalty was set to 12, the gap extension penalty was set to 4 and the comparison matrix selected was BLOSUM62. The sequences were also aligned using the UniProt Clustal Omega program (https://www.uniprot.org/align/). The similarities between both sequences were selected under the highlighted properties tab, the Q2G0P6:chain was selected under the select annotation tab and the alignment was viewed as wrapped as opposed to continuous.

2.1.2. Determination of the aptness of $McsB_{SA}$ for the thermal shift assay

The hydrophobicity of $McsB_{SA}$ was assessed and compared to the hydrophobicity of $McsB_{GS}$ by analysing the amino acid sequences of both $McsB_{SA}$ and $McsB_{GS}$ using the online tools available on the ExPASy Swiss Bioinformatics Resource portal (www.expasy.org). The ProtScale tool was accessed (https://web.expasy.org/protscale/) and the Kyte-Doolittle hydropathy index was selected to measure the hydrophobicity of the amino acid sequence for $McsB_{SA}$. The sequence was pasted into the window and the parameters were set to default (window size of 9, the relative weight of the window edges compared to the window centre set to 100%, the weight variation model set to linear while the option to normalise the scale from 0 to 1 was not selected). The full length of the amino acid sequence was selected to be analysed (amino acids 1 - 335).

2.2. McsB_pET-28a(+) plasmid synthesis and *E. coli* transformation.

The amino sequence for $McsB_{SA}$ was obtained from the UniProt database (Q2G0P6-MCSB_STAA8). The gene sequence coding for full length $McsB_{SA}$ was synthesised into a pET-28a (+) plasmid by GenScript (USA). This plasmid construct will be referred to as the $McsB_{SA}$ plasmid. The plasmid was obtained as lyophilized plasmid DNA which was reconstituted by adding 20 µl of Milli-Q water. The resuspended plasmid was aliquoted and stored at -20℃. *E. coli* BL21(DE3) cells were transformed using the calcium chloride transformation protocol (Chang *et al.*, 2017). A glycerol stock of *E. coli* BL21(DE3) cells available in our laboratory which was purchased from New England Biolabs (USA) was streaked onto 2xYT agar plates (16 mg/ml tryptone, 10 mg/ml yeast extract, 5 mg/ml NaCl, 1.5% (w/v) bacteriological agar (all purchased from MilliporeSigma, USA) and incubated overnight at 37℃. A single *E. coli* colony was selected and transferred to 2xYT liquid media (16 mg/ml tryptone, 10 mg/ml yeast extract, 5 mg/ml NaCl). The inoculated media was incubated overnight at 37℃ with agitation [200 revolutions per minute (RPM)]. This overnight culture was used to inoculate fresh 2xYT liquid media, with a ratio of 1:100, and was incubated at 37℃ with agitation (200 RPM) until the optical density (OD), measured at a wavelength of 600 nm reached 0.4-0.5. The culture was transferred to ice-cold centrifuge tubes and centrifuged at 5000 x *g* for 15 minutes at 4℃. The resulting pellet was resuspended in ice cold sterile $CaCl_2$ solution (60 mM CaCl2, 10 mM 4-(2-hydroxyethyl)-1-piperazineethanesulfonic acid (HEPES) buffer, pH 7.0 (all purchased from MilliporeSigma, USA). The resulting suspension was centrifuged at 5000 x *g* for 15 minutes at 4℃. The resulting pellet was resuspended in a $CaCl_2$ solution volume equal to 5% of the initial cell culture volume. The resulting solution served as competent cells required for transformation.

The competent cell mixture was incubated with the $McsB_{SA}$ plasmid in a ratio of 20:1 for 30 minutes on ice. The plasmid-cell mixture was heat shocked at 42℃ for 90 seconds which was followed by an incubation on ice for 2 minutes. The cell solution was then added 1:4 to Super Optimal broth with Catabolite repression (SOC) media (2% tryptone, 0.5% yeast extract, 10 mM NaCl, 2.5 mM KCl, 10 mM $MgCl_2$, 10 mM $MgSO_4$, 20 mM glucose (all purchased from MilliporeSigma, USA) and incubated at 37℃ for 1 hour with gentle agitation. The resulting cell mixture was plated onto freshly prepared 2xYT agar plates (16 mg/ml tryptone, 10 mg/ml yeast extract, 5 mg/ml NaCl, 50 µg/ml kanamycin, 1.5% (w/v) bacteriological agar (all purchased from MilliporeSigma, USA). The plates were incubated overnight at 37℃. Single colonies observed on the plate were used to generate glycerol stocks of the transformed *E. coli* BL21(DE3) cells by inoculating fresh 2xYT liquid media containing kanamycin (50 µg/ml) with

single colonies. The cells were allowed to grow at 37℃ overnight with agitation (200 RPM) Sterile glycerol was added to the overnight culture to a final concentration of 7.5%. The glycerol stocks were stored at -80℃.

2.3. Recombinant expression of soluble arginine kinase $McsB_{SA}$

2.3.1. Initial expression conditions

A glycerol stock of the transformed *E. coli* BL21(DE3) cells containing the $McsB_{SA}$ plasmid was used to perform a three-way streak onto 2xYT agar plates containing kanamycin (50 µg/ml). The plates were incubated at 37℃ for 16 hours. A single colony from the resulting plates was used to inoculate 2xYT broth (10 ml) containing kanamycin (50 µg/ml). The liquid media was incubated at 37℃ whilst shaking at 180 RPM for 16 hours. This overnight culture was used to inoculate four separate flasks containing 100 ml 2xYT liquid media with kanamycin (50 µg/ml), in a 1:100 dilution. The resulting culture was incubated at 37℃ whilst shaking at 180 RPM until the OD_{600} absorbance reached between 0.4 – 0.5 which was measured using the SpectraMax® ABS Plus absorbance ELISA microplate reader (Molecular Devices, USA) and analysed using SoftMax® Pro 7 Data acquisition and analysis software (Molecular Devices, USA). At this point, Isopropyl ß-D-1-thiogalactopyranoside (IPTG) was added to the flasks at the following concentrations of 0.1 mM, 0.3 mM, 0.5 mM and 1 mM. The set of cultures were induced at 16℃ whilst shaking at 180 RPM for 16 hours. Upon the completion of induction, the cultures were centrifuged at 5000 x *g* for 10 minutes at 4℃ to harvest the cells and discard the liquid media. The resulting pellets were resuspended in phosphate-buffered saline (PBS, pH 7.4.) supplemented with 1 mg / ml lysozyme (MilliporeSigma, USA), equal in volume to 10% of the starter culture volume. The resulting solution was sonicated on ice for 5 cycles where samples were sonicated for 30 seconds followed by a 30 second interval between cycles. The samples were centrifuged at 10 000 x *g* for 1 hour at 4℃. The supernatants were collected as the soluble fraction of the expressed $McsB_{SA}$ protein, and the pellet was resuspended in lysis buffer and stored at 4℃ as the insoluble fraction.

2.3.2. N- Lauroylsarcosine solubilization

A glycerol stock of the transformed *E. coli* BL21(DE3) cells containing the $McsB_{SA}$ plasmid was streaked onto 2xYT agar plates containing kanamycin (50 µg/ml). The plates were incubated at 37℃ for 16 hours. A single colony from the resulting plates was used to inoculate 2xYT broth (10 ml) containing kanamycin (50 µg/ml). The liquid media was incubated at 37℃ while shaking at 180 RPM for 16 hours. This overnight culture was used to inoculate three

separate flasks containing 100 ml 2xYT liquid media with kanamycin (50 µg/ml), in a 1:100 dilution. The resulting culture was incubated at 37℃ whilst shaking at 180 RPM until the OD_{600} absorbance reached between 0.4 – 0.5 which was measured using the SpectraMax® ABS Plus absorbance ELISA microplate reader (Molecular Devices, USA) and analysed using SoftMax® Pro 7 Data acquisition and analysis software (Molecular Devices, USA). At this point, IPTG was added to the flasks at a concentration of 0.5 mM. Cultures were induced at 37℃ whilst shaking at 180 RPM for 3 hours. Upon the completion of induction, the cultures were centrifuged at 5000 x *g* for 10 minutes at 4℃ to harvest the cells and discard the liquid media. The pellets were resuspended in PBS pH 7.4. Lysozyme was added at a final concentration of 1 mg/ml and incubated at 4℃ for 30 minutes. The solution was allowed to reach room temperature (RT) as N- Lauroylsarcosine (sarkosyl) may precipitate under low temperature conditions. A 30% sarkosyl stock was prepared and added to the cell suspension until a final concentration of 1% was attained, followed by a 1-hour incubation at RT. The cell suspensions were sonicated on ice for 12 rounds, with 10 second pulses at 10 second intervals. The cells were centrifuged at 20 000 x *g* for 20 minutes at 4℃. The supernatant (soluble fraction) was recovered and stored at 4℃. The insoluble pellet was resuspended in 2 ml of PBS pH 7.4. Sarkosyl (30% stock) was added to the resulting suspension until the final concentration of sarkosyl was 10%. The cell suspension with 10% sarkosyl was incubated overnight at RT. The next morning, the cells were centrifuged at 20 000 x *g* for 20 minutes at 4℃. The supernatant (soluble fraction) was stored at 4℃ and the pellet (insoluble fraction) was resuspended in 2 ml of PBS pH 7.4.

2.3.3. Optimised expression conditions

An overnight culture of *E. coli* BL21(DE3) cells with the $McsB_{SA}$ plasmid was prepared as previously described. This overnight culture was used to inoculate two separate flasks containing 2xYT liquid media (500 ml) containing kanamycin (50 µg/ml), in a 1:100 dilution. The resulting culture was incubated at 37℃ whilst shaking at 180 RPM until the OD_{600} absorbance reached between 0.4 – 0.5 which was measured using the SpectraMax® ABS Plus absorbance ELISA microplate reader (Molecular Devices, USA) and analysed using SoftMax® Pro 7 Data acquisition and analysis software (Molecular Devices, USA). At this point, IPTG was added to the flasks at a concentration of 0.5 mM. The cultures were induced at 18℃ whilst shaking at 120 RPM for 18 hours. Upon the completion of induction, the cultures were centrifuged at 5000 x g for 10 minutes at 4℃ to harvest the cells and discard the liquid media.

The resulting pellet was resuspended in lysis buffer (50 mM sodium phosphate, 300 mM NaCl, 1 mg/ml lysozyme and 1 mM phenylmethylsulfonyl fluoride, PMSF, pH 7.4) equal in volume to 10% of the starter culture volume. The resulting solution was stored at -20℃ overnight. The samples were thawed on ice which served as a single freeze thaw step to aid in cell lysis. The samples were also sonicated on ice for 5 cycles where samples were sonicated for 30 seconds followed by a 30 second interval between cycles. The samples were centrifuged at 10 000 x *g* for 1 hour at 4℃. The supernatants were collected as the soluble fraction of the expressed $McsB_{SA}$ protein, and the pellet was resuspended in lysis buffer as the insoluble fraction. All samples were stored at 4℃.

2.4. $McsB_{SA}$ expression analysis

2.4.1. Determination of the molecular weight of the expressed protein using reducing Sodium Dodecyl Sulphate-Polyacrylamide Gel Electrophoresis

The soluble and insoluble resulting fractions from the expression of $McsB_{SA}$ were separated using sodium dodecyl sulphate-polyacrylamide gel electrophoresis (SDS-PAGE) as previously described (Laemmli, 1970). Polyacrylamide gels (1 mm thick) composed of a 12.5% running gel and a 4% stacking gel were prepared. The gels were loaded with either the Spectra™ Multicolor Broad Range Protein Ladder molecular weight marker (Thermo Fisher Scientific, USA) or the Thermo Scientific PageRuler Plus (Thermo Fisher Scientific, USA). The protein samples loaded were treated with reducing treatment buffer (125 mM Tris-HCl, 4% SDS, 20% glycerol, 10% β-mercaptoethanol with bromophenol blue) in a 1:1 ratio and placed in a heating block for 10 minutes at 95℃ prior to being loaded onto the gel (equal volumes of each sample). The gels were electrophoresed at 20 mA per gel in tank buffer (250 mM Tris-HCl, 192 mM glycine, 0.1% (w/v) SDS). The resulting gels were stained using standard Coomassie blue staining whereby the gels were stained overnight in a Coomassie blue stain [0.025% (w/v) Coomassie brilliant blue R-250 (MilliporeSigma, USA), 40% (v/v) methanol (RadChem, USA), 7% (v/v) glacial acetic acid (RadChem, USA)]. The gels were destained by incubating the gels in a standard destain solution [40% (v/v) methanol (RadChem, USA), 7% (v/v) glacial acetic acid (RadChem, USA)] for 30 minutes followed by several washes of destain solution 2 [5% (v/v) methanol (RadChem, USA), 7% (v/v) glacial acetic acid (RadChem, USA)] until the bands became clearly visible and the background stain was visibly reduced. The gel image was captured using the Cleaver Scientific chemiPRO Chemiluminescence Imaging System and analysed using the GeneSys program (Version 1.8.0.0).

2.4.2. Confirmation of expressed protein as the arginine kinase $McsB_{SA}$ *via* western Blot

SDS-PAGE gels were prepared and loaded with samples as described above. The filter papers and nitrocellulose membranes (MilliporeSigma, USA) required were soaked in blotting buffer (25 mM Tris-HCl, 190 mM glycine, 20% (v/v) methanol, 0.1% (m/v) SDS) for the duration of the electrophoresis. The western blot was then prepared with the following components in order; two layers of 2.5 mm thick filter paper, a nitrocellulose membrane, the SDS-PAGE gel and two layers of 2.5 mm thick filter paper. The SDS-PAGE gel was carefully placed onto the nitrocellulose membrane to avoid any air bubbles. The sandwich was placed onto the Novex® Semi-Dry Blotter and the blot was run at 20 V for 1 hour. The gels were removed and stained using the Coomassie staining procedure as described in section 2.3.2 while the unoccupied sites on the nitrocellulose membranes were blocked for 1 hour using a 5% (w/v) low fat milk powder in tris buffered saline (TBS: 20 mM Tris, 200 mM NaCl, pH 7.4). The membranes were washed in TBS (3 x 5 minutes), followed by an overnight incubation at 4℃ with the 6x-His tag monoclonal antibody (HIS.H8) [cat#: MA1-21315, RRID: AB_557403, Thermo Fisher Scientific, USA) prepared in a 0.5% (w/v) bovine serum albumin (BSA)-TBS at a 5 000x dilution. The membranes were washed in TBS (2 x 5 minutes) followed by a one-hour incubation with the horseradish peroxidase enzyme (HRP)-conjugated secondary antibody [Pierce® goat anti-mouse IgG, (H + L), HRP conjugate, cat#: 31430, Thermo Fisher Scientific, USA] prepared in 0.5% (w/v) BSA-TBS solution at a 10 000 x dilution. The membranes were washed in TBS (3 x 5 minutes) and detected using Clarity Western ECL Substrate (Bio-Rad, USA). The images were captured using the Cleaver Scientific chemiPRO Chemiluminescence Imaging System and analysed using the GeneSys program (Version 1.8.0.0)

2.5. Purification of recombinantly expressed $McsB_{SA}$

The $McsB_{SA}$ soluble fraction obtained was purified by Ni-NTA affinity chromatography as per the manufacturer's instructions. Ni-NTA agarose resin (cat #: R90115, Thermo Fisher Scientific, USA) was first added to a sterile microcentrifuge tube and centrifuged for 1 min at 800 x *g* at 4℃. The supernatant was removed, and the resin was washed with distilled water. The tube containing the Ni-NTA agarose resin resuspended in distilled water was centrifuged using the same conditions and the supernatant was removed. The resin was equilibrated with equilibration buffer (50 mM sodium phosphate, 300 mM NaCl, pH 7.4), equal to 10 x the resin bed volume. The Ni-NTA agarose resin resuspended in equilibration buffer was centrifuged at 800 x *g* for one minute at 4℃. The supernatant was removed, and the equilibration step was repeated.

The $McsB_{SA}$ soluble fraction obtained through sarkosyl solubilisation was treated with 2% Triton X-100 and 20 mM 3-[(3-cholamidopropyl)dimethylammonium]-1-propanesulfonate (CHAPS) to aid in sarkosyl removal. The $McsB_{SA}$ soluble fractions (obtained through sarkosyl solubilisation and optimised expression conditions) were added to the equilibrated Ni-NTA agarose resin and incubated at 4℃ overnight (16 hours) which was followed by centrifugation for 1 min at 800 x *g*, and the supernatant was carefully removed without disturbing the resin bed. The resin was washed with 50 mM sodium phosphate, 300 mM NaCl, 20 mM imidazole, pH 7.4 (wash buffer). The resin resuspended in wash buffer was centrifuged and the supernatant was removed. The wash step was repeated a total of five times. Equilibration buffer supplemented with 300 mM imidazole was added to the resin and was incubated for an hour. This was followed by centrifugation 1 min at 800 x *g*, and the supernatant (eluted $McsB_{SA}$) was carefully removed without disturbing the resin bed. The elution step was carried out a total of three times.

2.6. Buffer exchange of purified $McsB_{SA}$ using the PD-10 column

The eluted $McsB_{SA}$ samples were buffer exchanged using PD-10 desalting columns as per the manufacturer's instructions (MilliporeSigma, USA) which contains 8.3 ml of Sephadex™ G-25 medium. The gravity protocol was conducted as per the manufacturer's instructions. The desalting column was prepared by removing the top cap and pouring off the column storage solution and thereafter cutting the sealed end of the column at the tip. The column was equilibrated by adding 5 ml of equilibration buffer (50 mM sodium phosphate, 150 mM NaCl, pH 7.4) and allowing the buffer to enter the packed bed completely. The equilibration step was repeated a total of five times and the flow-through was discarded. The cap was placed back onto the tip of the column and the $McsB_{SA}$ sample was added (maximum of 2.5 ml) and allowed to enter the packed resin bed. The cap was removed and the flow through was collected and stored at 4℃. The cap was placed back on the tip of the column and the protein was eluted by adding 5 ml of elution buffer (50 mM sodium phosphate, 150 mM NaCl, pH 7.4). The cap was removed, and the eluted protein sample was collected in 500 µl fractions. The flow-through and the eluted protein samples were analysed *via* SDS-PAGE as previously described in section 2.4.1.

2.7. Determination of protein concentration using the Bradford assay

The concentration for the purified $McsB_{SA}$ samples were determined by conducting a Bradford assay (Bradford, 1976). The assay was performed using a microplate reader (n=3). A stock solution of 1 mg/ml BSA was used to prepare protein standard solutions which ranged from

10 to 250 µg/ml. The constructed protein standard solutions were incubated for 10 minutes with Bradford reagent (Thermo Fisher Scientific, USA) in a 1:1 ratio and the absorbance was measured at 595 nm using the SpectraMax® ABS Plus absorbance ELISA microplate reader (Molecular Devices, USA) and analysed using SoftMax® Pro 7 Data acquisition and analysis software (Molecular Devices, USA). A standard curve was produced by plotting the average absorbance of the samples against concentration (Figure 2.1). The concentration of the $McsB_{SA}$ purified samples were determined by incubating the samples with Bradford reagent for 10 minutes in a 1:1 ratio and the absorbance was measured at 595 nm using the SpectraMax® ABS Plus absorbance ELISA microplate reader (Molecular Devices, USA) and analysed using SoftMax® Pro 7 Data acquisition and analysis software (Molecular Devices, USA). The resulting absorbance values recorded were used to extrapolate the concentration of the samples by referring to the constructed standard curve.

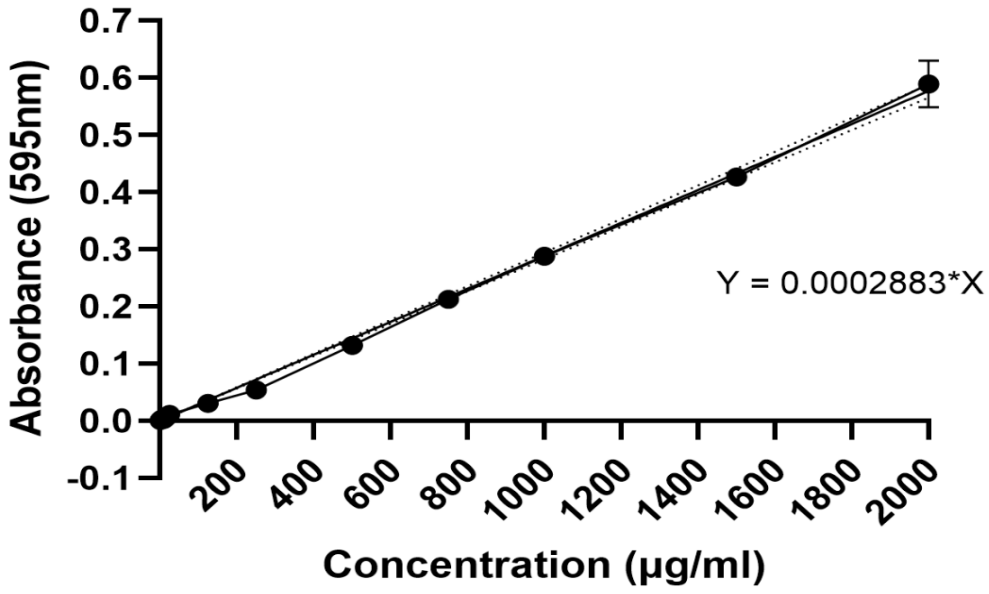

Figure 2.1. Standard curve obtained from the Bradford protein assay. Bovine serum albumin standards ranging from 10 to 250 µg/ml were added to Bradford reagent and the resulting absorbance values were measured at 595 nm after incubation at room temperature for 10 minutes. The mean absorbance calculated for each concentration was plotted (n=3). The equation of the trendline is y = 0.0002883x.

2.8. Thermal stability determination of $McsB_{SA}$

The thermal stability of $McsB_{SA}$ was evaluated through interrogation of the melting temperature of the protein which was investigated *via* the thermal shift assay and the identification of the aggregation temperature of $McsB_{SA}$ which was assessed using the cellular thermal shift assay.

2.8.1. Optimisation of the thermal shift assay (TSA)

A TSA using the Protein Thermal Shift™ Starter Kit was conducted as per the manufacturer's instructions (Thermo Fisher Scientific, USA). The reactions were prepared in clear 0.2 ml PCR strip tubes (Lasec, South Africa), on ice and in quadruplicate as described in Table 2.1. The reagents from the kit were used as provided except for the thermal shift dye. The dye was provided at a 1 000X concentration and was diluted to an 8X concentration using distilled water. The final concentration of the dye in the reaction is 1X.

Table 2.1.: Preparation of samples for the thermal shift assay using the Protein Thermal Shift™ Starter Kit

Sample	Control protein (1 µg/µl)	Control ligand (10 mM)	Thermal shift kit buffer	Distilled water	Thermal shift dye (8X)
1	2 µl	0 µl	5 µl	10.5 µl	2.5 µl
2	2 µl	0.2 µl	5 µl	10.3 µl	2.5 µl
3	2 µl	2 µl	5 µl	8.5 µl	2.5 µl
NPC[a]	0 µl	0 µl	5 µl	12.5 µl	2.5 µl
LOC[b]	0 µl	0.2 µl	5 µl	12.3 µl	2.5 µl

[a]NPC, no protein control
[b]LOC, ligand only control

The run was prepared by using the Design and Analysis software version 2.8.0 (Thermo Fisher Scientific, USA). The reaction volume was changed from 50µl to 20µl. A continuous thermal profile was set up (step 1: ramp rate=1.6 ℃/s, temperature = 25℃, time=2 minutes; step 2: ramp rate = 0.05 ℃/s, temperature=25–99℃, and step 3: hold at 99℃, time=2 minutes. The filter selected were X1 (excitation = 470 ± 15 nm) and M3 (Emission = 586 ± 10 nm). A passive reference was not selected, and the reporter dye and quencher dye were selected as ROX and none respectively. The reactions were typed in according to the position on the plate and the EDT file was saved. The TSA was performed using a QuantStudio 5 Real-Time PCR System (Thermo Fisher Scientific, USA). The melting temperatures were determined by analysis conducted using the Protein Thermal Shift software version 1.4 (Thermo Fisher Scientific, USA). The data was exported to GraphPad Prism (software version 10.4)

Papain was selected as a control protein for the TSA and the assay was prepared as described by Niesen and colleagues (Niesen *et al.*, 2007). Papain (MilliporeSigma, USA) was dissolved in a sodium phosphate buffer, pH 7 and a 2 mg/ml stock solution was prepared. The reactions

were prepared on ice and in duplicate. Papain was tested at 0.15, 0.25, 0.35 and 0.45 µg/µl whilst using a sodium phosphate buffer, pH 7 (n=3). The dye selected for the assay was the SYPRO orange dye (Thermo Fisher Scientific, USA) which was diluted in sodium phosphate buffer, pH 7 to a final concentration of 100X. The final concentration of the dye in the reactions were 5X and 10X when the final reaction volume was 20 µl. The TSA setup was performed as described above.

2.8.2. Thermal shift assay optimisation for $McsB_{SA}$

$McsB_{SA}$ was tested at 0.5 µg in a final reaction volume of 20 µl. The SYPRO orange dye was added at a final concentration of 5X and 10X and a 0.05 M sodium phosphate buffer, pH 7.4 was used. The dye working stock solution (100X) was prepared by diluting the 5000X dye stock in 0.05 M sodium phosphate buffer, pH 7.4. The experimental setup was carried out as described above.

The thermal stability of $McsB_{SA}$ was evaluated under different pH conditions through the screening of a buffer library (n=3). The buffer library consisted of 0.1 M sodium acetate pH 5, 0.5 M 4-Morpholineethanesulfonic acid (MES) buffer pH 6.5, 1 M HEPES buffer pH 7, 0.5 M sodium citrate pH 7, 0.5 M sodium phosphate buffer pH 7, 0.05 M sodium phosphate buffer pH 7.4, 0.05 M sodium phosphate buffer supplemented with 2% (v/v) glycerol, 10 mM β-mercaptoethanol and 12 mM $MgCl_2$, pH 7.4, 1 M Tris-HCl buffer pH 7.5, 1 M Tris-HCl buffer, 2% (v/v) glycerol, 10 mM β-mercaptoethanol and 12 mM $MgCl_2$, pH 7.5 and 0.5 M Bicine buffer pH 7.5 (all buffer reagents were purchased from MilliporeSigma, USA). $McsB_{SA}$ was evaluated at 1 µg and SYPRO orange dye was added at a final concentration of 10X. The experimental setup was carried out as described above where the final reaction volume was 20 µl.

2.8.3. Optimisation of the cellular thermal shift assay (CETSA)

The CETSA protocol was adapted from Hart *et al*, 2019. An overnight culture of *E. coli* $McsB_{SA}$ cells were prepared as previously described in section 2.3. The overnight culture was used to inoculate fresh 2xYT media containing 50 µg/ml kanamycin (ratio of 1:100) and was incubated at 37℃ until the OD_{600} reached 0.5-0.6 and IPTG was added at 0.5 mM. Induction was allowed to proceed for 16 hours at 18℃ with shaking at 150 RPM. The cell culture was transferred to sterile PCR tubes. A broad range of temperatures were selected for initial CETSA's. The nine temperatures selected were 39℃, 41℃, 43℃, 45℃, 47℃, 49℃, 51℃, 53℃, and 55℃. The samples were held at each temperature for 6 minutes using the ProFlex PCR system (Thermo Fisher Scientific, USA) followed by cooling for 6 minutes on ice. The samples were centrifuged

at 5 000 x *g* for 5 minutes at 4℃ and resuspended in 100 µl of lysis buffer (50 mM sodium phosphate, 300 mM NaCl, 1mM PMSF, 1% Triton X -100, pH 7.4). Samples were kept on ice and the cells were lysed using the freeze-thaw method where the tubes were placed in liquid nitrogen for 1 minute followed by thawing out on ice (this process was repeated a total of 5X). The samples were centrifuged at 20 000 x *g* for 1 hour at 4℃. The supernatant (soluble $McsB_{SA}$) was removed and analysed *via* western blot as per section 2.4.2. Densitometry was performed on the resulting images using the Image J 1.54g software (Schneider *et al.*, 2012). The relative band intensities were measured and normalized into percentages where the largest intensity was designated a value of 100% and smallest intensity was designated a value of 0%. The normalized data was transferred to GraphPad Prism (software version 10.4) and the T_{agg} was determined using the Boltzmann sigmoidal non-linear regression (curve fit) analysis (n=3).

The experimental protocol was repeated testing a narrower range of temperatures (47℃, 48℃, 49℃, 50℃, 51℃, 52℃, 53℃, 54℃ and 55℃). The protocol was amended to have a constant concentration of soluble protein in each PCR tube. Firstly, an overnight culture of $McsB_{SA}$ was prepared as previously stated. The overnight culture was used to inoculate fresh 2xYT media containing 50 µg/ml kanamycin (ratio of 1:100) and was incubated at 37℃ until the OD_{600} reached 0.5-0.6. IPTG was added at 0.5 mM. and induction was allowed to proceed for 16 hours at 18℃ with shaking at 150 RPM. The cell culture was lysed by freeze thawing using liquid nitrogen and the process was repeated a total of three times. The samples were sonicated on ice for a total of 5 pulse cycles (30 seconds on and 30 seconds off) and were centrifuged at 20 000 x *g* for 30 minutes at 4℃ and the soluble fraction was collected. This soluble fraction was aliquoted into each PCR tube (100 µl). The temperatures selected were 47℃, 48℃, 49℃, 50℃, 51℃, 52℃, 53℃, 54℃ and 55℃. The samples were held at each temperature for 6 minutes and cooled on ice for six minutes and thereafter centrifuged at 20 000 x *g* for 30 minutes at 4℃. The soluble fractions were collected and the CETSA analysis was conducted as described above.

2.8.4. Evaluation of the cellular thermal shift assay to detect ligand binding of $McsB_{SA}$

The amended CETSA protocol testing a narrower temperature range and utilising a constant concentration of soluble protein as described above was used to detect the binding of the N-terminally acetylated CtsR-derived sequence, Ac-KRGGGGYIKIIKV-OH peptide designed by Suskiewicz and co-workers (Suskiewicz *et al.*, 2019) and synthesised in-house by Professor Fernando Albericio and Professor Beatriz Garcia De la Torre (Discipline of Chemistry,

University of KwaZulu-Natal). The synthesised peptide was dissolved in autoclaved Milli-Q water to prepare a 1 mM stock solution. An overnight culture of $McsB_{SA}$ was prepared and used to inoculate fresh 2xYT media (ratio of 1:100) which was incubated at 37℃ until the OD_{600} reached 0.5-0.6. IPTG was added at 0.5 mM and induction was allowed to proceed for 16 hours at 18℃ with shaking at 150 RPM. The cell culture was lysed by freeze thawing using liquid nitrogen and the process was repeated a total of three times. The samples were sonicated on ice for a total of five cycles (30 seconds on and 30 seconds off) and were centrifuged at 20 000 x *g* for 30 minutes at 4℃ after which the soluble fraction was collected. The soluble fraction was transferred to two 1.5 ml sterile centrifuge tubes and the peptide was added to one of the tubes at a final concentration of 100 µM (by adding 150 µl of the 1 mM stock solution). The two tubes were incubated for 24 hours at 4℃. The samples were transferred to PCR tubes to test the designed temperature range (47℃ - 55℃) as described above. The samples were held at each temperature for 6 minutes and cooled on ice for six minutes and thereafter centrifuged at 20 000 x g for 30 minutes at 4℃. The soluble fractions were collected and the CETSA analysis was conducted as described above (n=3).

2.9. Pandemic Response Box screening

The Pandemic Response Box was prepared as per the manufacturer's instructions. The compounds were prepared in dimethyl sulfoxide (DMSO) [MilliporeSigma, USA], and stock plates were prepared at 1 mM. The compounds were screened against $McsB_{SA}$ by means of the thermal shift assay and further evaluated using the cellular thermal shift assay.

2.9.1. Identification of novel $McsB_{SA}$ ligands through thermal shift analysis

The 400 compounds present in the Pandemic Response Box were initially screened by creating 40 cocktails. Each cocktail contained 10 compounds with each of the compounds added at a final concentration of 10 µM (a total of 2 µl per cocktail). The composition of each cocktail is described in APPENDIX E. Each cocktail (2 µl) was incubated with 1 µg of $McsB_{SA}$ and 50 mM sodium phosphate buffer, pH 7.4 for 1 hour at 4℃ followed by the addition of SYPRO orange (10X). The 100X SYPRO orange dye working stock solution was created by diluting the 5000X stock in 50 mM sodium phosphate buffer, pH 7.4. The run was prepared by using the Design and Analysis software version 2.8.0 (Thermo Fisher Scientific, USA). The reaction volume was changed from 50µl to 20µl. A continuous thermal profile was set up (step 1: ramp rate=1.6 ℃/s, temperature = 25℃, time=2 minutes; step 2: ramp rate = 0.05 ℃/s, temperature=25–99℃, and step 3: hold at 99℃, time=2 minutes. The filter selected were X1 (excitation = 470 ± 15 nm) and M3 (Emission = 586 ± 10 nm). A passive reference was not

selected, and the reporter dye and quencher dye were selected as ROX and none respectively. The reactions were typed in according to the position on the plate and the EDT file was saved. The TSA was performed using a QuantStudio 5 Real-Time PCR System (Thermo Fisher Scientific, USA). The melting temperatures were determined by analysis conducted using the Protein Thermal Shift software version 1.4 (Thermo Fisher Scientific, USA). The data was exported to GraphPad Prism (software version 10.4). The cocktail screening was conducted once (n=1).

The top four cocktails (A1, B4, C3 and E3) that resulted in a positive shift in the melting temperature of $McsB_{SA}$ were further evaluated (n=3). Cocktail A1 was evaluated first, by testing each compound present in the cocktail individually at a concentration of 10 µM. The cocktail was subsequently split into cocktails A1.1 [containing compounds MMV1634492 (A1), MMV002731 (A2), MMV003143 (A3), MMV1578560 (A4) and MMV1782223 (A5)] and A1.2 (containing compounds MMV1782351 (A6), MMV1593535 (A7), MMV1579783 (A8), MMV1633967 (A9), and MMV1581551 (A10). Cocktail A1.1 was further evaluated by testing pairs of compounds, each at 10 µM, specifically compounds A1+A2, A1+A3, A1+A4, A1+A5, A2+A3, A2+A4, A2+A5, A3+A4, A3+A5, A4+A5 and lastly, a combination of compounds A1+A2+A3 was tested. $McsB_{SA}$ was evaluated at 1 µg and SYPRO orange dye was added in at a final concentration of 10X. The experimental setup was carried out as described above where the final reaction volume was 20 µl.

Finally, each of the compounds present in the remaining three cocktails (B4, C3 and E3) were tested individually at a concentration of 10 µM (by adding 0.2 µl of the 1 mM stock) (n=3). $McsB_{SA}$ was screened at 1 µg, SYPRO orange dye was added in at a final concentration of 10X and the experimental setup was carried out as described above where the final reaction volume was 20 µl. The nine compounds which were determined to induce an increase in the melting temperature of $McsB_{SA}$ were thereafter evaluated at 5 µM (using 0.1 µl of the 1 mM stock) and 10 µM (using 0.2 µl of the 1 mM stock) whilst the experimental setup was performed as described above.

2.9.2. Validation of identified novel $McsB_{SA}$ ligands *via* the cellular thermal shift assay (CETSA)

The nine positive hits identified from the thermal shift assay (compounds MMV1593539, MMV1578899, MMV1634391, MMV1593531, MMV1580485, MMV1633968, MMV658803, MMV1782213 and MMV1782355) were further analysed using the amended CETSA protocol

(n=3). An overnight culture of $McsB_{SA}$ was prepared. The overnight culture was used to inoculate fresh 2xYT media supplemented with 50 µg/ml kanamycin (ratio of 1:100) and was incubated at 37℃ until the OD_{600} reached 0.5-0.6. IPTG was added at 0.5 mM and induction was allowed to proceed for 16 hours at 18℃ with shaking at 150 RPM. The cell culture was lysed by freeze thawing using liquid nitrogen and the process was repeated a total of three times. The samples were sonicated on ice for a total of five cycles (30 seconds on and 30 seconds off) and were centrifuged at 20 000 x *g* for 30 minutes at 4℃ and the soluble fractions were collected. The soluble fractions were transferred to ten 1.5 ml sterile centrifuge tubes and were incubated for 24 hours with 1% DMSO in tube one, and 1 µM of compound (one compound per tube for tubes two – ten). Each of the tubes were aliquoted into fourteen PCR tubes (100 µl). The temperatures selected were 43℃, 44℃, 45℃ 46℃, 47℃, 48℃, 49℃, 50℃, 51℃, 52℃, 53℃, 54℃, 55℃ and 56℃. The samples were held at each temperature for 6 minutes and cooled on ice for six minutes and thereafter centrifuged at 20 000 x *g* for 30 minutes at 4℃. The supernatants (soluble $McsB_{SA}$) were removed and analysed *via* western blot as per section 2.4.2. Densitometry was performed on the resulting images using the Image J 1.54g software (Schneider *et al.*, 2012). The relative band intensities were measured and normalized into percentages where the largest intensity was designated a value of 100% and smallest intensity was designated a value of 0%. The normalized data was transferred to GraphPad Prism (software version 10.4) and the T_{agg} was determined using the Boltzmann sigmoidal non-linear regression (curve fit) analysis.

2.10. Isothermal dose-response fingerprint cellular thermal shift assay

An isothermal dose-response fingerprint CETSA ($ITDRF_{CETSA}$) was conducted (n=3) as described by Jafari and co-workers (Jafari *et al.*, 2014), using the compounds which produced the highest shift in T_m (TSA) and T_{agg} (CETSA) which were compounds MMV1593539, MMV1580485, MMV1633968 and MMV1782213. These compounds were tested at 1 µM, 10 µM and 30 µM. $McsB_{SA}$ soluble protein was incubated with each of the compounds at the desired concentration for 1 hour at 4℃. The samples were exposed to a constant temperature of 48℃ for 6 minutes and cooled on ice for 6 minutes. The samples were centrifuged at 20 000 x *g* for 30 minutes at 4℃ to separate and collect the soluble fraction. The soluble $McsB_{SA}$ samples were analysed using western blot analysis whereby the $McsB_{SA}$ samples were probed and detected as previously described. Relative band intensities were determined using ImageJ software and further analysed using GraphPad Prism (software version 10.4).

2.11. *Staphylococcus aureus* minimum inhibitory concentration assay

A minimum inhibitory concentration assay was performed using 2xYT media and a glycerol stock of *S. aureus* (ATCC25923). The ATCC25923 strain is commonly used as a control for antibiotic susceptibility testing (Treangen *et al.*, 2014). Firstly, the glycerol stock of *S. aureus* (ATCC25923) was streaked onto 2xYT agar plates [16 mg/ml tryptone, 10 mg/ml yeast extract, 5 mg/ml NaCl, 1.5% (w/v) bacteriological agar (all purchased from MilliporeSigma, USA)]. The plates were grown overnight at 37℃. A single colony from the plate was used to inoculate fresh 2xYT media [16 mg/ml tryptone, 10 mg/ml yeast extract, 5 mg/ml NaCl (all purchased from MilliporeSigma, USA)]. The culture was incubated overnight at 37℃ whilst shaking at 180 RPM. The overnight culture of *S. aureus* was diluted to obtain an OD_{600} of 0.10. The diluted culture was transferred to a 96-well plate. Compounds MMV1593539, MMV1578899, MMV1634391, MMV1633968, MMV1782355 and MMV1782213 were tested at a range of 0.078 µM – 20 µM (20 µM was the starting concentration whilst ciprofloxacin was tested as a positive control in a range of 0.078 µg/ml – 20 µg/ml). A two-fold serial dilution was prepared from 20 µM until a concentration of 0.078 µM (µg/ml for ciprofloxacin control) was reached. The OD_{600} readings were recorded at 0 hour (h) using the SpectraMax® ABS Plus absorbance ELISA microplate reader (Molecular Devices, USA) and analysed using SoftMax® Pro 7 Data acquisition and analysis software (Molecular Devices, USA). The plates were incubated at 37℃ for 24 hours and the OD_{600} readings were recorded thereafter. The readings were normalised by subtracting the 0 h OD_{600} reading from the 24 h OD_{600} reading and the relative growth was determined by using the 0 µM DMSO control as 100% (n=3).

2.12. In silico analysis of $McsB_{SA}$

2.12.1. Assessing the drug-likeness of novel $McsB_{SA}$ ligands

The six compounds identified as $McsB_{SA}$ ligands were assessed for drug-like properties using the in silico tools SwissADME SwissDrugDesign web tool (operated by the Molecular Modelling Group of the University of Lausanne and the SIB Swiss Institute of Bioinformatics, http://www.swissadme.ch/, accessed last in October 2024) (Daina *et al.*, 2017) and the OSIRIS Molecular Property Explorer (https://www.organic-chemistry.org/prog/peo/, accessed last in October 2024).

2.12.2. Molecular modelling of $McsB_{SA}$

A pairwise structural alignment was first performed using the pairwise structure alignment tool available from the Research Collaboratory for Structural Bioinformatics Protein Data Bank (RCSB PDB) [Accessed in December 2024]. The crystal structure for $McsB_{SA}$ (PDB: 8GQD)

(Lu *et al.*, 2024) as well as the $McsB_{GS}$ structure (PDB: 6FH3) (Suskiewicz *et al.*, 2019) were used. The monomeric forms of $McsB_{SA}$ and $McsB_{GS}$ were aligned using the TM-align (where TM = template modelling) algorithm and the computed root mean square deviation (RMSD) and TM-score was recorded (Bittrich *et al.*, 2024).

Molecular modelling was performed using the Schrödinger drug discovering suite (Maestro, version 2022-1) provided by the Centre for High Performance Computing, Cape Town, South Africa. The crystal structure for $McsB_{SA}$ (PDB: 8GQD) (Lu *et al.*, 2024) as well as two $McsB_{GS}$ structures (PDB: 6FH3 and 6FH2) (Suskiewicz *et al.*, 2019) were used. The $McsB_{GS}$ structures were crystallised as a dimer whereas the $McsB_{SA}$ structure was crystallised as a tetramer. Both McsB structures were modelled as dimers, and this was attained by removing two of the monomers from the tetrameric structure of $McsB_{SA}$. All McsB protein structures were prepared using the protein preparation wizard with default settings. The putative binding sites on the $McsB_{SA}$ dimer were identified using SiteMap. The Protein Structure Alignment tool was used to align each of the identified putative $McsB_{SA}$ binding sites with either $McsB_{GS}$ bound with AMP-PN or $McsB_{GS}$ bound with pArg. The $McsB_{SA}$ sites which aligned with the binding sites of $McsB_{GS}$ were used for subsequent docking analyses.

2.12.3. Molecular docking of novel $McsB_{SA}$ binders

The Schrödinger drug discovering suite (Maestro, version 2022-1) provided by the Centre for High Performance Computing (Cape Town, South Africa) was used to perform all molecular docking analyses. The six compounds, MMV1593539, MMV1578899, MMV1634391, MMV1633968, MMV1782355 and MMV1782213, identified to bind $McsB_{SA}$ *in vitro* as well as AMP-PN, ATP, pArg and Arg were imported into the Schrödinger drug discovering suite. All of the ligands were prepared using the LigPrep tool with default settings. The AMP-PN and pArg sites of $McsB_{GS}$ as well as the putative ATP and pArg sites of $McsB_{SA}$ were prepared for docking analyses using the Receptor Grid Generation tool. All docking analyses were performed using the Glide software in XP mode and the compounds were ranked using the obtained docking, XP glide and glide emodel scores. Firstly, ATP and AMP-PN or pArg and Arg were docked into the respective predicted/known binding sites of $McsB_{SA}$ and $McsB_{GS}$ and the scores were compared. Secondly, Arg was docked into the predicted ATP $McsB_{SA}$ binding site and AMP-PN was docked into the predicted pArg $McsB_{SA}$ binding site. After which, all identified ligands shown to bind to $McsB_{SA}$ *in vitro*, were docked into the predicted ATP and pArg *S. aureus* binding sites.

2.12.4. Molecular dynamics of $McsB_{SA}$

Molecular dynamics (MD) was performed on the $McsB_{SA}$ monomer with no ligand present or in the complex with ATP, MMV1782355 and MMV1593539 for 50 ns using Desmond with Isothermal-Isobaric ensemble class, 300 K temperature, 1.01 bar pressure and 150 mM NaCl. The RMSD over time, radius of gyration (RoG) over time, root mean square fluctuation (RMSF) per residue, bond interaction counts and ligand interaction diagrams as snapshots at 0, 10, 20, 30, 40 and 50 ns (where applicable) were calculated for each simulation within the drug discovery suite and were used to assess conformational stability and ligand topology of the two binders.

2.13. Statistical analysis

All statistical analyses performed were conducted using GraphPad Prism (software version 10.4) where descriptive statistical analysis was calculated [mean, standard deviation (SD) and standard error (SE)] and either a Student's t-test or a one-way ANOVA with Dunnett's multiple comparison test were used as described in each respective figure legend.

CHAPTER 3: RESULTS

3.1. Sequence analysis for $McsB_{SA}$

3.1.1. Comparative sequence alignment of $McsB_{SA}$ and $McsB_{GS}$

The sequences for $McsB_{SA}$ and $McsB_{GS}$ were analysed for sequence similarity by using the Clustal Omega program and the SIM tool. The alignment outputs [Figure 3.1 and APPENDIX A (Figure A1)] revealed the best alignment for the sequences and highlights the amino acid regions which are common in both sequences. The Clustal Omega alignment calculated an overall similarity index of 41.79% between both sequences (Figure 3.1). The sequence similarity shared was low and the result was verified using the SIM tool available from ExPASy. The result was verified as the SIM alignment identified a 43.8% sequence identity in a 349 residue overlap (2 N-terminal and 12 C-terminal residues were not considered) between the 363 amino acid sequence of $McsB_{GS}$ and the 335 amino acid sequence of $McsB_{SA}$ (APPENDIX A, Figure A1).

3.1.2. Determination of the aptness of $McsB_{SA}$ for the thermal shift assay

The amino acid sequence for $McsB_{SA}$ was analysed and the amino acids contributing towards protein hydrophobicity were scored using the Kyte and Doolittle index as per Table 3.1. The $McsB_{SA}$ sequence consists of 335 amino acids of which 123 were scored as hydrophobic (either alanine, cysteine, isoleucine, leucine, methionine, phenylalanine or valine) as per the Kyte and Doolittle scale (Table 3.1). Isoleucine and valine return the highest scores of 4.5 and 4.2, respectively. These amino acids account for 38.21% of the hydrophobicity observed for $McsB_{SA}$. The hydrophobicity of $McsB_{SA}$ was thereafter visualised through a Kyte and Doolittle hydrophobicity plot (Figure 3.2). The hydrophobicity plot revealed a larger portion of the sequence being composed of hydrophilic residues as highlighted by the red rectangle in Figure 3.2.

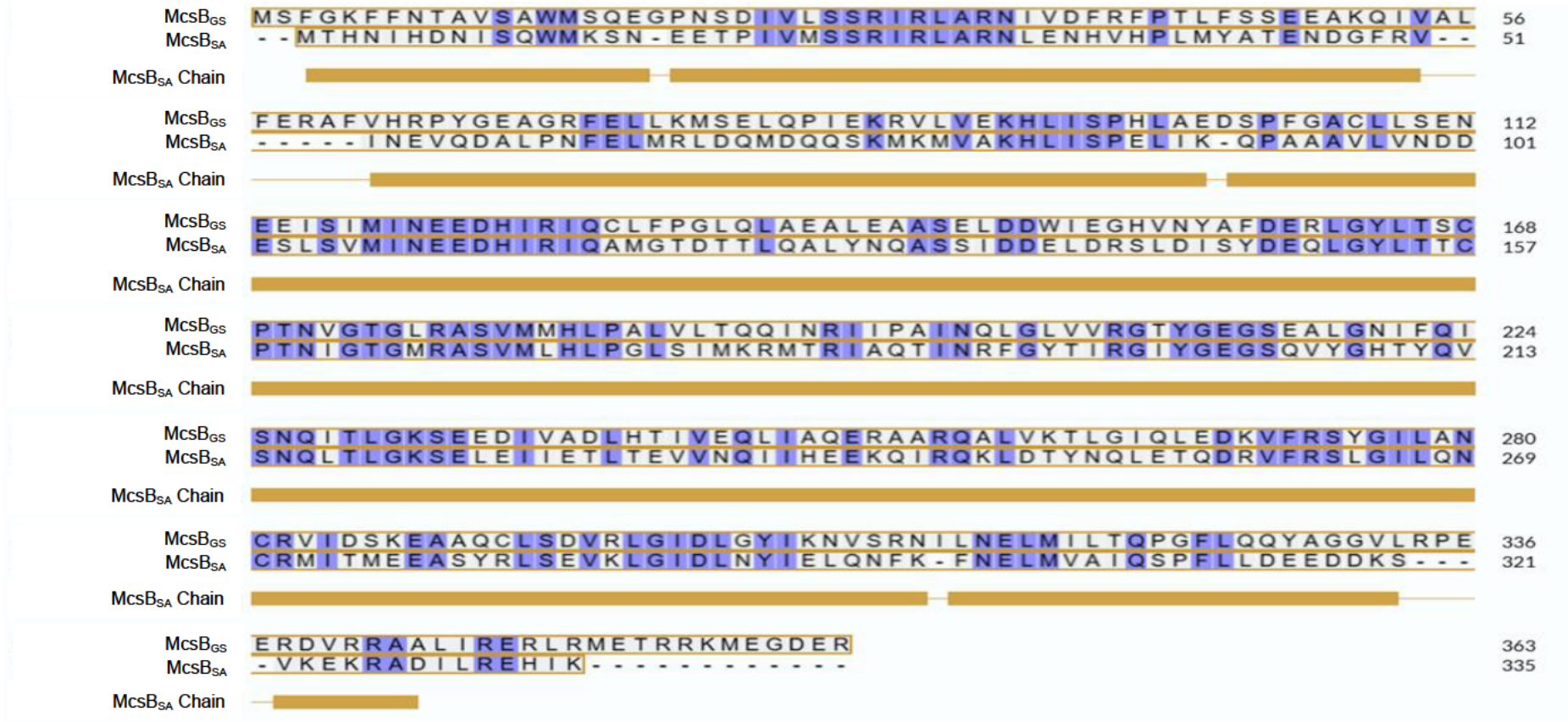

Figure 3.1. The Clustal Omega alignment output for McsB$_{SA}$ and McsB$_{GS}$. The highlighted amino acids in blue represent the common amino acids between the two sequences analysed. The dashes (-) indicate the missing residues in the sequence of McsB$_{SA}$, The McsB$_{SA}$ chain was selected and was displayed by the brown bar which becomes a thin line where there are missing residues.

Table 3.1.: The total number of hydrophobic amino acids present in the $McsB_{SA}$ and $McsB_{GS}$ sequences with the relative hydrophobic scores as per the Kyte and Doolittle index.

			$McsB_{SA}$	**$McsB_{GS}$**
Hydrophobic amino acid	Symbol	Kyte and Doolittle score	Total number of Amino Acids	Total number of Amino Acids
Alanine	A	1.8	15	29
Cysteine	C	2.5	2	5
Isoleucine	I	4.5	30	30
Leucine	L	3.8	35	43
Methionine	M	1.9	17	9
Phenylalanine	F	2.8	7	15
Valine	V	4.2	17	22
Total			123	153

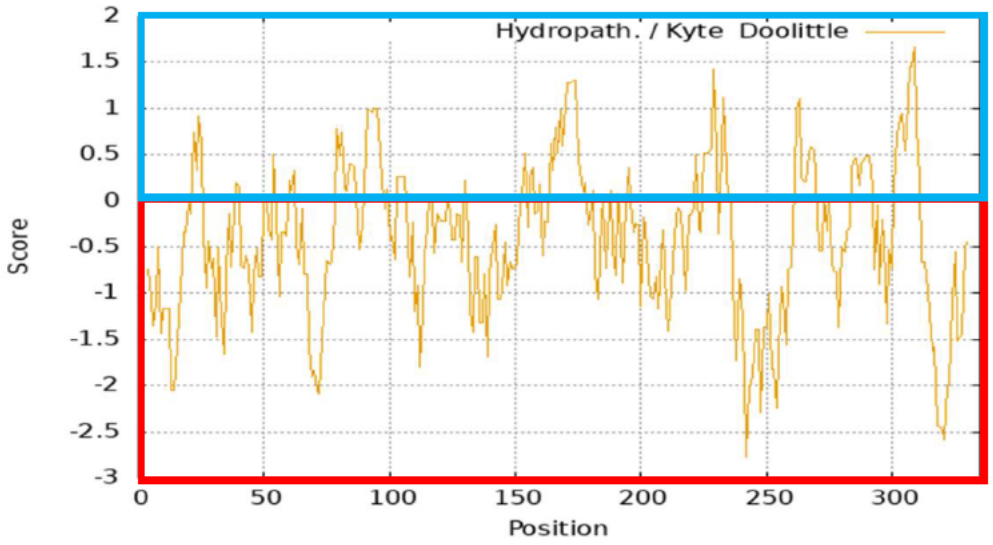

Figure 3.2. Plot of the hydrophobicity score for the amino acid sequence of $McsB_{SA}$ using the Kyte and Doolittle index. The blue rectangle highlights the hydrophobic portion of the sequence, and the red rectangle highlights the hydrophilic portion of the sequence.

3.2. Recombinant expression of soluble arginine kinase $McsB_{SA}$

3.2.1. Initial expression conditions

The *E. coli* BL21(DE3) cells transformed with the $McsB_{SA}$ plasmid expressed a protein with a size of approximately 42 kDa. The protein was expressed prominently in the insoluble fraction as observed in Figure 3.3. Both the insoluble and soluble fractions were separated and analysed *via* SDS-PAGE gels (Figure 3.3). Induction of protein expression with 0.1 mM IPTG and 0.3 mM IPTG resulted in seemingly higher yields of protein as observed by the intense banding pattern observed in lanes 3 and 5 of Figure 3.3. These expression conditions were not optimal as they resulted in the protein being expressed in the insoluble form. The largest levels of protein available in the soluble form was obtained following induction with 0.5 mM IPTG as observed in lane 6 of Figure 3.3.

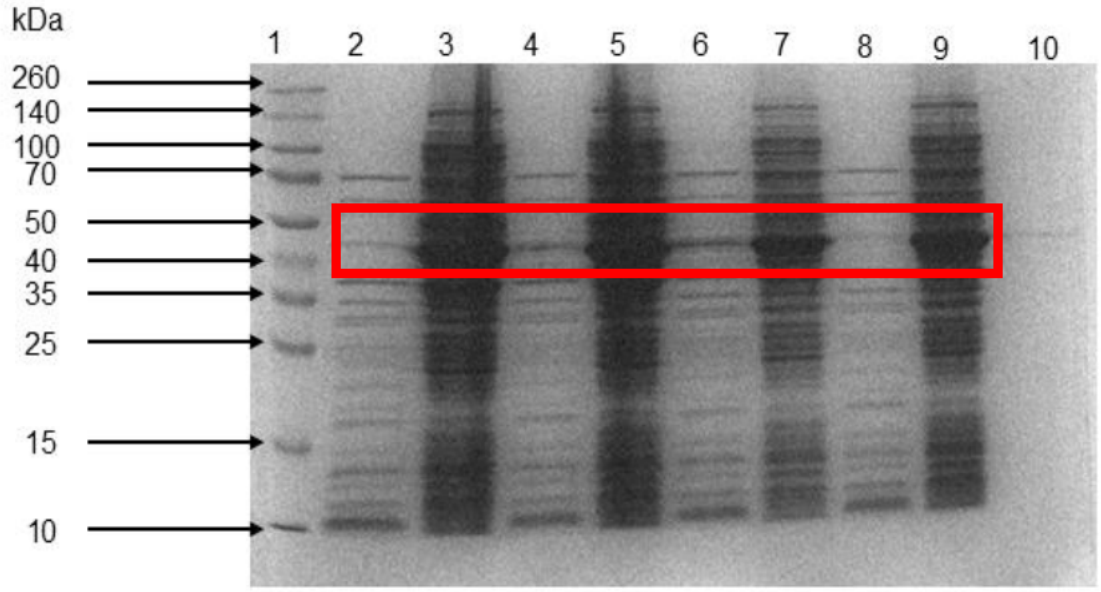

Figure 3.3. Recombinantly expressed protein in *E. coli* BL21(DE3) cells. All cell cultures were induced overnight at 16°C using various concentrations of Isopropyl ß-D-1-thiogalactopyranoside (IPTG). The protein, expressed under varying conditions, was separated into the soluble and insoluble fractions. These fractions were separated and visualised through reducing SDS-PAGE by loading equal volumes of each sample (20 µl). The 12,5% gel was stained with Coomassie blue R250 stain. The Spectra™ Multicolour Broad Range Protein Ladder was run in lane 1. The expressed protein samples were run as follows: lane 2: soluble fraction from 0.1 mM IPTG induced sample, lane 3: insoluble fraction from 0.1 mM IPTG induced sample, lane 4: soluble fraction from 0.3 mM IPTG induced sample, lane 5: insoluble fraction from 0.3 mM IPTG induced sample, lane 6: soluble fraction from 0.5 mM IPTG induced sample, lane 7: insoluble fraction from 0.5 mM IPTG induced sample, lane 8: soluble fraction from 1 mM IPTG induced sample, lane 9: insoluble fraction from 1 mM IPTG induced sample and lane 10: reducing treatment buffer. The red box highlights the band with a molecular weight of approximately 42 kDa.

3.2.2. N-Lauroylsarcosine solubilization

The expressed protein was prominently displayed in the insoluble fraction regardless of the induction conditions tested. Two methods were employed to obtain soluble recombinantly expressed protein, the first, obtained soluble protein from previously insoluble expressed protein *via* sarkosyl solubilisation whilst the second method relied on optimised expression conditions to obtain soluble recombinantly expressed protein. In the first instance, the expressed protein was solubilised using a 2% sarkosyl solution. The previously insoluble expressed protein was solubilised using sarkosyl as observed *via* SDS-PAGE gel analysis, specifically in lanes 4 and 8 of Figure 3.4. which displays the soluble fraction obtained after sarkosyl solubilization. SDS-PAGE analysis revealed protein present in the insoluble fractions as observed in lanes two and six of Figure 3.4 however it was substantially less than previously detected (Figure 3.3).

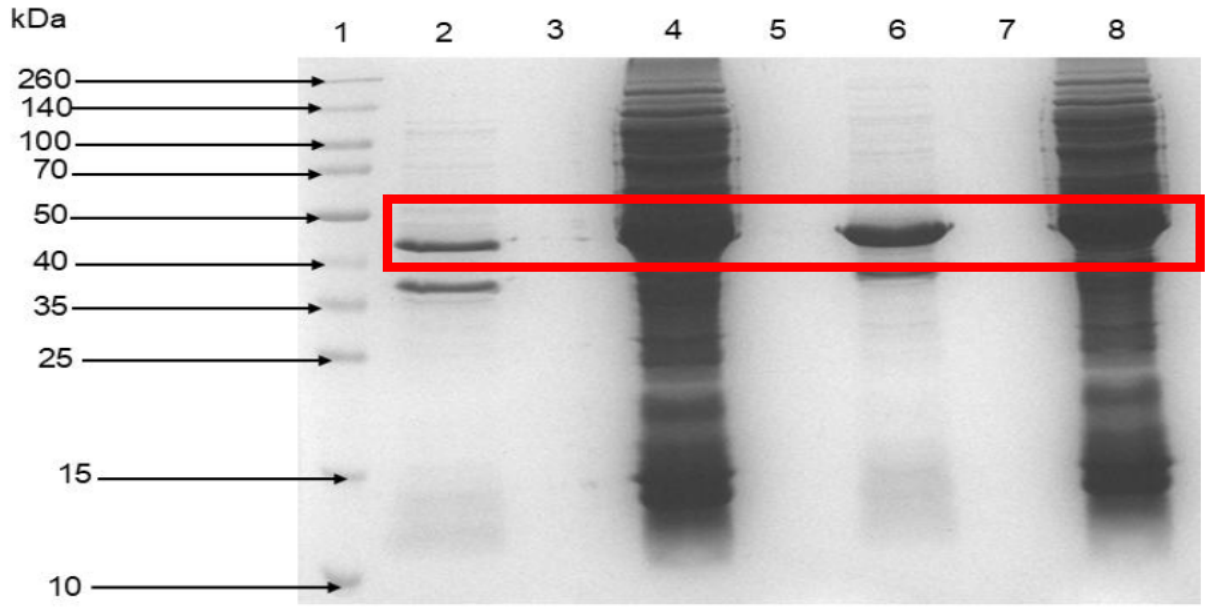

Figure 3.4. Recombinantly expressed protein solubilised using 2% N-Lauroylsarcosine (sarkosyl). All cell cultures were induced overnight at 16°C using 0.5 mM of Isopropyl ß-D-1-thiogalactopyranoside (IPTG). The insoluble fraction was incubated with 2% sarkosyl and thereafter was separated into the soluble and insoluble fractions. These fractions were separated and visualised through reducing SDS-PAGE (loading equal volumes). The 12,5% gel was stained with Coomassie blue R250 stain. The Spectra™ Multicolour Broad Range Protein Ladder was run in lane 1. The expressed protein samples were run as follows: lane 2: insoluble fraction from 0.5 mM IPTG induced $McsB_{SA}$ sample 1, lane 3: reducing treatment buffer, lane 4: soluble fraction from 0.5 mM IPTG induced $McsB_{SA}$ sample 1, lane 5: reducing treatment buffer, lane 6: insoluble fraction from 0.5mM IPTG induced $McsB_{SA}$ sample 2, lane 7: reducing treatment buffer, lane 8: soluble fraction from 0.5 mM IPTG induced $McsB_{SA}$ sample 2. The red box highlights the band present at the expected molecular weight of expressed $McsB_{SA}$.

3.2.3. Optimised expression conditions

In the second instance, the protein was overly expressed in the soluble fraction through optimised expression conditions (without the use of sarkosyl) as observed in Figure 3.5. (lanes two and four). A large fraction of the expressed protein was insoluble (lanes three and five, Figure 3.5.). The western blot confirmed that the band present in the soluble fraction was a His-tagged protein as it was detected when probed with 6x-His tag monoclonal antibody (Figure 3.5.B). The detected band was at the approximate molecular weight of expressed $McsB_{SA}$ (approximately 42 kDa).

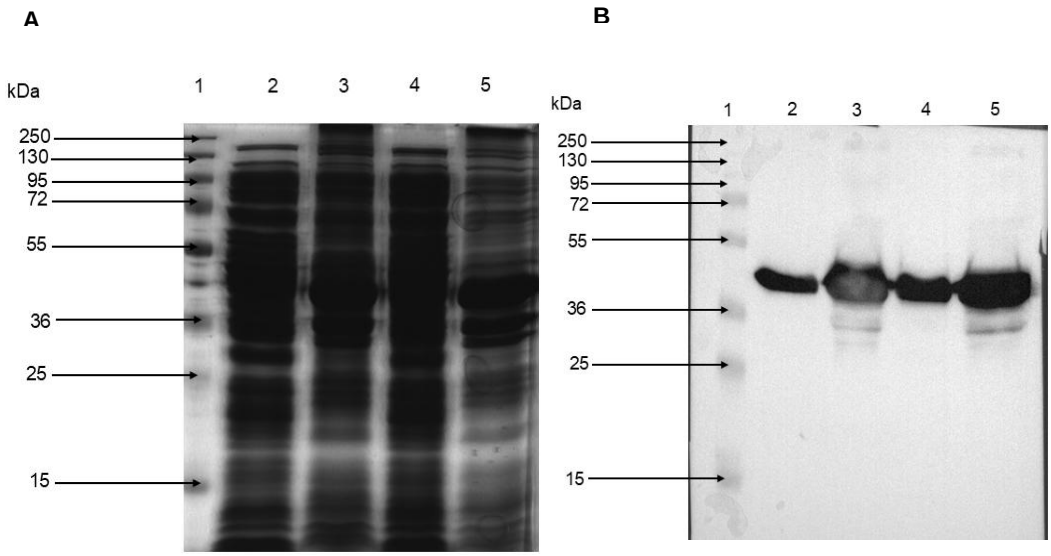

Figure 3.5. Analysis of overexpressed $McsB_{SA}$ optimised for soluble expression. (A) Expressed protein samples were separated and visualised through reducing SDS-PAGE. The expression was tested in duplicate. The Thermo Scientific PageRuler Plus was run in lane 1. The expressed protein samples were run as follows: lane 2: insoluble fraction from 0.5 mM induced sample 1, lane 3: soluble fraction from 0.5 mM induced sample 1, lane 4: insoluble fraction from 0.5 mM induced sample 2, lane 5: soluble fraction from 0.5 mM induced sample 2. (B)The samples were separated as per the SDS-PAGE in (A) and transferred to a nitrocellulose membrane. The membrane was probed with 6x-His tag monoclonal antibody (HIS.H8) [cat#: MA1-21315, RRID: AB_557403, Thermo Fisher Scientific, USA) and horseradish peroxidase enzyme (HRP)-conjugated secondary antibody [Pierce® goat anti-mouse IgG, (H + L), HRP conjugate, cat#: 31430, Thermo Fisher Scientific, USA].

3.3. Purification of recombinantly expressed $McsB_{SA}$

The soluble fraction of $McsB_{SA}$ obtained through optimised expression conditions was purified using Ni-NTA agarose (cat #: R90115, Thermo Fisher Scientific, USA). The soluble fraction along with the eluted products were separated by SDS-PAGE (Figure 3.6). The soluble fraction revealed contaminating proteins present from the expression process (Figure 3.6, lane 2). Majority of these contaminating proteins were, however, not present in the eluted fractions with the exception of faint bands being observed at 100 kDa and 140 kDa which suggested that there may be non-specific binding, and a more stringent wash step was required (Figure 3.6, lanes 3- 5). The samples were then transferred to nitrocellulose membrane and probed

with anti-HIS primary antibody. The probed western blot revealed a single band detected at the approximate molecular weight of $McsB_{SA}$ at approximately 42 kDa (Figure 3.7). The band was detected in lane 2 which contained the soluble fraction and in lanes 3 and 5 of the blot containing the $McsB_{SA}$ eluted samples (Figure 3.7). The band was not detected in lane 4 which could be explained by a poor transfer between the SDS-PAGE gel and the nitrocellulose membrane.

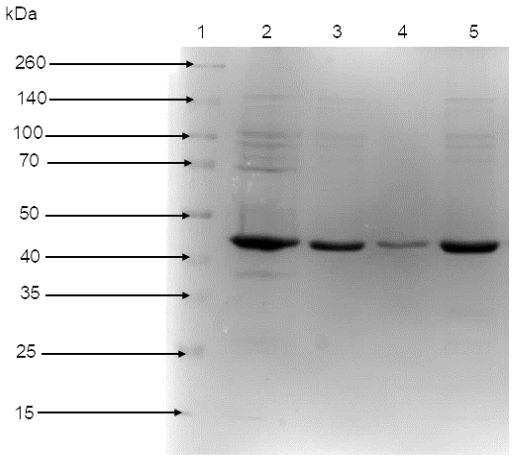

Figure 3.6. SDS-PAGE analysis of a representative purification of $McsB_{SA}$ from *E. coli*. $McsB_{SA}$ eluted samples from the Ni-NTA agarose resin (cat #: R90115, Thermo Fisher Scientific, USA) were analysed and separated *via* a 12.5% reducing SDS-PAGE. The gel was stained with Coomassie blue R250 stain. The gel was loaded as follows: lane 1: Spectra™ Multicolour Broad Range Protein Ladder, lane 2: $McsB_{SA}$ protein (diluted soluble fraction which was incubated with the Ni-NTA agarose resin), lane 3: $McsB_{SA}$ elution 01, lane 4: $McsB_{SA}$ elution 02 and lane 5: $McsB_{SA}$ elution 03.

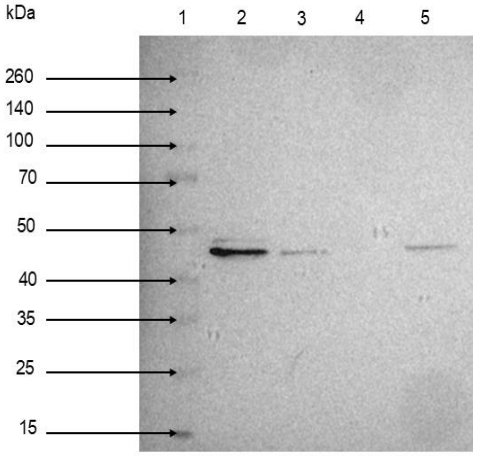

Figure 3.7. Western blot analysis of a representative purification of $McsB_{SA}$. The representative SDS-PAGE gel loaded with $McsB_{SA}$ eluted samples from the Ni-NTA agarose resin was transferred to a nitrocellulose membrane. The membrane was probed with 6x-His tag monoclonal antibody (HIS.H8) [cat#: MA1-21315, RRID: AB_557403, Thermo Fisher Scientific, USA) and horseradish peroxidase enzyme (HRP)-conjugated secondary antibody [Pierce® goat anti-mouse IgG, (H + L), HRP conjugate, cat#: 31430, Thermo Fisher Scientific, USA]. The lanes were loaded as follows: lane 1: Spectra™ Multicolour Broad Range Protein Ladder, lane 2: $McsB_{SA}$ protein (diluted soluble fraction which was incubated with the Ni-NTA agarose resin), lane 3: $McsB_{SA}$ elution 01, lane 4: $McsB_{SA}$ elution 02 and lane 5: $McsB_{SA}$ elution 03.

3.4. Buffer exchange of purified $McsB_{SA}$ using the PD-10 column

The $McsB_{SA}$ eluted samples obtained from the Ni-NTA agarose resin were pooled together and a buffer exchange was performed to remove the imidazole present in the eluted samples using the PD-10 column. The buffer exchanged $McsB_{SA}$ products were analysed *via* SDS-PAGE. The first two eluted samples loaded in lanes 2 and 3 of Figure 3.8 showed no protein present thus indicating that the protein was only eluted from the resin after the first millilitre of buffer had passed through. The remaining collected eluted samples from lane 4 to lane 10 revealed a protein band with an approximate molecular weight of 42 kDa. The eluted samples obtained were pooled together and the concentration of $McsB_{SA}$ was determined using the Bradford assay. The average concentration of $McsB_{SA}$ samples after the buffer exchange was determined to be 251.11 µg/ml (0.25 µg/µl).

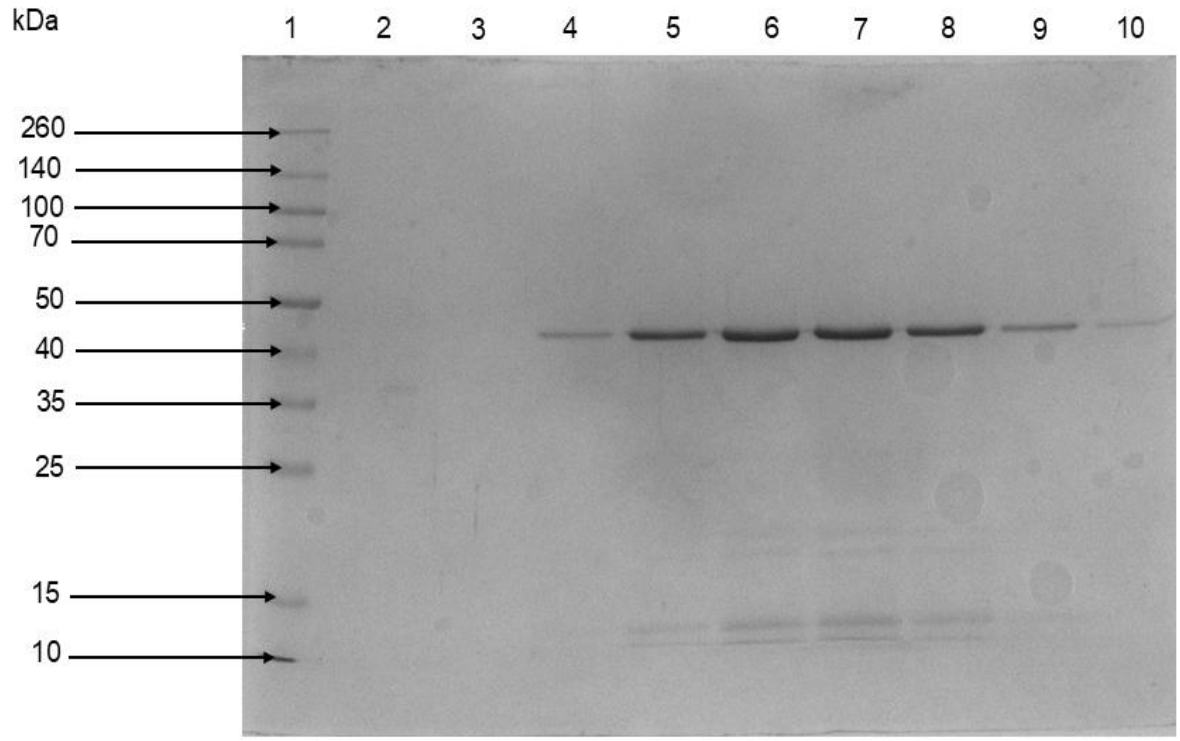

Figure 3.8. Analysis of $McsB_{SA}$ eluted protein samples after buffer exchange. $McsB_{SA}$ eluted samples from the Ni-NTA agarose resin were buffer exchanged using PD-10 columns. The buffer exchanged $McsB_{SA}$ elutions were separated on a 12.5% SDS-PAGE. The gel was loaded as follows: lane 1: Spectra™ Multicolour Broad Range Protein Ladder, lane 2: collected flow through (waste), lanes 3 – 10: $McsB_{SA}$ elutions 01 – 08. The gel was stained using standard Coomassie blue R250.

3.5. Thermal stability determination of $McsB_{SA}$

3.5.1. Optimisation of the thermal shift assay (TSA)

Firstly, the thermal shift assay was validated as a tool to detect ligands of $McsB_{SA}$ by assessing the thermal shift kit (Thermo Fisher Scientific, USA). The model protein provided was investigated at a final concentration of 0.1 µg/µl while the control ligand was evaluated at 0.1 mM and 1 mM. The raw fluorescence obtained for the model protein was compared to the raw fluorescence obtained for the model protein when incubated with the ligand at each concentration as displayed in APPENDIX D (Figure D1). The raw fluorescence obtained was used to calculate the first derivative (dF/dT) and this was plotted against temperature (℃) as displayed in APPENDIX D (Figure D2).

The derivative graph in Figure D2 defines the melting temperature of the samples as the peak of the sigmoidal curve and delineates the temperature at which 50% of the protein had unfolded. The melting temperature of the control protein increased significantly to 46.91℃ ($p<0.0001$, Figure 3.11) when incubated with 0.1 mM of the control ligand and increased further when incubated with 1 mM of the control ligand as a difference of 7.43℃ ($p<0.0001$, Figure 3.11) was noted which indicated that the control ligand bound to the control protein as expected and resulted in an increase in thermal stability. A fluorescence signal was not detected at any temperature point for either the NPC or the LOC as was anticipated since the NPC sample did not have any protein present and thus confirmed that the dye would only fluoresce when bound to the control protein. The lack of fluorescence signal obtained for the LOC was also expected as the Protein Thermal Shift Kit was designed to contain a control ligand which would not interact with the dye.

Papain was selected as a control protein owing to the protein having a molecular weight similar to $McsB_{SA}$ with a molecular weight of approximately 39 kDa, an amino acid length of 345 amino acids and a hydrophobicity index similar to $McsB_{SA}$ (APPENDIX B). Papain consisted of 115 amino acid residues which contributed towards the obtained hydrophobicity plot and 40.87% of this hydrophobicity was attributed to isoleucine and valine. The thermal stability of papain was determined by evaluating numerous concentrations of papain against two SYPRO orange dye concentrations (5X and 10X). The observed raw fluorescence from the thermal shift run was used to calculate the derivative (dF/dT) and a plot of the derivative against temperature was constructed (Figure 3.9).

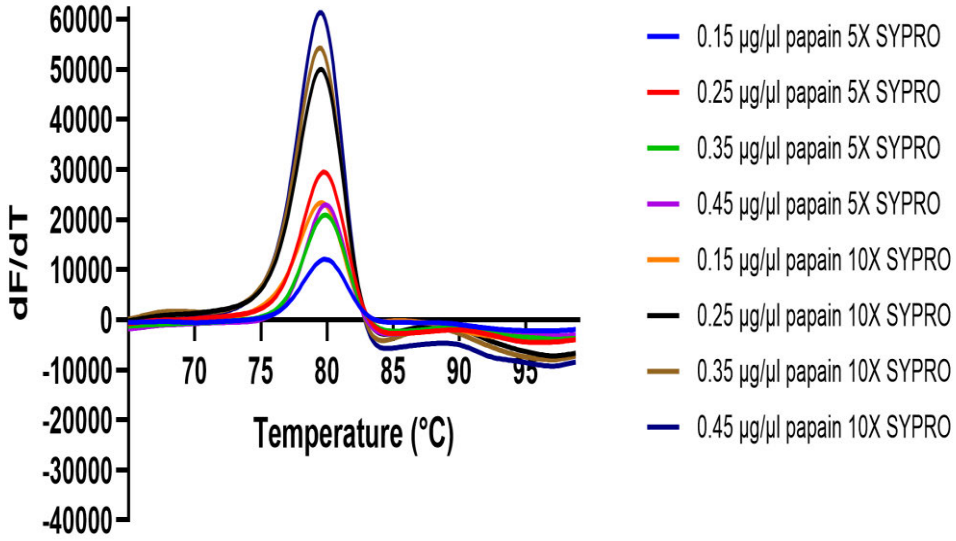

Figure 3.9. A representative thermal shift analysis obtained for different concentrations of papain under two concentrations of SYPRO orange dye. The melting temperature of papain was determined to be approximately 80℃ regardless of protein or dye concentration.

The hydrophobicity profile of papain proved adequate in deriving a melting temperature through the implementation of the TSA, more specifically, was compatible with the recommended dye (SYPRO orange) for the assay. The fluorescence signal intensity increased with an increase in papain protein concentration (Figure 3.9) when using 5X SYPRO orange. The same trend was followed when 10X SYPRO orange was used and the fluorescence signals obtained were higher compared to using 5X SYPRO orange. It was concluded that increasing protein and dye concentration resulted in higher fluorescence intensity but importantly did not affect the melting temperature derived for papain. The melting temperature of papain was determined to be 80℃ which concurred with the T_m previously derived through DSC (Sathish *et al.*, 2007).

3.5.2. Thermal shift assay optimisation for $McsB_{SA}$

The $McsB_{SA}$ purified protein samples were analysed *via* the thermal shift assay where a single concentration of the protein at 0.25 µg/µl was tested against 5X and 10X concentrations of SYPRO orange dye. The raw fluorescence observed from the thermal shift assay was transformed into the derivative (dF/dT) data and plotted against temperature as shown in Figure 3.10. The T_m (49.60±0.37℃) obtained for $McsB_{SA}$ when examined with 5X SYPRO orange dye was similar to the T_m (49.52±0.21℃) obtained when $McsB_{SA}$ was examined with 10X SYPRO orange dye (Table 3.2) as was the trend observed above for the control protein

papain. The obtained T_m for $McsB_{SA}$ is 9.1 ℃ higher than the T_m reported by Lu and co-workers (T_m of $McsB_{SA}$ = 40.50 ± 0.02℃)(Lu *et al.*, 2024).

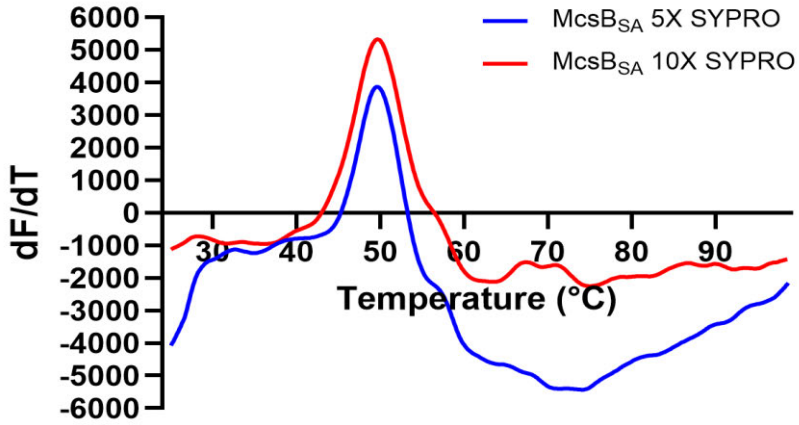

Figure 3.10. Thermal shift analysis for the purified protein $McsB_{SA}$ under various concentrations of SYPRO orange dye. The derivative (d/F/dT) was calculated from the raw fluorescence obtained and plotted against temperature (℃). The melting temperature obtained for $McsB_{SA}$ in the presence of 5X and 10X SYPRO orange dye was determined to be 49.60±0.37℃ (blue curve) and 49.52±0.21℃ (red curve) respectively (n≥3)

Table 3.2.: Derivative melting temperatures obtained for $McsB_{SA}$ when evaluating SYPRO orange dye concentration.

SYPRO Orange Concentration	Melting Point (℃ ± Standard Deviation)
5X	49.60±0.37
10X	49.52±0.21

A buffer library comprising ten different buffers with a pH range of 5 – 7.5 was screened against $McsB_{SA}$. The thermal stability of $McsB_{SA}$ was evaluated with each buffer *via* the TSA using 10X SYPRO orange dye. The raw fluorescence obtained from the TSA was analysed and the derivative (dF/dT) was calculated. The derivative was plotted against the temperature profile in Figure 3.11. A single T_m (T_m1) was obtained for $McsB_{SA}$ when evaluated with eight of the buffers (buffers 1-6, 8 and 10, Table 3.3, n=3). Two melting temperatures were observed for $McsB_{SA}$, T_m1 and T_m2 respectively, when evaluating buffer 7 and 9 (Table 3.3., n=3) which were supplemented with 2% (v/v) glycerol, 10 mM β-mercaptoethanol and 12 mM $MgCl_2$.

The derived T_m values were obtained from technical replicates utilizing a single expressed and purified $McsB_{SA}$ protein sample and thus accounts for the low standard deviation observed between the obtained melting temperatures (Table 3.3, n=3). The highest thermal stability for $McsB_{SA}$ (determined by T_m1 alone) was obtained when evaluated with sodium phosphate pH

7.4 (T_m1 = 49.73±0.21℃, represented by the purple line, Figure 3.11). This T_m1 for $McsB_{SA}$ was expected as it was derived in SYPRO dye optimisation assays using the same buffer (sodium phosphate, pH 7.4, buffer 6).

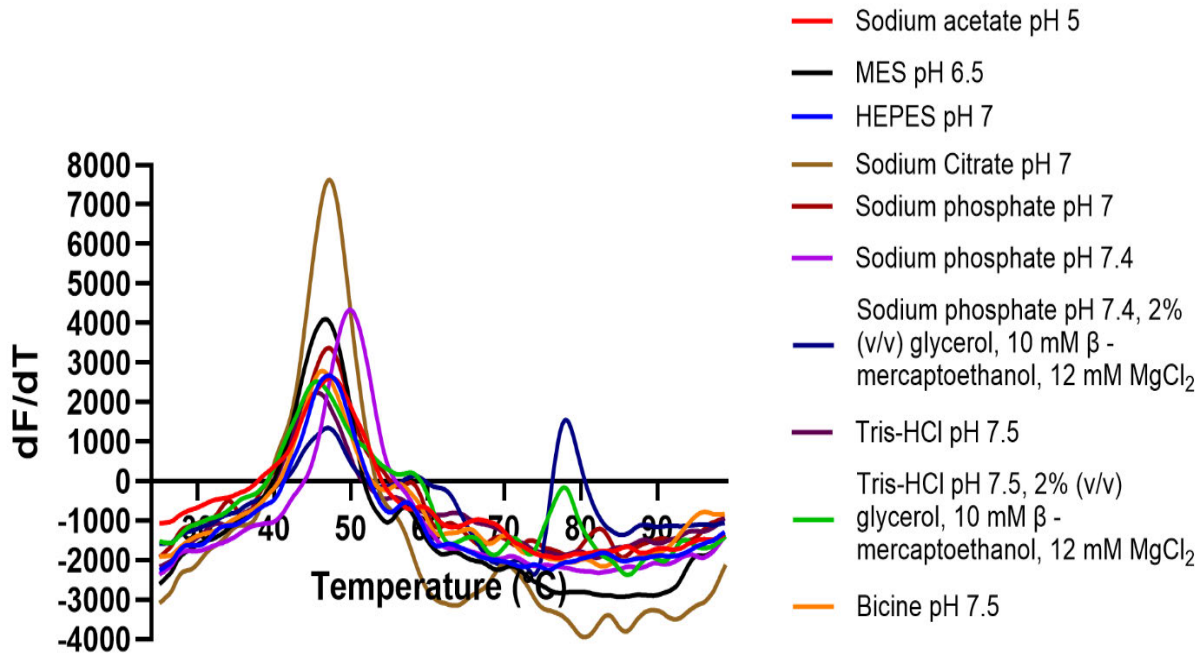

Figure 3.11. Thermal shift analysis obtained for $McsB_{SA}$ in the presence of various buffers. The derivative (dF/dT) was calculated from the raw fluorescence obtained and was plotted against the temperature (℃). A single melting temperature (T_m1) and a second melting temperature (T_m2) were observed under specific buffer conditions. The highest T_m1 was observed for $McsB_{SA}$ in the presence of sodium phosphate pH 7.4 (49.73 ± 0.21℃) (purple line) and the lowest T_m1 was observed for $McsB_{SA}$ in the presence of Tris-HCl pH 7.5 (45.35 ± 0.34℃) (dark purple line).

The T_m1 obtained for $McsB_{SA}$ in sodium phosphate, pH 7.4, was 4.38℃ higher than the T_m1 obtained for $McsB_{SA}$ when evaluated with Tris-HCl pH 7.5 (represented by the dark purple line, Figure 3.11). The sodium phosphate buffer supplemented with 2% (v/v) glycerol, 10 mM β-mercaptoethanol and 12 mM $MgCl_2$, pH 7.4 (represented by the dark blue line, Figure 3.11) also resulted in a higher thermal stability (for both T_m1 and T_m2) obtained for $McsB_{SA}$ as compared to the Tris-HCl buffer supplemented with 2% (v/v) glycerol, 10 mM β-mercaptoethanol and 12 mM $MgCl_2$ (represented by the green line, Figure 3.11) where there was a 1.09℃ difference observed for T_m1 and a 0.38℃ difference observed for T_m2. The melting temperatures obtained for $McsB_{SA}$ with each buffer is displayed in Table 3.3. Screening of $McsB_{SA}$ against the designed buffer library suggested that $McsB_{SA}$ favoured a slightly basic pH of 7.4 as thermal stability was reduced under acidic pH conditions (Table 3.3.). Interestingly, the thermal stability was reduced when the pH increased to 7.5 as indicated by the T_m1 obtained for $McsB_{SA}$ with buffers 8-10. The arginine kinase also had the lowest thermal stability in the presence of Tris-HCl buffers (45.35 ± 0.34 and 45.76 ± 0.20 for buffers

8 and 9 respectively) as a higher melting temperature (T_m1) was observed for $McsB_{SA}$ using bicine buffer at the same pH of 7.5. The reduced T_m1 obtained for $McsB_{SA}$ in the presence of Tris-HCl was also reported by Lu and co-workers as they derived the T_m of $McsB_{SA}$ to be 40.50±0.02℃ using a gel filtration buffer [20 mM Tris-HCl, 300mM NaCl and 1 mM Tris(2-carboxyethyl)phosphine (TCEP), pH 7.5] (Lu *et al.*, 2024).

Table 3.3.: Derivative melting temperatures obtained for $McsB_{SA}$ screened against a buffer library.

No.	Buffer	Melting Point 1 (℃ ± Std Dev[a])	Melting Point 2 (℃ ± Std Dev[a])
1	Sodium acetate pH 5.0	47.46 ± 0.07	NA
2	MES pH 6.5	46.48 ± 0.20	NA
3	HEPES pH 7.0	47.15 ± 0.10	NA
4	Sodium citrate pH 7.0	47.22 ± 0.00	NA
5	Sodium phosphate pH 7.0	47.07 ± 0.00	NA
6	Sodium phosphate pH 7.4	49.73 ± 0.21	NA
7	Sodium phosphate, 2% (v/v) glycerol, 10 mM β-mercaptoethanol, 12 mM $MgCl_2$, pH 7.4	46.85 ± 0.10	78.32 ± 0.41
8	Tris-HCl pH 7.5	45.35 ± 0.34	NA
9	Tris-HCl, 2% (v/v) glycerol, 10 mM β-mercaptoethanol, 12 mM $MgCl_2$, pH 7.5	45.76 ± 0.20	77.94 ± 0.01
10	Bicine pH 7.5	46.20 ± 0.21	NA

[a] Standard deviation

3.5.3. Optimisation of the cellular thermal shift assay (CETSA)

The initial CETSA protocol was evaluated as previously described (Hart *et al.*, 2019). The initial protocol proved inadequate due to the inconsistency observed in $McsB_{SA}$ solubility (Figure 3.12.). This inconsistency inhibited the establishment of an aggregation temperature for $McsB_{SA}$.

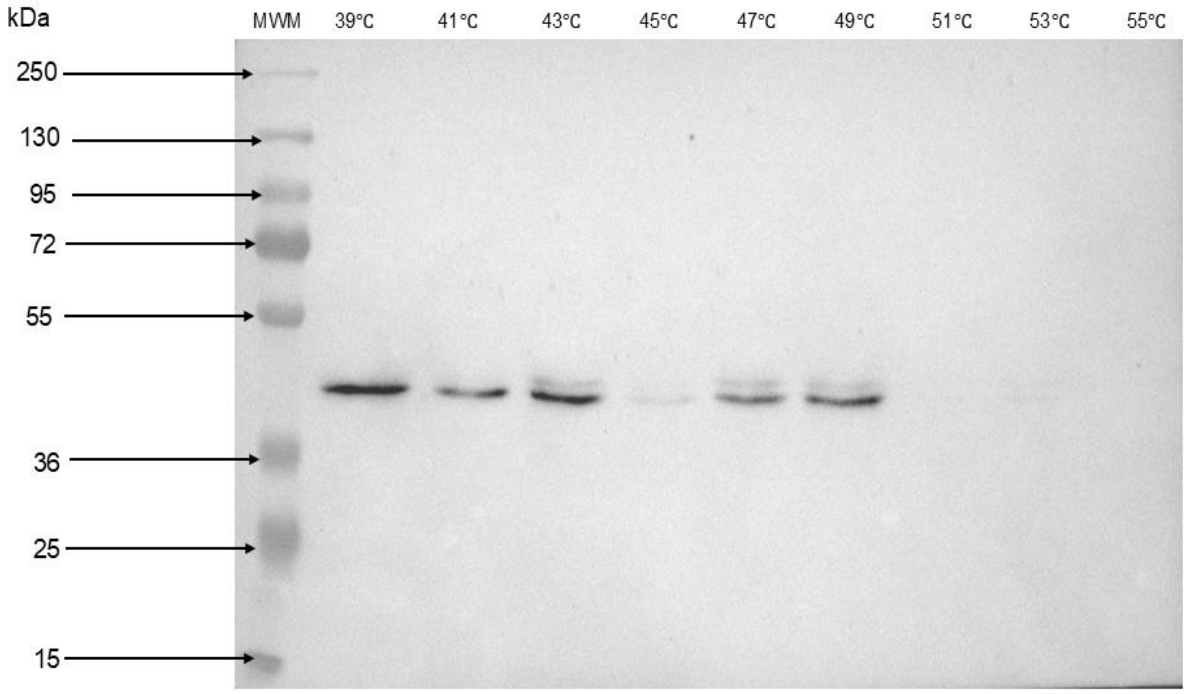

Figure 3.12. A representative western blot for a cellular thermal shift assay (CETSA) performed on $McsB_{SA}$. The resulting western blot from the CETSA of $McsB_{SA}$. The Spectra™ Multicolour Broad Range Protein Ladder was loaded into the lane marked MWM (molecular weight marker) and samples exposed to the 39℃, 41℃, 43℃, 45℃, 47℃, 49℃, 51℃, 53℃ and 55℃ temperatures were loaded in the corresponding marked lanes. The membrane was probed with 6x-His tag monoclonal antibody (HIS.H8)[cat#: MA1-21315, RRID: AB_557403, Thermo Fisher Scientific, USA) overnight at 4℃, washed with TBS (three times) and incubated with horseradish peroxidase enzyme (HRP)-conjugated secondary antibody [Pierce® goat anti-mouse IgG, (H + L), HRP conjugate, cat#: 31430, Thermo Fisher Scientific, USA] for one hour at room temperature.

The CETSA protocol was amended to account for the inconsistency observed in the intensities of detected $McsB_{SA}$. The issue was resolved by preparing a single soluble fraction of $McsB_{SA}$ after expression and aliquoting the same volume into separate tubes to ensure the concentration of soluble $McsB_{SA}$ was constant. The temperature range was also optimised, and temperatures were tested from 47-55℃ (in 1℃ increments). A representative western blot for the amended CETSA of $McsB_{SA}$ is shown in Figure 3.13 which clearly shows a decreased band intensity from 47℃ to 55℃. The assay was repeated to obtain n=3 where each assay was independently conducted from $McsB_{SA}$ expression to CETSA assaying and culminated in the detection of $McsB_{SA}$ utilising 6x-His tag monoclonal antibody(HIS.H8) [cat#: MA1-21315, RRID: AB_557403, Thermo Fisher Scientific, USA) and horseradish peroxidase enzyme (HRP)-conjugated secondary antibody [Pierce® goat anti-mouse IgG, (H + L), HRP conjugate, cat#: 31430, Thermo Fisher Scientific, USA].

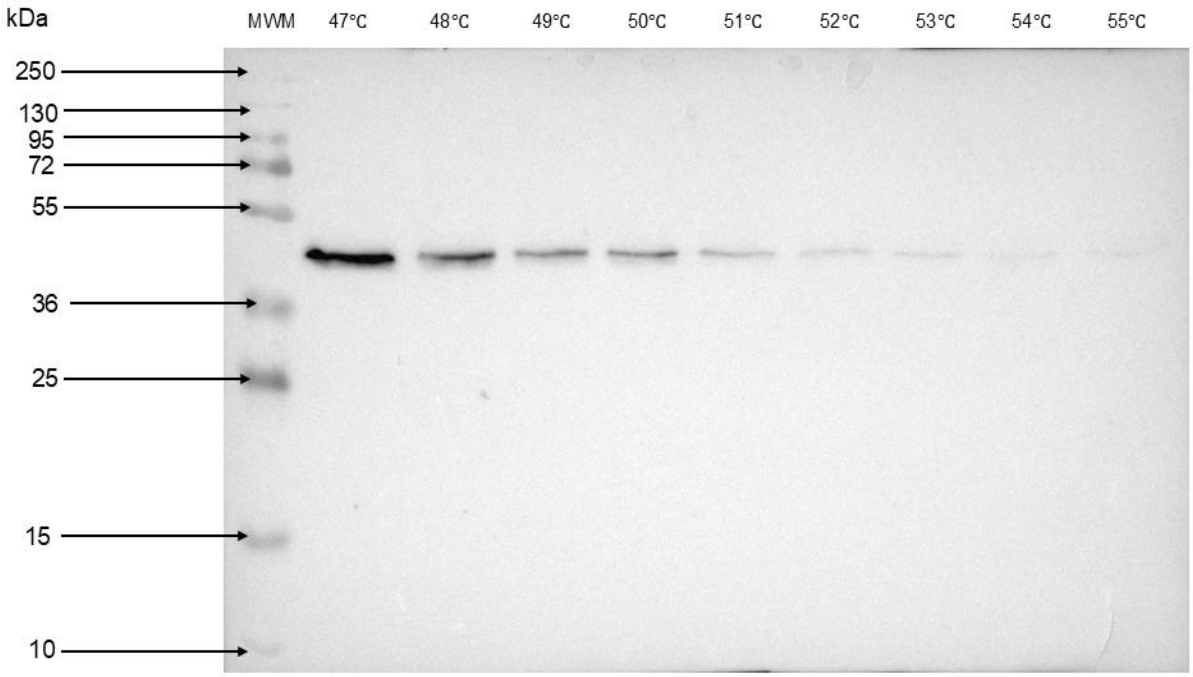

Figure 3.13. A representative western blot for a cellular thermal shift assay (CETSA) performed on $McsB_{SA}$ with an optimal protocol for aggregation temperature evaluation. The CETSA protocol was amended to evaluate the aggregation temperature (T_{agg}) for $McsB_{SA}$. The Spectra™ Multicolour Broad Range Protein Ladder was loaded into the lane marked MWM (molecular weight marker) and samples exposed to the 47-55℃ temperature range were loaded in the corresponding marked lanes. The membrane was probed with 6x-His tag monoclonal antibody (HIS.H8)[cat#: MA1-21315, RRID: AB_557403, Thermo Fisher Scientific, USA) and horseradish peroxidase enzyme (HRP)-conjugated secondary antibody [Pierce® goat anti-mouse IgG, (H + L), HRP conjugate, cat#: 31430, Thermo Fisher Scientific, USA].

The captured blots from the CETSA of $McsB_{SA}$ were analysed using ImageJ software to determine the relative band intensities of the detected protein. The relevant band intensities were normalised by setting the highest band intensity as 100% (For Figure 3.13, the band detected at 47℃) and the lowest band intensity as 0% (For Figure 3.13, the band detected at 55℃). The normalised data was transferred to GraphPad Prism (software version 10.4) and Boltzmann sigmoidal non-linear regression analysis was performed on the dataset (Figure 3.14). The T_{agg} for $McsB_{SA}$ was determined to be 48.28±0.18℃ which was the temperature at which 50% of the protein had aggregated. The T_{agg} of $McsB_{SA}$ was slightly lower than the derived T_m of 49.73 ± 0.21 (when evaluated in sodium phosphate, pH 7.4). The T_{max} was delineated as the maximum temperature at which $McsB_{SA}$ detection was possible (and a band intensity could be measured by the ImageJ software) and was determined to be 53℃ for the reference blot in Figure 3.13. To our knowledge, this is the first reported aggregation temperature for any orthologue of McsB and more specifically the first reported T_{agg} for $McsB_{SA}$.

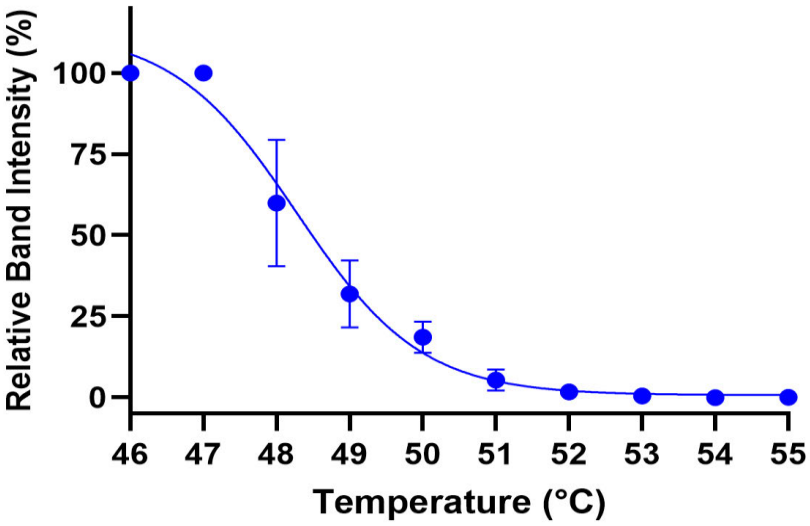

Figure 3.14. Cellular thermal shift analysis for $McsB_{SA}$. The relative band intensities obtained were normalised (by setting the highest intensity for each data set as 100% and setting the lowest intensity for each data set as 0%) and a Boltzmann sigmoidal non-linear regression was performed using GraphPad Prism (software version 10.4) to generate a sigmoidal curve. The mean relative band intensities are plotted with the error bars representing the standard deviation. The aggregation temperature for $McsB_{SA}$ was determined to be 48.28 ± 0.18℃ (n=3).

3.5.4. Evaluation of the cellular thermal shift assay to detect ligand binding of $McsB_{SA}$

The N-terminally acetylated CtsR-derived sequence, Ac-KRGGGGYIKIIKV-OH peptide designed by Suskiewicz and co-workers (Suskiewicz *et al.*, 2019) was synthesised in-house (Discipline of Chemistry, University of KwaZulu-Natal) and evaluated against $McsB_{SA}$. $McsB_{GS}$ was previously shown to phosphorylate the peptide thus suggesting that $McsB_{GS}$ could detect the arginine residue present in the peptide (Suskiewicz *et al.*, 2019). The T_{agg} of $McsB_{SA}$ was evaluated through the CETSA after incubation with 100 µm of the Ac-KRGGGGYIKIIKV-OH peptide at 4℃ for 24 hours. A representative western blot captured (Figure 3.15) was analysed using ImageJ software to measure the relative band intensities detected from 47-55℃. The data was normalised as described above and Boltzmann sigmoidal non-linear regression analysis was performed using GraphPad Prism (software version 10.4). The sigmoidal plot of $McsB_{SA}$ with 100 µM peptide was compared to the sigmoidal plot for $McsB_{SA}$ alone (Data from Figure 3.14) and a significant increase in T_{agg} of 1.13±0.09℃ was delineated for $McsB_{SA}$ evaluated with the peptide (Figure 3.16). This suggested that $McsB_{SA}$ could detect the N-terminally acetylated CtsR-derived sequence, Ac-KRGGGGYIKIIKV-OH peptide in an endogenous environment and confirmed the CETSA's efficacy to monitor ligand binding through changes in T_{agg} of $McsB_{SA}$.

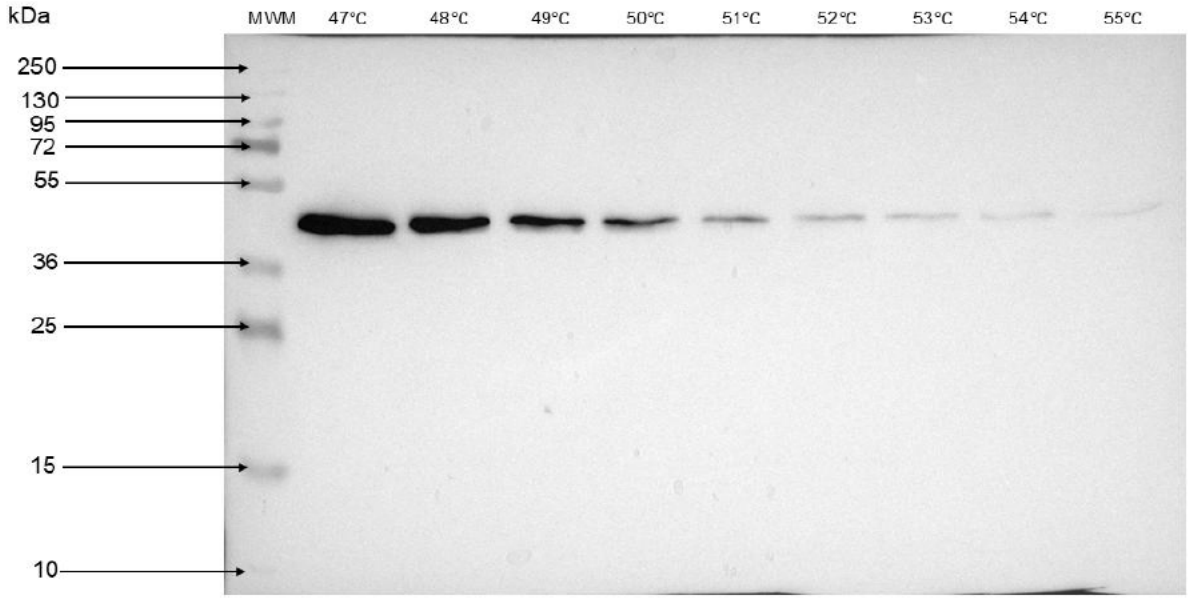

Figure 3.15. A representative western blot for a cellular thermal shift assay (CETSA) performed on $McsB_{SA}$ after a 24-hour incubation with 100 µM of the Ac-KRGGGGYIKIIKV-OH peptide. The CETSA protocol was amended to evaluate the aggregation temperature (T_{agg}) for $McsB_{SA}$ after a 24-hour incubation with 100µM peptide. The nitrocellulose membrane was probed with 6x-His tag monoclonal antibody (HIS.H8)[cat#: MA1-21315, RRID: AB_557403, Thermo Fisher Scientific, USA) and horseradish peroxidase enzyme (HRP)-conjugated secondary antibody [Pierce® goat anti-mouse IgG, (H + L), HRP conjugate, cat#: 31430, Thermo Fisher Scientific, USA].

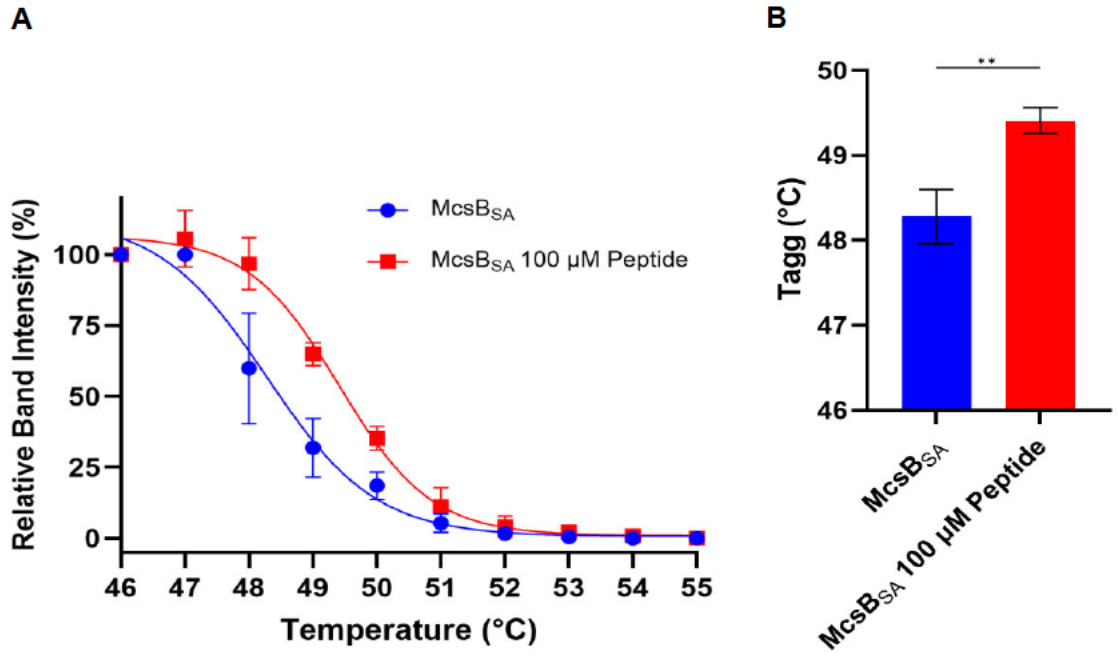

Figure 3.16. Cellular thermal shift analysis for the $McsB_{SA}$ alone and for $McsB_{SA}$ with 100µM peptide. (A) The relative band intensities obtained were normalised (by setting the highest intensity for each data set as 100% and setting the lowest intensity for each data set as 0%) and a non-linear regression was performed using GraphPad Prism (software version 10.4) to generate a sigmoidal curve. (B) The mean ± standard error (SE) aggregation temperature (T_{agg}) calculated from the sigmoidal curves were analysed (n = 3). Statistical analysis was performed using Student's t-test, *p<0.05, **p<0.01, ***p<0.001, ns: not significant (α = 0.05, CI 95%).

3.6. Pandemic Response Box Screening

3.6.1. Identification of novel $McsB_{SA}$ ligands through thermal shift analysis

$McsB_{SA}$ was screened against the Pandemic Response Box of compounds and the T_m of $McsB_{SA}$ was determined *via* the TSA. The initial screening was performed by dividing the 400 compounds into 40 cocktails with each cocktail containing 10 compounds at 10 µM. Sodium phosphate buffer, Ph 7.4 was selected for the screen as $McsB_{SA}$ had the highest T_m when assessed with this buffer during optimisation experiments. The Pandemic Response Box comprised of five plates (plate A -E, with each plate containing 80 compounds) and eight cocktails were generated per plate. The T_m obtained for $McsB_{SA}$ when incubated with each cocktail was compared to the T_m obtained for the DMSO control (10% DMSO, represented by the blue diamond in Figure 3.17) which was determined to be 54.47℃. The T_m obtained for $McsB_{SA}$ containing 10% DMSO (2 µl in a total reaction volume of 20 µl) was assessed to be 4.74℃ higher than the T_m obtained for $McsB_{SA}$ with sodium phosphate pH 7.4 (49.73 ± 0.21, Table 3.3.).

Thermal shift analysis conducted on the screening of the 40 cocktails revealed that 29 out of the 40 cocktails when incubated with $McsB_{SA}$ induced an increase in $McsB_{SA}$ T_m as compared to the DMSO control sample whereas 11 of the 40 cocktails (cocktails B1, B2, B3, C5, C6, C7, C8, D1, D2, D7 and D8) when incubated with $McsB_{SA}$ destabilized $McsB_{SA}$ as evident by the decrease in T_m compared to the DMSO control sample as observed in Figure 3.17 (The points which fall above and below the black line respectively). This decrease in T_m, in comparison to the protein without any ligand, has previously been attributed to compounds binding to the protein in the unfolded state as opposed to the native state and thus result in a decreased T_m (Waldron and Murphy, 2003, Cimmperman *et al.*, 2008). The observed increase in the T_m of $McsB_{SA}$ induced by >70% of the designed cocktails was unexpected and would suggest that the compounds present in the cocktails demonstrated an additive or synergistic effect when combined. An induced increase in the T_m of $McsB_{SA}$ (≤ 8℃) was detected for 25 of the cocktails (represented by the points which fall in the area between the black and red line, Figure 3.17) and four of the cocktails caused the T_m of $McsB_{SA}$ to increase by ≥ 8℃ (represented by the points above the red line, Figure 3.17). These four cocktails (cocktail A1, B4, C3 and E3) were selected for further evaluation to identify potential $McsB_{SA}$ ligands as they induced the greatest increases in $McsB_{SA}$ T_m.

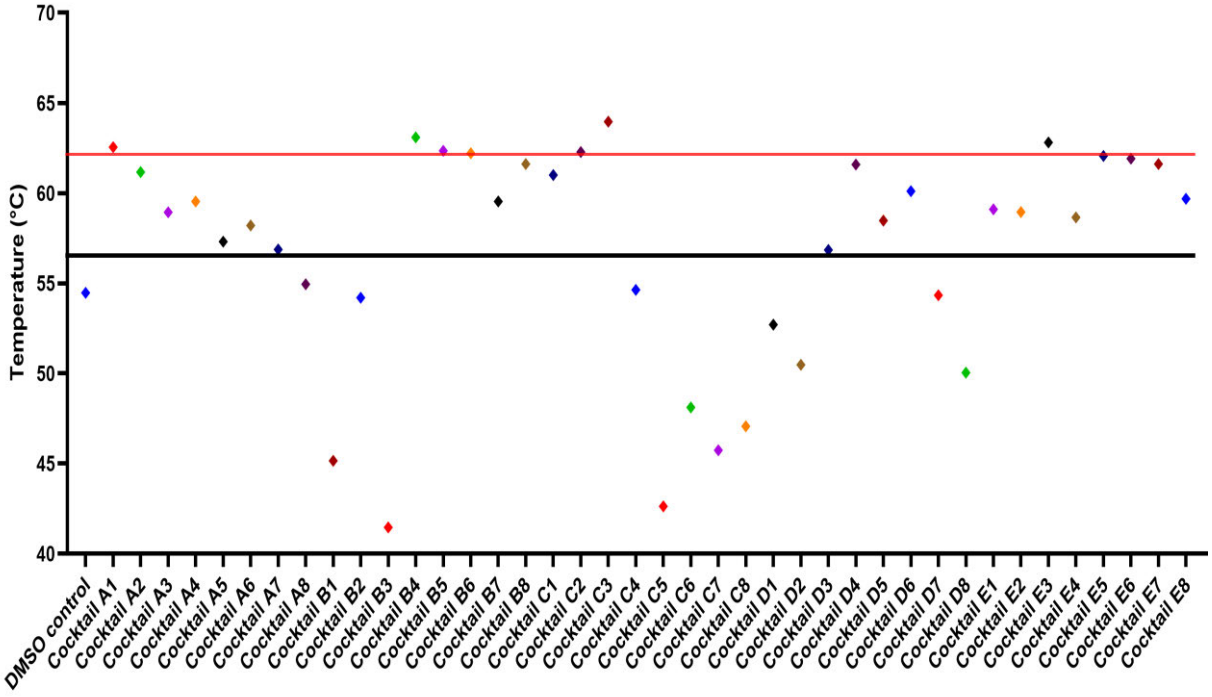

Figure 3.17. The derivative melting temperature (T_m) obtained for $McsB_{SA}$ when incubated with each cocktail overnight at 4℃. The melting temperatures of $McsB_{SA}$ which fall below 54.47℃ (as indicated as the area underneath the black line) represent the cocktails which did not cause an increase the melting temperature of $McsB_{SA}$. The area between the red and black line represents the cocktails which induced an increase in the melting temperature of $McsB_{SA}$ when compared to $McsB_{SA}$ in the presence of a 10% DMSO control and the four cocktails found above the red line, which were cocktails A1, B4, C3 and E3, induced an increase in the T_m of $McsB_{SA}$ >8℃.

First, compounds present in cocktail A1 were assessed individually (at 10µM) as potential $McsB_{SA}$ ligands. Interestingly, none of the ten compounds induced an increase in the T_m of $McsB_{SA}$ even though cocktail A1 caused an increase in T_m (>8℃) which further supported the compounds exhibiting an additive/synergistic effect when grouped. Cocktail A1 was further divided into cocktails A1.1 (containing compounds A1-A5) and cocktail A1.2 (containing compounds A6-A10) and thermal shift analysis conducted revealed that cocktail A1.1 caused an increase in the T_m of $McsB_{SA}$ (8.173±0.43, $p<0.0001$, Figure 3.18) whereas cocktail A1.2 caused a decrease in the T_m of $McsB_{SA}$ (3.91±0.67, Figure 3.18) which suggested that the induced increase in T_m by cocktail A1 was due to the additive/synergistic effects of compounds A1-A5 (compounds MMV1634492, MMV002731, MMV003143, MMV1578560, and MMV1782223). These five compounds were tested in pairs, and a distinct pattern of stabilization could not be delineated, however it was observed that a combination of compounds MMV1634492 with MMV002731, MMV003143 with MMV1578560, and MMV1578560 with MMV1782223 induced an increase in the T_m of $McsB_{SA}$ [1.483±0.25℃

(p<0.01), 1.96±0.23℃ (p<0.0001) and 1.97±0.33℃ (p<0.0001) respectively]. These observations provide further evidence of a synergistic/additive effect existing between compounds when grouped.

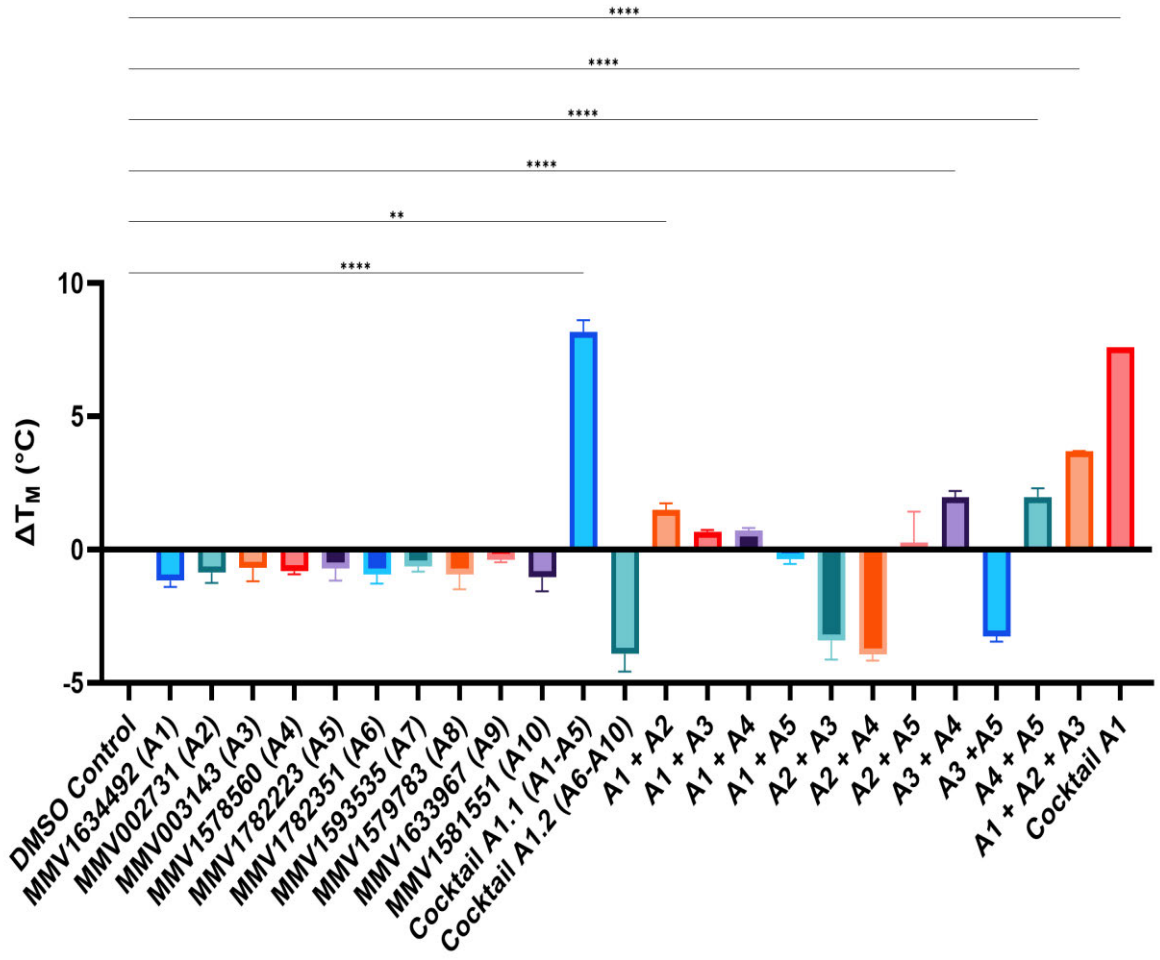

Figure 3.18. The change in the derivative melting temperature (ΔT_m) obtained for $McsB_{SA}$ when incubated with compounds from cocktail A1. The ΔT_m was calculated by selecting the DMSO control T_m as the reference T_m**.** Statistical analysis was performed using a one-way ANOVA. *p<0.05, **p<0.01, ***p<0.001 and ****p<0.0001 (α=0.05, CI 95%).

The remaining three cocktails identified from the screening of the Pandemic Response Box were further evaluated by testing each compound present in cocktails B4, C3 and E3 individually at 10 µM. Thermal shift analysis of the 30 compounds present in the cocktails was conducted to assess the effect on the T_m of $McsB_{SA}$ (Figure 3.19). Nine compounds were identified to induce an increase in the T_m of $McsB_{SA}$ when compared to the DMSO control (1% DMSO) whereby the T_m of $McsB_{SA}$ was derived to be 47.10 ± 0.21℃ (Figure 3.19 and 3.20). The compound MMV1593539 (present in cocktail B4) caused an increase in the T_m of $McsB_{SA}$

by 1.19℃ ($p<0.001$) and was the highest shift obtained for $McsB_{SA}$ for each of the 30 compounds evaluated (Figure 3.20).

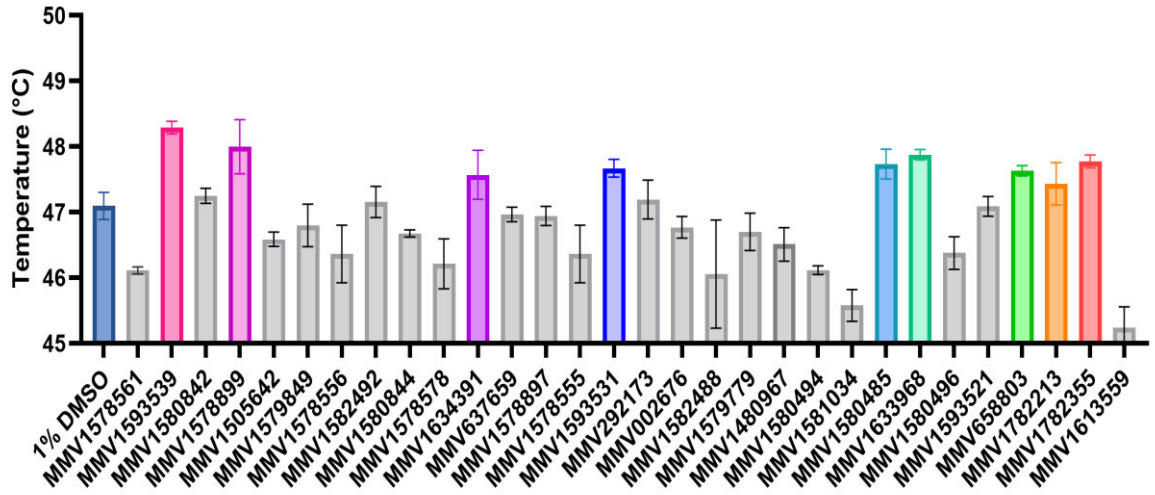

Figure 3.19. The thermal derivative melting temperatures obtained for $McsB_{SA}$ when incubated with individual compounds from cocktails B4, C3 and E3 of the Pandemic Response Box of compounds. The nine compounds which resulted in the largest increase in the T_m of $McsB_{SA}$ are represented in various colours whilst those compounds which did not induce an increase in $McsB_{SA}$ T_m are displayed in grey and the T_m of $McsB_{SA}$ with 1% DMSO is represented in dark blue (n=3).

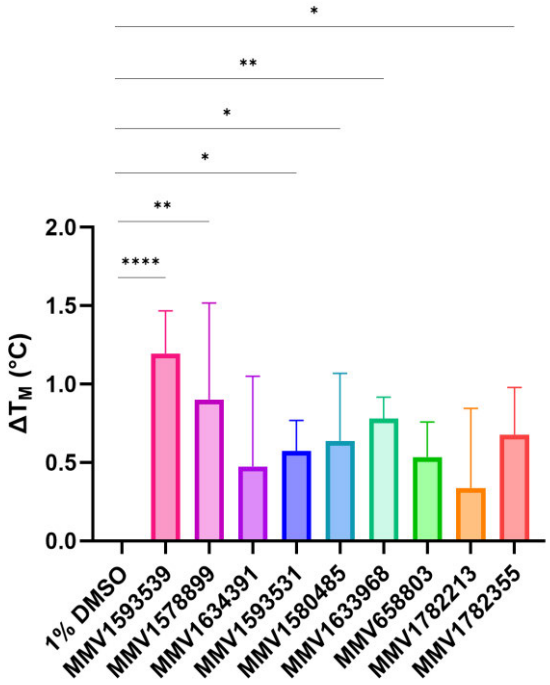

Figure 3.20. The change in melting temperature (ΔT_m) of $McsB_{SA}$ induced by the nine identified compounds from cocktails B4, C3 and E3. The ΔT_m obtained for $McsB_{SA}$ when incubated with each compound was established through comparisons to the melting temperature obtained for $McsB_{SA}$ with 1% DMSO (n=3). Statistical analysis was performed using a one-way ANOVA. *p<0.05, **p<0.01, ***p<0.001 and ****p<0.0001 (α=0.05, CI 95%).

The nine identified hits detected from the cocktail screening were further evaluated at 5 µM and 20 µM to determine if there were any dose response effects observed. The change in T_m observed was plotted against the concentration of compound tested (Figure 3.21). Each of the compounds induced non-significant shifts in the T_m ($p>0.05$) of $McsB_{SA}$ when evaluated at 5 µM (Figure 3.21.A) which indicated that a ligand concentration of 5 µM was not optimal when evaluating the T_m of $McsB_{SA}$ at 0.25 µg/µl. Compounds MMV1578899, MMV1634391, and MMV658803 did not induce significant shifts in T_m ($p>0.05$) at 20 µM however compound MMV1578899 did induce a significant shift ($p<0.01$) at 10 µM (Figure 3.20) which suggested that the compound may be poorly soluble. The compound MMV1593539 induced the greatest increase in T_m at each concentration which indicated that this compound may be the best binder out of the nine detected ligands.

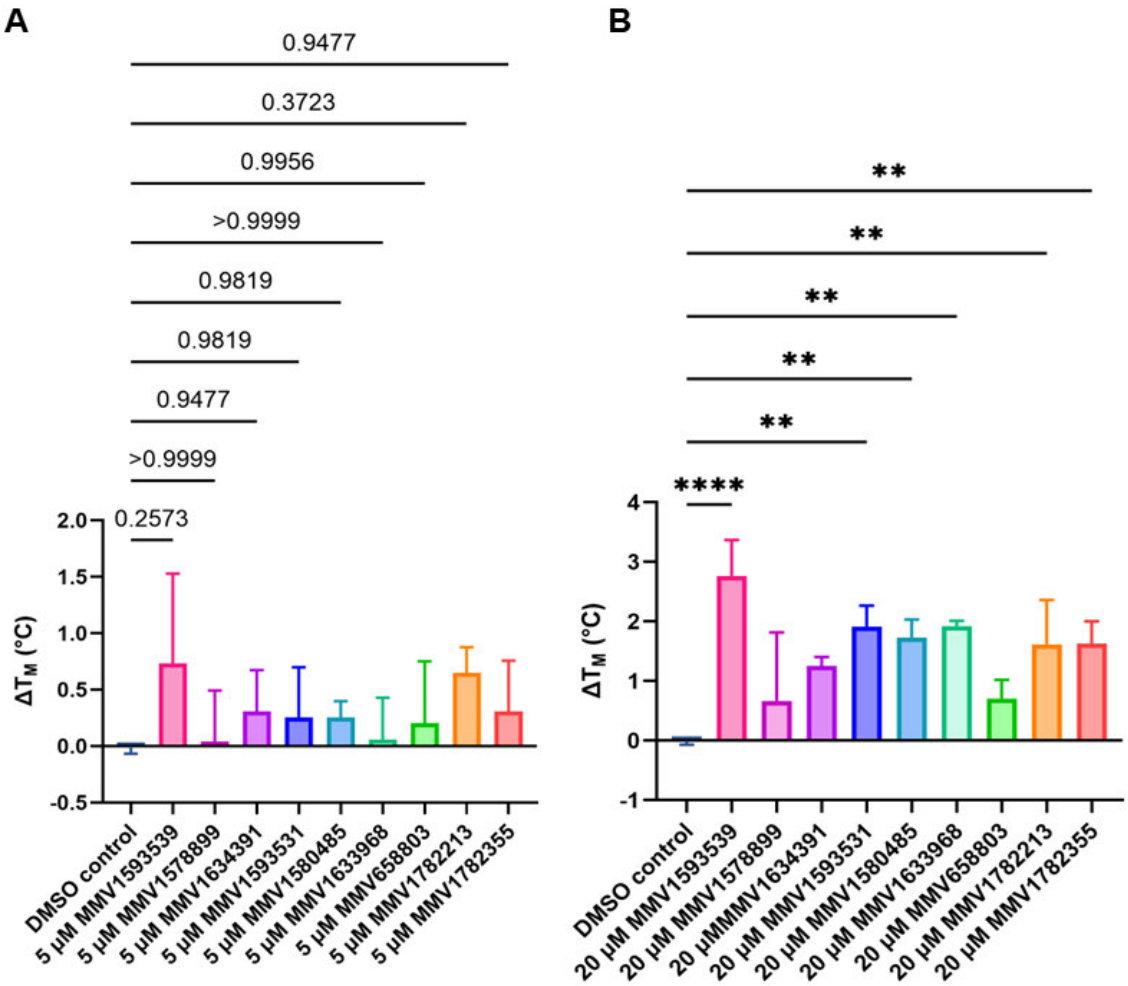

Figure 3.21. The effect of increasing ligand concentration of the nine identified compounds against the melting temperature (T_m) of $McsB_{SA}$. The changes in melting temperature obtained for $McsB_{SA}$ when incubated with each compound (A) at 5 µM, and (B) at 20 µM was compared to the melting temperature obtained for $McsB_{SA}$ (DMSO control, 0.5% for 5 µM and 2% for 10 µM) (n=3). Statistical analysis was performed using a one-way ANOVA. *p<0.05, **p<0.01, ***p<0.001 and ****p<0.0001 (α=0.05, CI 95%).

A dose response effect was detected for each of the identified compounds except for compounds MMV1578899 and MMV1782213 (Figure 3.22.). Although compound MMV1782213 did induce a significant shift at 20 µM which was similar to that of compound MMV1782355. The dose response effects instigated by the compounds further validate their binding to $McsB_{SA}$ as novel $McsB_{SA}$ ligands. The compound MMV1593539 displayed a significant dose response from 10µM ($p<0.05$) which indicated that the compound displayed good solubility and was determined to be the best identified binder.

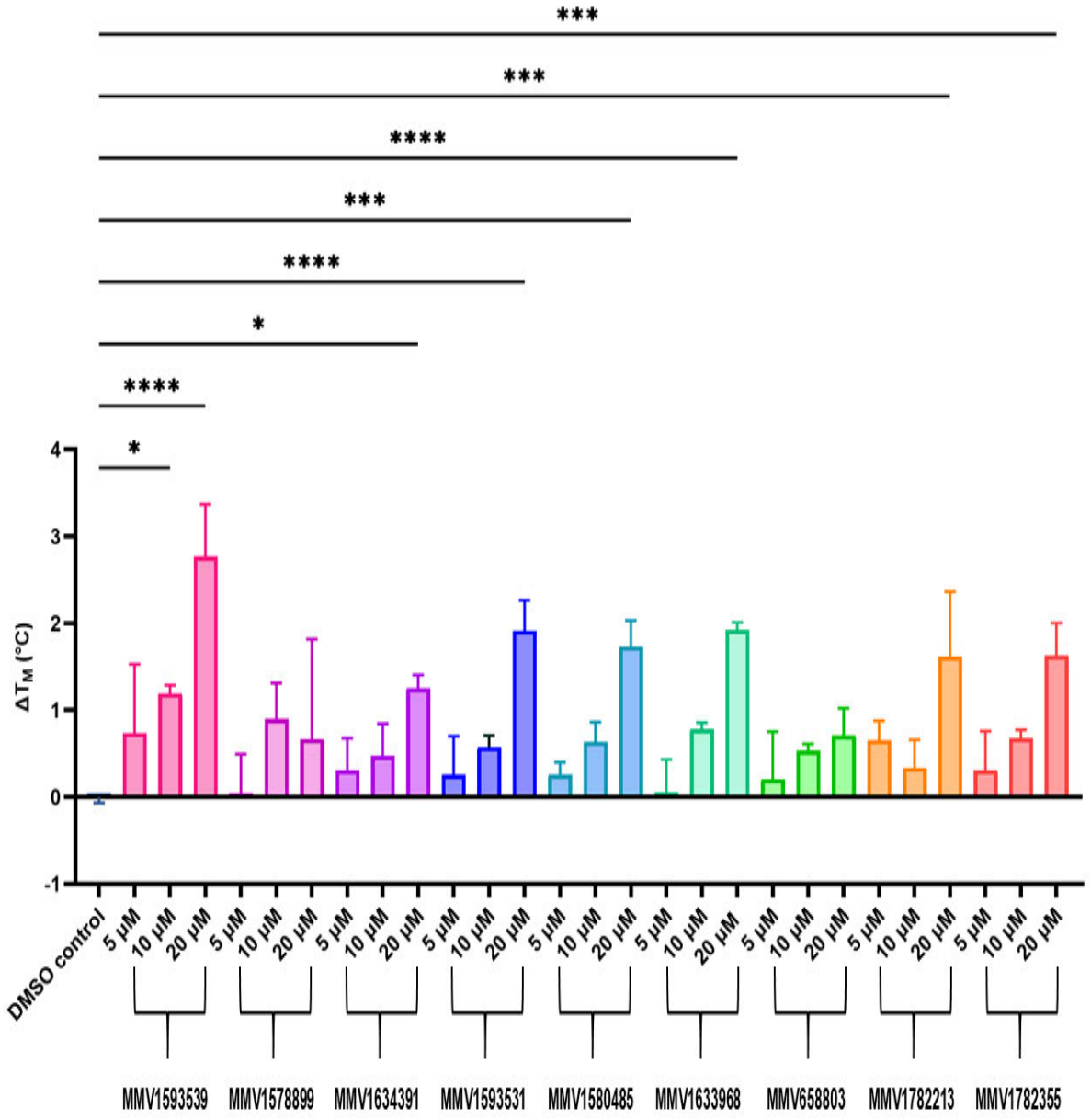

Figure 3.22. The observed dose response effect of increasing ligand concentration on melting temperature (T_m) of $McsB_{SA}$. The changes in melting temperature obtained for $McsB_{SA}$ when incubated with each compound at increasing concentrations (5-20 µM) was compared to the melting temperature obtained for $McsB_{SA}$ (DMSO control) (n=3). Statistical analysis was performed using a one-way ANOVA. *p<0.05, **p<0.01, ***p<0.001 and ****p<0.0001 (α=0.05, CI 95%).

3.6.2. Validation of identified novel $McsB_{SA}$ ligands *via* the cellular thermal shift assay

The CETSA was performed to further investigate the binding efficacy of the nine compounds (compounds MMV1593539, MMV1578899, MMV1634391, MMV1593531, MMV1580485, MMV1633968, MMV658803, MMV1782213 and MMV1782355) identified as McsB ligands through the TSA screen. A representative western blot captured for $McsB_{SA}$ incubated overnight with 1% DMSO as a control (loaded with samples prepared over a temperature range of 43℃ - 56℃, with 1℃ increments) and detected with anti-HIS primary antibody is shown in Figure 3.23. A 42 kDa band was detected (approximately the same molecular weight as recombinantly expressed $McsB_{SA}$). The most intense band was observed at 43℃ and decreased in intensity as the temperature increased until the band became undetectable at temperatures above 50℃. The T_{agg} and T_{max} of $McsB_{SA}$ derived from the reference blot were 46.50℃ and 50℃ respectively which was lower than derived values for $McsB_{SA}$ alone thus suggesting DMSO caused a reduction in both T_{agg} and T_{max} of $McsB_{SA}$.

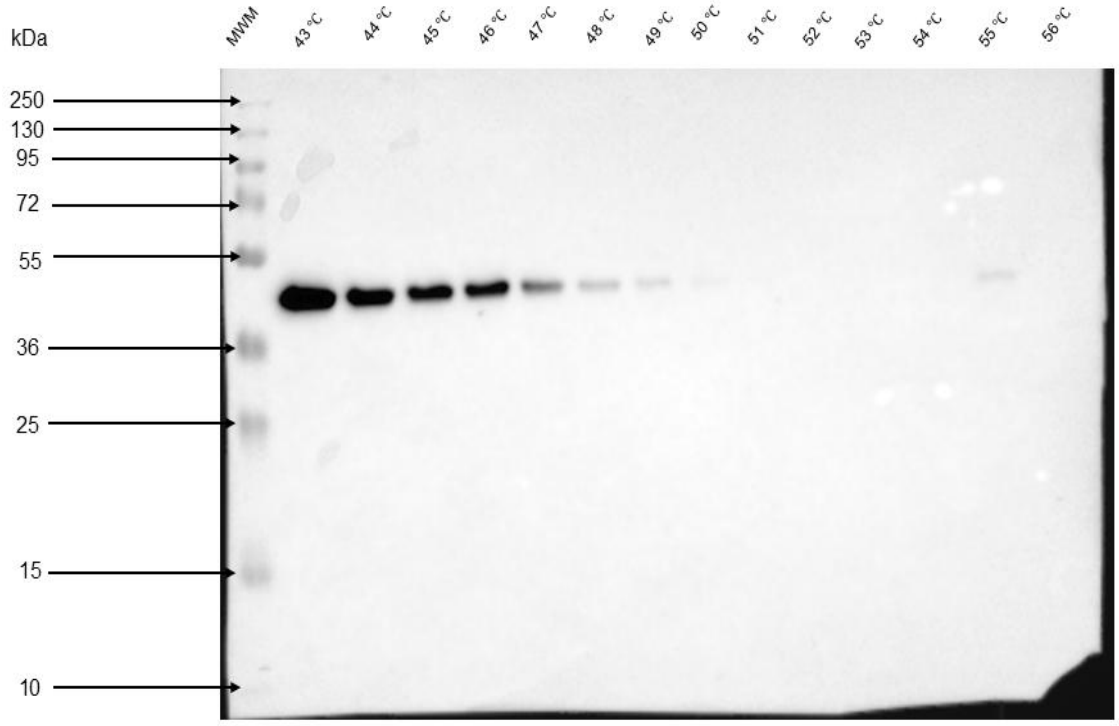

Figure 3.23. A representative western blot for a cellular thermal shift assay performed on $McsB_{SA}$ when incubated with 1% DMSO overnight. $McsB_{SA}$ samples incubated with 1% DMSO were aliquoted and exposed to different temperatures (43℃ -56℃, 1℃ increments). The samples were analysed via SDS-PAGE and transferred onto a nitrocellulose membrane. A single protein band of approximately 42 kDa (the approximate molecular weight for recombinantly expressed $McsB_{SA}$) was detected at each temperature point using 6x-His tag monoclonal antibody (HIS.H8)[cat#: MA1-21315, RRID: AB_557403, Thermo Fisher Scientific, USA) and horseradish peroxidase enzyme (HRP)-conjugated secondary antibody [Pierce® goat anti-mouse IgG, (H + L), HRP conjugate, cat#: 31430, Thermo Fisher Scientific, USA].

The protocol utilized for the representative CETSA assay was employed for evaluation of the nine compounds. The captured western blots from these CETSA assays are displayed as Figure 3.24. A single band of approximately 42 kDa (the expected molecular weight of recombinantly expressed $McsB_{SA}$) was detected for each of the captured western blots in Figure 3.24. The band detected at 43℃ was the most intense band observed for each blot. The general trend observed amongst each of the captured western blots was a decrease in band intensity as the temperature increased which was expected as this allowed for the T_{agg} to be calculated. $McsB_{SA}$ melt profiles were generated through CETSA analysis of the captured western blots. These melt profiles were generated by measuring the relative band intensities of each band and normalizing the intensities for each data set by defining the highest band intensity as 100% and the lowest band intensity as 0% and plotting these intensities against the corresponding temperature (℃) (Figure 3.25.A). The T_{agg} for each $McsB_{SA}$ sample was determined from these sigmoidal curves and was compared to the T_{agg} of the DMSO control sample (Figure 3.25.B)

A T_{agg} of 46.5 ± 0.11℃ was observed for the $McsB_{SA}$ DMSO control sample similar to the determined T_m (47.10 ± 0.21℃) of the $McsB_{SA}$ 1% DMSO control sample from the TSA screen evaluating cocktails A1, B4, C3 and E3 (Figure 3.19). The T_{agg} was lower than the T_m of the $McsB_{SA}$ 1% DMSO control sample, as previously observed between the T_{agg} and T_m of $McsB_{SA}$ alone. The T_{agg} of $McsB_{SA}$ when incubated with compound MMV1593539 was observed to be 47.8 ± 0.16℃ which is 1.3℃ higher than the T_{agg} observed for the $McsB_{SA}$ control ($p<0.001$). The T_{agg} difference observed was similar to the 1.19℃ difference ($p<0.001$) in T_m induced by compound MMV1593539 through the TSA. Incubation of $McsB_{SA}$ with compounds MMV1593531 and MMV1633968 resulted in aggregation temperatures significantly lower than the T_{agg} observed for the control (45.94 ± 0.26 and 45.84 ± 0.32 ℃ respectively, $p<0.05$). A decrease in the T_{agg} of $McsB_{SA}$ was also observed when incubated with compounds MMV1580485 and MMV658803 [46.26 ± 0.62℃ ($p>0.05$) and 45.85 ± 0.40℃ ($p>0.05$)] however this decrease was non-significant for both compounds (Figure 3.25). The remaining four compounds significantly increased the T_{agg} of $McsB_{SA}$ with compound MMV1578899 resulting in a 0.78℃ increase ($p<0.05$), compound MMV1634391 inducing in a 0.78℃ increase ($p<0.001$), compound MMV1782213 causing a 0.63℃ increase ($p<0.05$) and compound MMV1782355 resulting in 0.95℃ increase ($p<0.01$). Compounds MMV1634391 and MMV1782213 induced non-significant increases in the T_m of $McsB_{SA}$ when screened at 5 and 10 µM however caused significant increases in the T_{agg} thus suggesting that these ligands bind $McsB_{SA}$ in an endogenous environment. Conversely, compound MMV1580485 caused a

significant increase in the T_m of $McsB_{SA}$ (0.63 ± 0.43°C, $p<0.05$), but induced a non-significant decrease in the T_{agg} of $McsB_{SA}$ (0.24 ± 0.62°C, $p>0.05$), suggesting that the native environment hindered the binding of the compound.

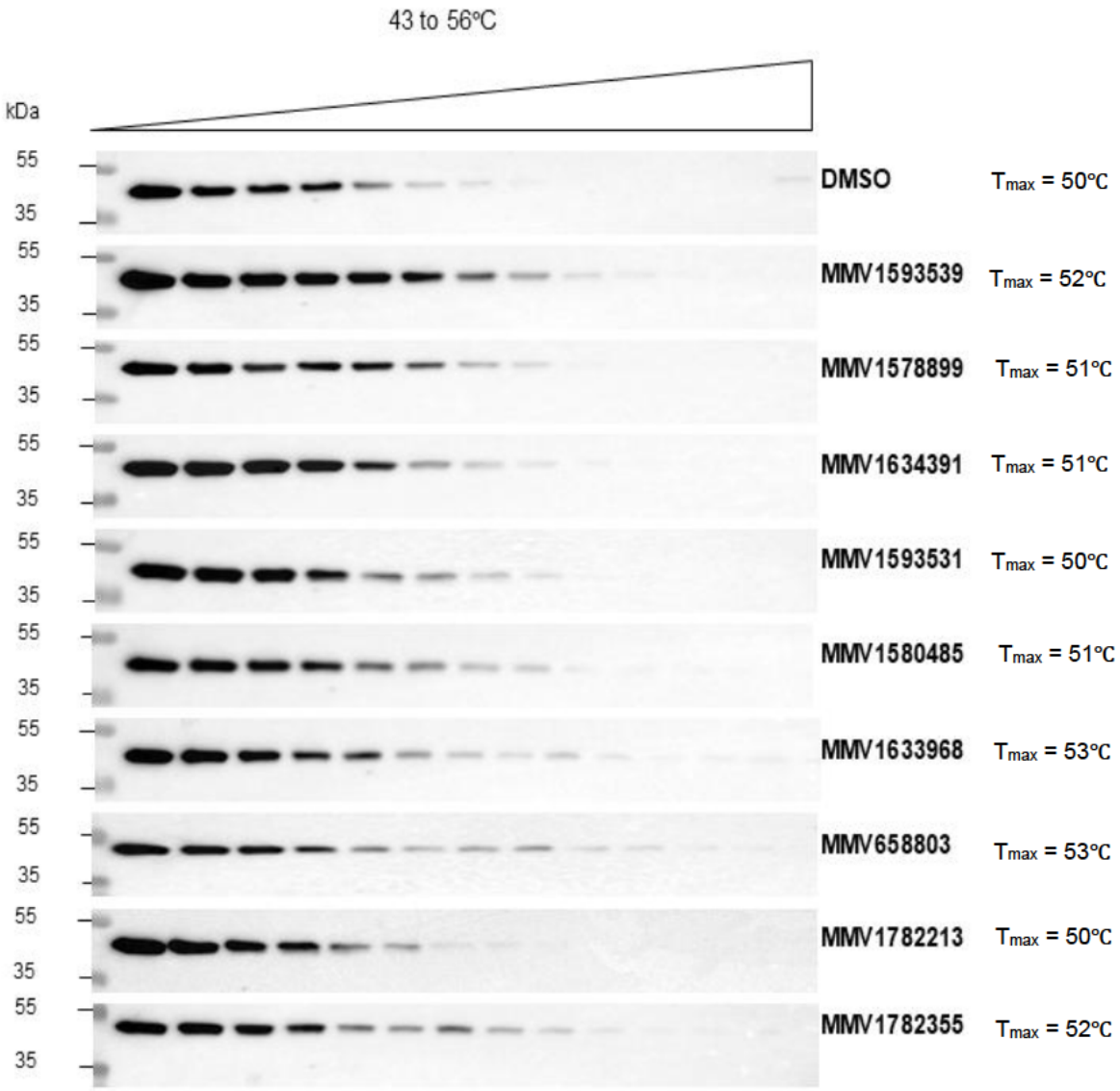

Figure 3.24 Cellular thermal shift assay western blots captured for the nine compounds determined to increase the melting temperature of $McsB_{SA}$. $McsB_{SA}$ samples, which were incubated with 1% DMSO or each of the nine compounds, were aliquoted and exposed to different temperatures (43°C -56°C, 1°C increments). These samples were analysed *via* reducing SDS-PAGE and transferred onto a nitrocellulose membrane where a single protein band of approximately 42 kDa (the approximate molecular weight for recombinantly expressed $McsB_{SA}$) was detected at each temperature point using anti-HIS tag primary antibody (HIS.H8)[cat#: MA1-21315, RRID: AB_557403, Thermo Fisher Scientific, USA) and horseradish peroxidase enzyme (HRP)-conjugated secondary antibody [Pierce® goat anti-mouse IgG, (H + L), HRP conjugate, cat#: 31430, Thermo Fisher Scientific, USA]. The T_{max} for $McsB_{SA}$ observed for the DMSO control blot, and the nine compounds tested are highlighted to the right of each captured blot.

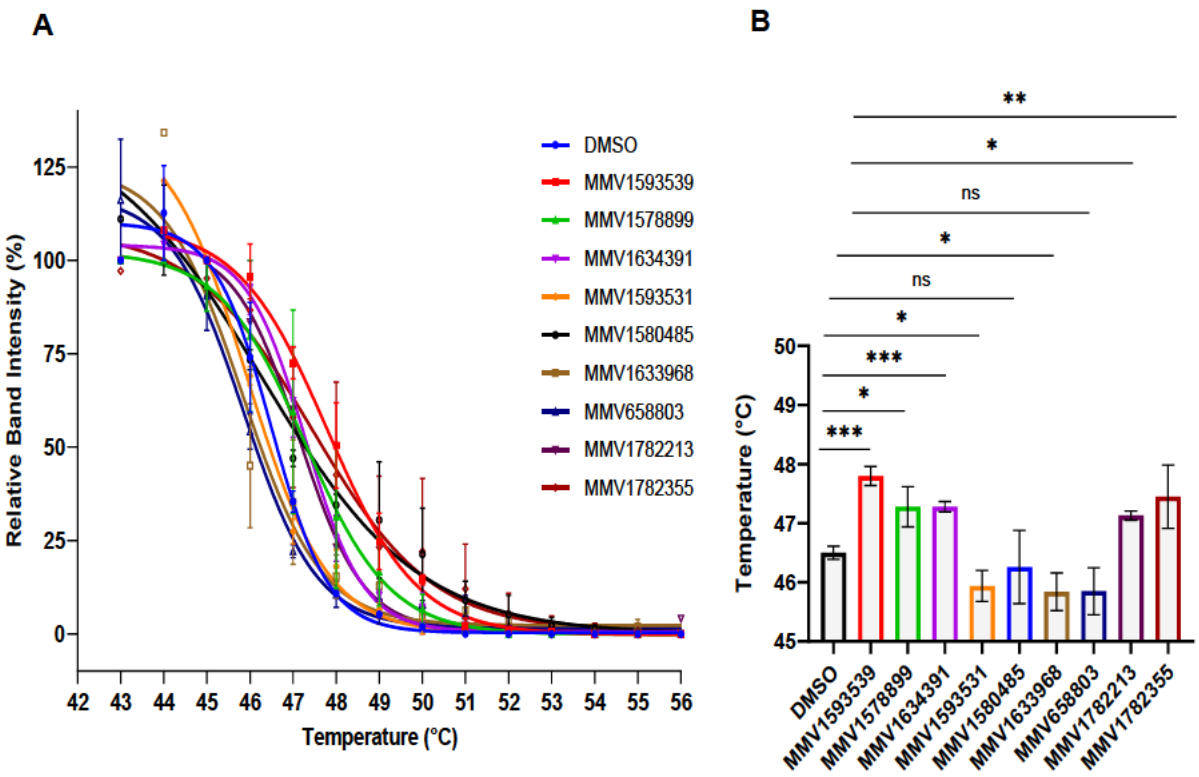

Figure 3.25. Cellular thermal shift analysis for the nine compounds determined to increase the melting temperature of $McsB_{SA}$. (A) The relative band intensities obtained were normalised (by setting the highest intensity for each data set as 100% and setting the lowest intensity for each data set as 0%) and a non-linear regression was performed using GraphPad Prism (software version 10.4) to generate a sigmoidal curve. (B) The mean ± standard error (SE) aggregation temperature (T_{agg}) calculated from the sigmoidal curves were analysed (n = 3). Statistical analysis was performed using Student's t-test, *p<0.05, **p<0.01, ***p<0.001, ns: not significant (α = 0.05, CI 95%).

3.7. Isothermal dose-response fingerprint cellular thermal shift assay

An $ITDRF_{CETSA}$ was conducted for $McsB_{SA}$ and compounds MMV1593539, MMV1580485, MMV1633968 and MMV1782213 were further evaluated. Compound MMV1593539 was selected to further validate the compound as the strongest $McsB_{SA}$ binder whilst compounds MMV1580485, MMV1633968 and MMV1782213 were selected to further assess discrepancies in binding of the compounds noted between derived T_m and T_{agg} analysis. The compounds were evaluated at 1 µM, 10 µM and 30 µM, and were compared to a DMSO control sample. A representative western blot captured (Figure 3.26) showed detection of a single band with a molecular weight of approximately 42 kDa (the expected molecular weight of recombinantly expressed $McsB_{SA}$). The $ITDRF_{CETSA}$ was performed at 48℃ as CETSA analysis (Figure 3.24) revealed this temperature to be a checkpoint at which degradation could be detected for the unliganded protein.

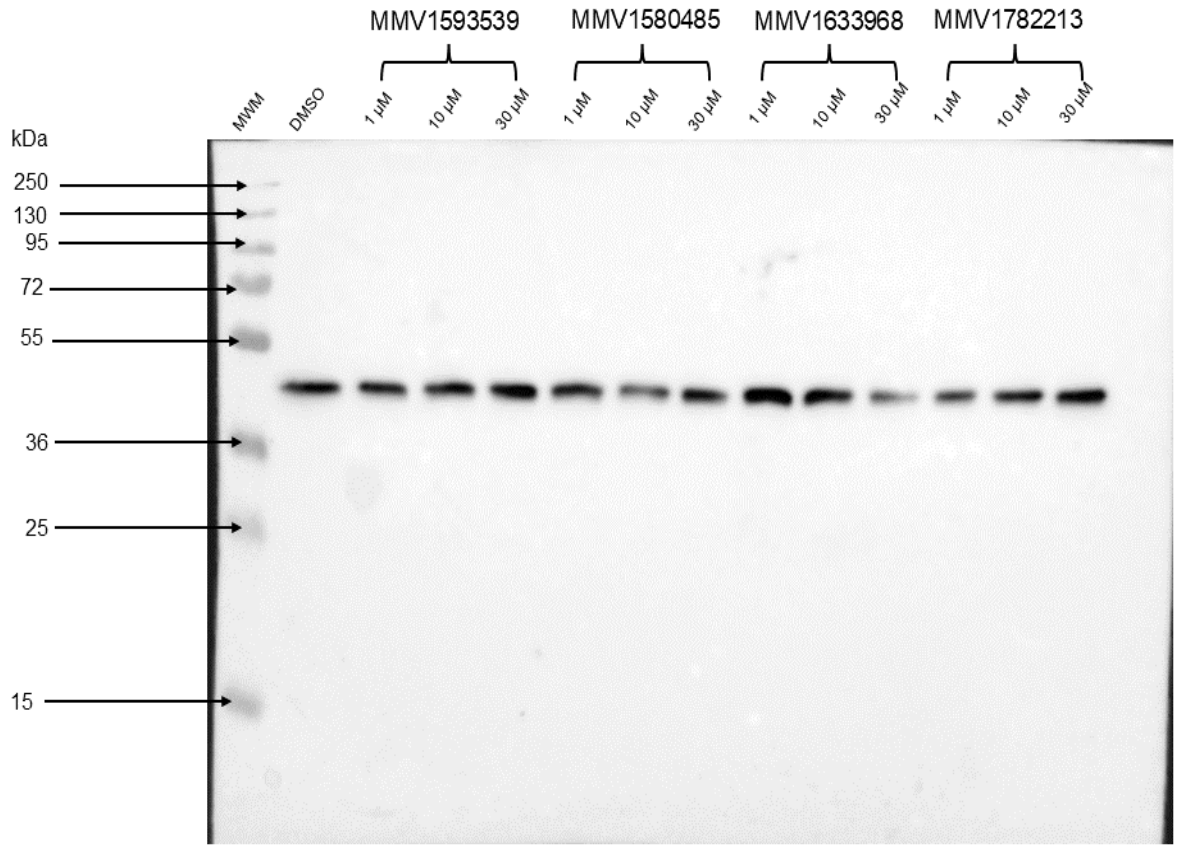

Figure 3.26. A representative isothermal dose response fingerprint cellular thermal shift assay (ITDRF$_{CETSA}$) for McsB$_{SA}$ incubated with increasing concentrations of compounds MMV1593539, MMV1580485, MMV1633968 and MMV1782213. The ITDRF$_{CETSA}$ was conducted by incubating *E. coli* lysate containing McsB$_{SA}$ with either 1, 10, or 30 µM of each ligand or DMSO only (control) for 1 hour at 4℃. The samples were incubated at 48℃ for 6 minutes and the soluble fraction was collected. The samples were analysed *via* western blot and the nitrocellulose membrane was probed using anti-His primary antibodies [cat#: MA1-21315, RRID: AB_557403, Thermo Fisher Scientific, USA) and horseradish peroxidase enzyme (HRP)-conjugated secondary antibody [Pierce® goat anti-mouse IgG, (H + L), HRP conjugate, cat#: 31430, Thermo Fisher Scientific, USA]. The detected protein band has a molecular weight of approximately 42 kDa. The relative band intensities for each band were analysed. The concentration of McsB$_{SA}$ was observed to increase as ligand concentrations increased for compounds MMV1593539 and MMV1782213 however there was no trend observed when evaluating compounds MMV1580485 and MMV1633968.

Densitometry was carried out for detected bands obtained from the conducted ITDRF$_{CETSA}$ assays and were used to measure the relative increase in McsB$_{SA}$ levels (%) per sample when compared to the DMSO control (Figure 3.27). A more prominent dose response was observed for compound MMV1593539 as compared to compound MMV1782213. Similar relative increases in McsB$_{SA}$ levels were observed for compound MMV1782213 at 1 and 10 µM however McsB$_{SA}$ levels increased significantly at 30 µM ($p<0.01$). Interestingly, a dose response was observed for compound MMV1580485 however compound MMV1580485 failed to induce an increase in the levels of McsB$_{SA}$ for each concentration tested (1, 10 and 30 µM) when compared to the DMSO control and resulted in a non-significant increase at each

concentration (p>0.5). Compound MMV1633968 caused a significant increase in $McsB_{SA}$ levels when evaluated at 1 µM (p<0.01) and 10 µM (p<0.05) similar to that of compounds MMV1593539 and MMV1782213, however a non-significant increase in $McsB_{SA}$ levels were observed when the compound was evaluated at 30 µM. The trend observed for compound MMV1633968 did not reveal a dose response; rather, the $McsB_{SA}$ levels were observed to decrease as the ligand concentration increased which suggested that the compound could be poorly soluble under the assay conditions.

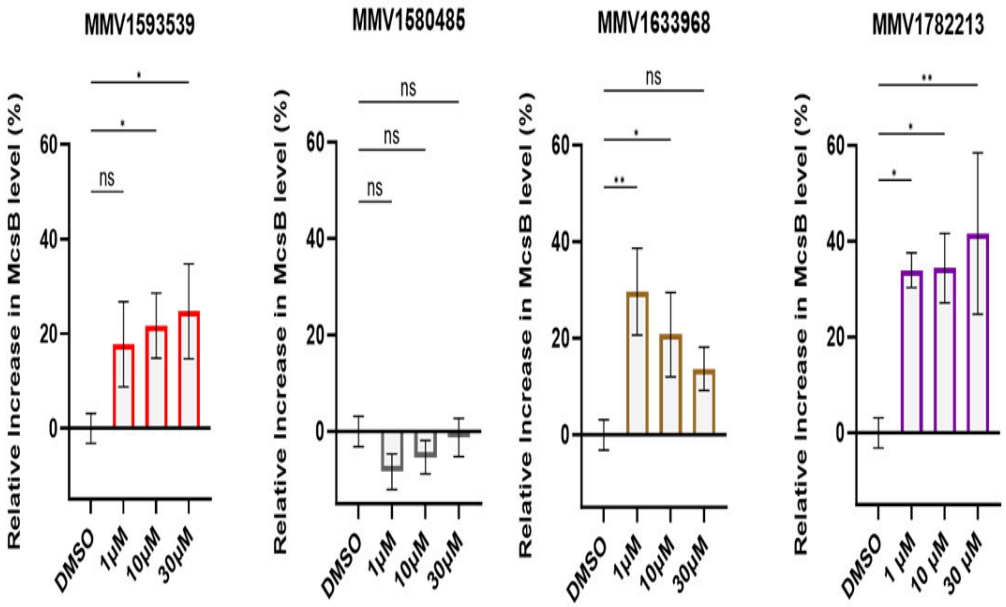

Figure 3.27. Isothermal dose response fingerprint cellular thermal shift assay ($ITDRF_{CETSA}$) analysis for $McsB_{SA}$ incubated with increasing concentrations of compounds MMV1593539, MMV1580485, MMV1633968 and MMV1782213. $ITDRF_{CETSA}$ was conducted by incubating *E. coli* lysate containing $McsB_{SA}$ with either 1, 10, or 30 µM of each ligand or DMSO only (control) for 1 hour at 4℃. The samples were incubated at 48℃ for 6 minutes and the soluble fraction was collected. The samples were analysed *via* western blot and the nitrocellulose membrane was probed using anti-His primary antibodies. The detected protein band has a molecular weight of approximately 42 kDa. The relative band intensities for each band were analysed and the relative increase in soluble $McsB_{SA}$ levels were calculated (n=3). Statistical analysis was conducted using one-way ANOVA with Dunnett's post hoc, *p<0.05, **p<0.01, ns: not significant (α=0.05, CI 95%).

3.8. *Staphylococcus aureus* minimum inhibitory concentration assay

Thermal stability screens of the Pandemic Response Box revealed that at least six compounds bound to $McsB_{SA}$ in varying capacities. Ciprofloxacin inhibited the growth of *S. aureus* similarly to reported MIC_{50} and MIC_{90} values of 0.25 µg/ml and 0.5 µg/ml respectively as observed in APPENDIX F, Figure F1 (Smith and Eng, 1985, Yasir *et al.*, 2021). The inhibitory effect of compounds MMV1593539, MMV1578899, MMV1634391, MMV1633968, MMV1782355 and MMV1782213 were evaluated against the growth of *S. aureus*. Compounds MMV1593539,

MMV1578899 and MMV1634391 were classed as anti-bacterial agents whilst compounds MMV1633968, MMV1782355 and MMV1782213 were classed as antiviral agents.

The relative growth (%) of *S. aureus* when exposed to the three anti-bacterial $McsB_{SA}$ ligands are displayed in Figure 3.28. Compounds MMV1593539 and MMV1634391 were not able to inhibit the growth of *S. aureus* completely but did result in decreased growth of *S. aureus* at 20 µM when compared to the control whilst compound MMV1578899 did not have any effect on the growth of *S. aureus*. The ligand MMV1593539, was established as our best binder from the three anti-bacterial compounds but failed to completely inhibit the growth of *S. aureus* which agreed with previous results establishing the compound to be inactive against *S. aureus* up to 20 µM (Zoraghi *et al.*, 2014).

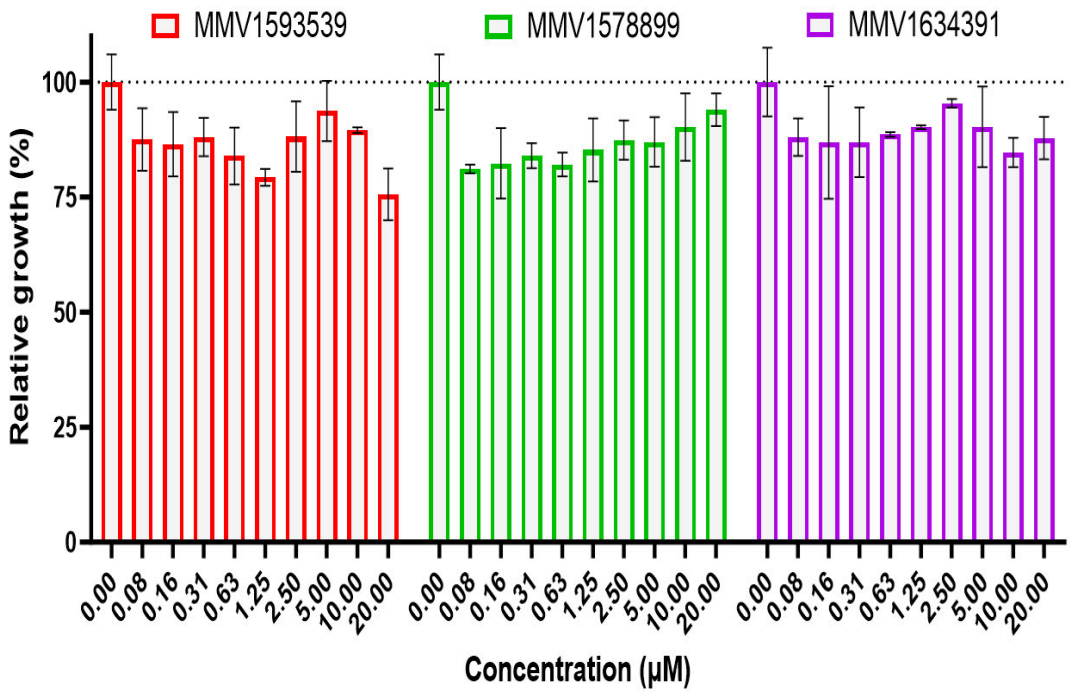

Figure 3.28. The effect of identified anti-bacterial $McsB_{SA}$ ligands on *Staphylococcus aureus* growth using a minimum inhibitory concentration assay. *S. aureus* was incubated with the three identified anti-bacterial $McsB_{SA}$ ligands. The compounds were tested at a range of 0.078 µM – 20 µM (where 20 µM was the highest concentration tested, and a two-fold serial dilution was prepared until the lowest concentration of 0.078 µM was reached). An OD_{600} reading was taken at 0 h and once again after a 24 h incubation period at 37℃. The relative growth of *S. aureus* was assessed by treating the 0 µM DMSO control as 100%.

The relative growth (%) of *S. aureus* when exposed to the three anti-viral $McsB_{SA}$ ligands are displayed in Figure 3.29. Compounds MMV1633968, MMV1782213 and MMV1782355 were unable to inhibit the growth of *S. aureus* completely (Figure 3.29). The ligand MMV1782355,

peldesine or BCX-34, was identified as our best binding anti-viral ligand but displayed little to no inhibitory effect on the growth of *S. aureus* from 0.08 µm to 20 µM. Peldesine has been reported as a potent purine nucleoside phosphorylase inhibitor and had been tested as a possible treatment therapy for cutaneous T-cell lymphoma however has not been explored as a potential treatment for *S. aureus* infections (Duvic *et al.*, 2001). The MIC data revealed that the binding of the identified $McsB_{SA}$ ligands does not have any toxic effects on the *S. aureus* (ATCC25923) bacterial strain.

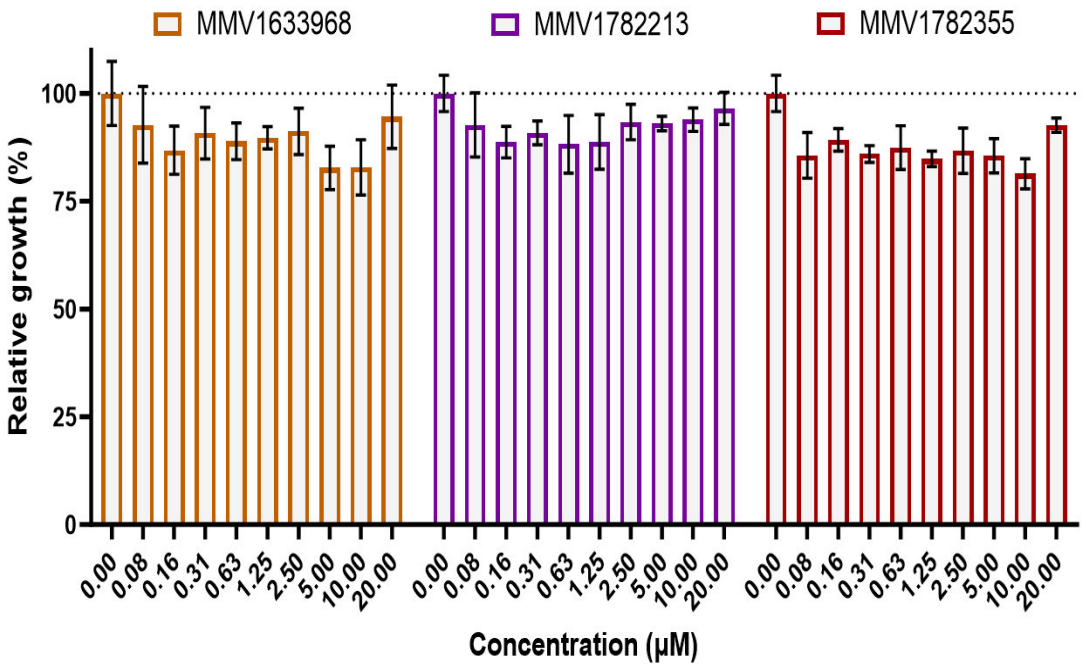

Figure 3.29. The effect of identified anti-viral $McsB_{SA}$ ligands on *Staphylococcus aureus* growth using a minimum inhibitory concentration assay. *S. aureus* was incubated with the three identified anti-viral $McsB_{SA}$ ligands. The compounds were tested within a range of 0.078 µM – 20 µM (a two-fold serial dilution was prepared from 20 µM until the concentration of 0.078 µM was reached). An OD_{600} reading was taken at 0 h and once again after a 24 h incubation period at 37℃. The relative growth of *S. aureus* was assessed by treating the 0 µM control as 100%.

3.9. In silico analysis of $McsB_{SA}$

3.9.1. Assessing the drug-likeness of novel $McsB_{SA}$ ligands

The in silico drug like properties measured for the six novel $McsB_{SA}$ ligands are displayed in Table 3.4, specifically, the following properties were assessed, toxic risks, hydrophilicity, solubility, absorption, pharmacokinetics and drug likeness. Compounds MMV1578899 and MMV1782213 were the only two compounds which had predicted toxicity risks. The first having a high risk of being an irritant whilst the latter was predicted to be more potent as it had high risks of inducing mutations and tumour development, as well as being a mild irritant.

Compounds MMV1633968 and MMV1782213 were the only two compounds which had two solubility scores [specifically Log S (Ali) mg/ml and Log S (SILICOS-IT) mg/ml solubility scores] classifying the compounds as poorly soluble. This corroborates the findings from the $ITDRF_{CETSA}$ conducted on compounds MMV1633968 and MMV1782213. Compound MMV1782213 was also predicted to have two violations against the Lipinski rule of 5 which was observed for compound MMV1634391 as well (2 violations). Importantly, none of the identified novel $McsB_{SA}$ ligands were described as pan assay interference structures (PAINS). Drug scores calculated using the OSIRIS Property Explorer tool suggested our best binding anti-bacterial compound MMV1593539 (0.35) to be less drug-like than compound MMV1633968 (0.43), our best binding anti-viral compound MMV1782213 to be the least drug-like compound overall (0.05) and compound MMV1782355 to be the most drug-like with a predicted drug score of 0.94.

3.9.2. Molecular modelling of $McsB_{SA}$

The crystal structures of $McsB_{SA}$ (PDB: 8GQD) and $McsB_{GS}$ (PDB: 6FH3) were compared using Protein structural alignment tools. The $McsB_{SA}$ and $McsB_{GS}$ structures were modelled as dimers and monomers and the structural superposition of $McsB_{GS}$ and $McsB_{SA}$ is displayed in Figure 3.30.A and B respectively. The structural alignment tool was used to align all residues from both $McsB_{SA}$ and $McsB_{GS}$ structures and is displayed in APPENDIX G, Figure G1. An alignment score of 0.336 was obtained from the structural alignment and a RMSD value of 2.825 Å was obtained for the dimeric structural alignment whilst a TM-score of 0.88 (TM-score range is 0-1, >0.5 generally indicate proteins have the same protein fold) and a RMSD value of 2.62 Å was obtained for the monomeric structural alignment. Both the structural alignments shared a similar RMSD value <3 which suggested a good alignment as an RMSD value <3 was pronounced typical between homologous proteins (Reva *et al.*, 1998).

Table 3.4.: The predicted drug-like properties of identified $McsB_{SA}$ ligands using the in silico tools SwissADME and OSIRIS Molecular Property Explorer.

Property	Measurement	$McsB_{SA}$ Ligands					
		MMV1593539	**MMV1578899**	**MMV1634391**	**MMV1633968**	**MMV1782213**	**MMV1782355**
Toxicity risks	Mutagenic	No	No	No	No	Yes, high risk	No
	Tumorigenic	No	No	No	No	Yes, high risk	No
	Irritant	No	Yes, high risk	No	No	Yes, medium risk	No
	Reproductive effect	No	No	No	No	No	No
Hydrophilicity	cLogP[a]	3.45	2.89	3.43	3.85	4.98	0.81
Solubility	Log S (ESOL)[b] mg/ml	-4.71	-2.93	-5.34	-5.47	-7.11	-1.88
	Log S (Ali)[c] mg/ml	-5.56	-3.35	-5.47	-6.46	-8.54	-1.75
	Log S (SILICOS-IT)[d] mg/ml	-7.34	-4.09	--9.54	-7.72	8.46	4.64
	Class[e]	Moderately, moderately, poorly soluble	Soluble, Soluble, moderately soluble	Moderately, moderately, poorly soluble	Moderately, poorly, poorly soluble	Poorly soluble	Very soluble, very soluble, moderately soluble
Absorption	Molecular weight	305.30	192.30	631.70	370.30	557.80	241.20
	GI absorption[f]	High	High	High	High	Low	High
	BBB Permeant[g]	No	Yes	No	No	No	No
	P-gp Substrate[h]	No	No	Yes	No	No	No
Pharmacokinetics	Cytochromes inhibited (out of 5)[i]	4	1	3	4	4	1
Drug likeness	Lipinski (Rule of 5)[j]	Yes, 0 violations	Yes, 0 violations	No, 2 violations	Yes, 0 violations	No, 2 violations	Yes, 0 violations
	Bioavailability score[k]	0.55	0.55	0.17	0.55	0.56	0.55
	PAINS[l]	0	0	0	0	0	0
	Drug-score (0-1)[m]	0.35	0.27	0.43	0.23	0.05	0.94

[a] The consensus Log $P_{o/w}$ is an average of the Log $P_{o/w}$ (iLOGP), Log $P_{o/w}$ (XLOGP3), Log $P_{o/w}$ (WLOGP), Log $P_{o/w}$ (MLOGP), Log $P_{o/w}$ (SILICOS-IT)(Wildman and Crippen, 1999, Lipinski *et al.*, 2012, Daina *et al.*, 2014)
[b] The topological solubility score (Delaney, 2004)
[c] The topological solubility score (Ali *et al.*, 2012)
[d] The fragmented solubility score calculated by FILTER-IT program, version 1.0.2, courtesy of SILICOS-IT
[e] The Log S scale, insoluble<-10<poorly<-6<moderately soluble<-4<soluble<-2<very soluble<0<highly soluble
[f] Gastrointestinal absorption
[g] Blood brain barrier permeation
[h] p-glycoprotein substrate
[i] The predicted number of P450 cytrochrome enzymes inhibted, the five cytochromes tested are cytochrome P450 1A2, cytochrome P450 2C19, cytochrome P450 2C9, cytochrome P450 2D6, cytochrome P450 3A4.
[j] The Lipinski rule of 5 filter (MW≤500, MLOGP≤4.15, N or O≤10 and NH or OH≤5)
[k] Abbot bioavailability score (Martin, 2005)
[l] Pan Assay Interference Structures (PAINS) (Baell and Holloway, 2010)
[m] The OSIRIS drug score is a calculated score factoring in the drug likeness, cLogP, LogS, molecular weight and toxicity risks of a compound to estimate the overall potential of the compound to qualify for a drug.

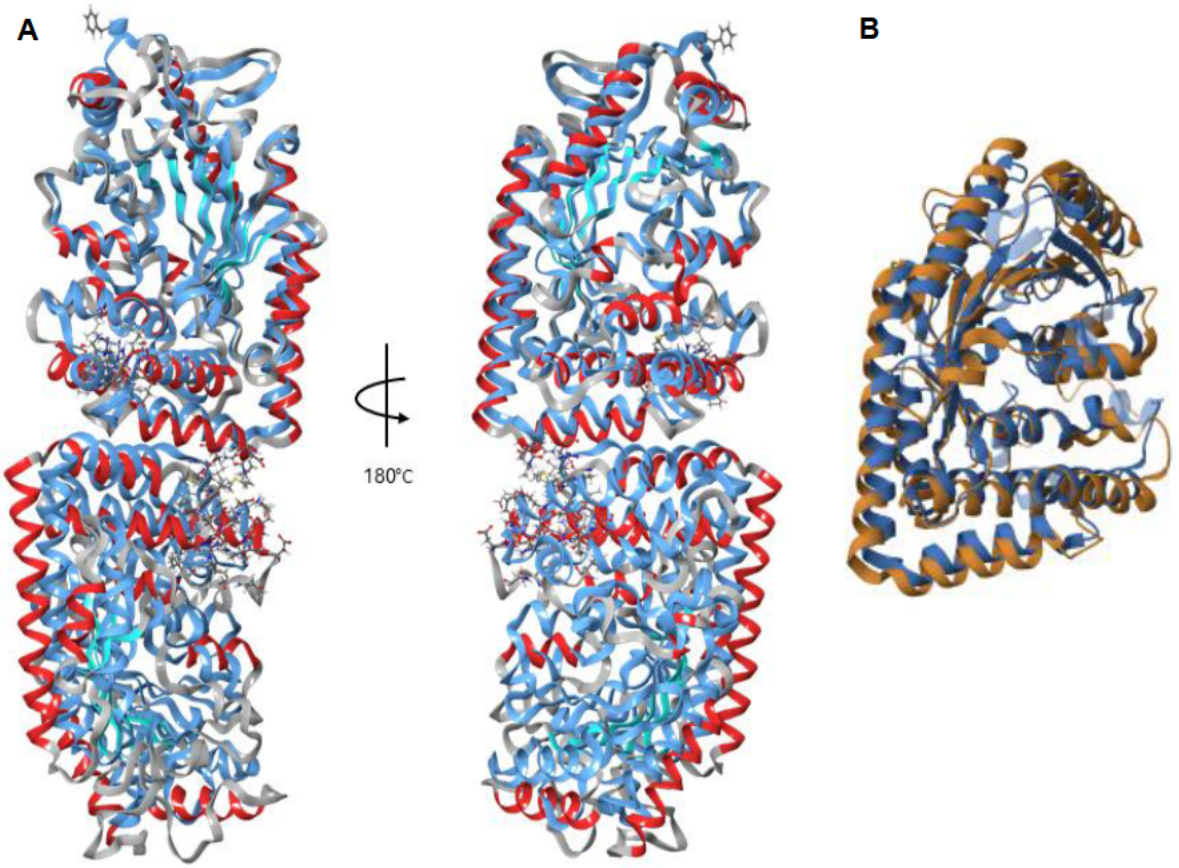

Figure 3.30. Structural superposition of $McsB_{SA}$ (PDB: 8GQD) and $McsB_{GS}$ (PDB: 6FH3). (A) Structural superposition of dimeric forms of $McsB_{SA}$ and $McsB_{GS}$ obtained using the structural alignment tool in the Schrödinger drug discovering suite (Maestro, version 2022-1). $McsB_{SA}$ is displayed as a grey, red and cyan cartoon model and $McsB_{GS}$ is displayed as a blue cartoon model. (B) Structural superposition of monomeric forms of $McsB_{SA}$ and $McsB_{GS}$ obtained using the pairwise structure alignment tool from the Research Collaboratory for Structural Bioinformatics Protein Data Bank (RCSB PDB) [Accessed in December 2024]. $McsB_{SA}$ is displayed as a brown cartoon model and $McsB_{GS}$ is displayed as a blue cartoon model.

3.9.3. Molecular docking of novel $McsB_{SA}$ binders

A comparison of the $McsB_{SA}$ and $McsB_{GS}$ structures allowed for the identification of the putative $McsB_{SA}$ ATP and pArg binding sites. The binding of ATP and Amp-PN within the putative $McsB_{SA}$ ATP binding site was compared to the binding within the known $McsB_{GS}$ ATP binding site and the binding of pArg and Arg into the putative $McsB_{SA}$ pArg binding site was compared to the known $McsB_{GS}$ pArg site (Table 3.5.). All ligands tested (ATP, AMP-PN, pArg and Arg) were observed to dock favourably with negative docking scores obtained for each case. The docking of pArg into the putative pArg binding site in $McsB_{SA}$ resulted in a docking score of -5.488 which is similar to the docking score obtained for the docking of pArg into the known pArg binding site of $McsB_{GS}$ (-5.018). The docking scores for ATP docked into the putative ATP binding site of $McsB_{SA}$ and for ATP docked into the known ATP binding site of $McsB_{GS}$ were also similar (-12.616 and -12.230 respectively).

Table 3.5.: The protein-ligand docking scores between $McsB_{SA}$ and $McsB_{GS}$.

McsB	Ligand			
Orthologues	**AMP-PN[a]**	**ATP[a]**	**pArg[b]**	**Arg[b]**
	Docking scores (kcal/mol)			
$McsB_{SA}$	-7.095	-12.616	-5.488	-5.094
$McsB_{GS}$	-10.230	-12.230	-5.018	-7.383

[a] Ligands were docked into the putative/known ATP binding sites of $McsB_{SA}$/$McsB_{GS}$
[b] Ligands were docked into the putative/known pArg binding sites of $McsB_{SA}$/$McsB_{GS}$

Based on analysed data from the TSA, CETSA and $ITDRF_{CETSA}$, and MIC, six of the identified novel $McsB_{SA}$ ligands (MMV1593539, MMV1578899, MMV1634391, MMV1633968, MMV1782355 and MMV1782213) were selected for docking into both identified putative ATP and pArg binding sites or $McsB_{SA}$. The structures and IUPAC nomenclature for each $McsB_{SA}$ ligand is displayed in APPENDIX H, Table H1. The docking scores of the six novel $McsB_{SA}$ ligands docked into the predicted ATP $McsB_{SA}$ binding site and the predicted pArg binding site are displayed in Table 3.6. and Table 3.7. respectively. Ligands MMV1593539, MMV1634391, MMV1633968 and MMV1782355 all had glide scores higher than -4.302 kcal/mol (docking score of pArg, negative control) when docked into the putative ATP binding site of $McsB_{SA}$ whilst compounds MMV1578899 and MMV1782213 had glide scores lower than that observed for pArg docked in the putative ATP binding site of $McsB_{SA}$ (Table 3.6). The highest docking scores were obtained for MMV1782355 and MMV1593539 (-7.873 and -6.518 kcal/mol respectively).

Table 3.6.: The best protein-ligand docking scores obtained for the six novel $McsB_{SA}$ ligands docked into the putative ATP binding site of $McsB_{SA}$.

Ligand	Docking score	XP glide	Glide emodel
ATP[a]	-12.616	-12.616	-95.614
AMP-PN[a]	-7.095	-7.095	-52.703
MMV1593539	-6.518	-6.518	-63.139
MMV1578899	-4.179	-4.179	-33.906
MMV1634391	-6.114	-6.319	-82.107
MMV1633968	-5.398	-5.398	-47.67
MMV1782355	-7.873	-7.907	-56.45
MMV1782213	-3.616	-3.616	-68.003
pArg[b]	-4.302	-4.302	-38.842

[a] ATP and AMP-PN ligands were docked as positive controls
[b] pArg ligand was docked as a negative control

Table 3.7.: The best protein-ligand docking scores obtained for the six novel $McsB_{SA}$ ligands docked into the putative pArg binding site of $McsB_{SA}$.

Ligand	Docking score	XP glide	Glide emodel
pArg[a]	-5.488	-7.478	-69.504
Arg[a]	-5.094	-5.094	-27.755
MMV1593539	-4.167	-4.167	-44.037
MMV1578899	-4.035	-4.035	-28.768
MMV1634391	-2.492	-3.238	-69.74
MMV1633968	-1.074	-1.074	-35.22
MMV1782355	-4.486	-4.52	-49.107
MMV1782213	-2.324	-2.325	-54.718
AMP-PN[b]	-4.317	-4.317	-54.966

[a] pArg and Arg ligands were docked as positive controls.
[b] AMP-PN ligand was docked as a negative control.

All ligands docked to the putative pArg binding site of $McsB_{SA}$ were observed to have glide scores lower than -4.317 kcal/mol (docking score of AMP-PN, negative control), with the exception of ligand MMV1782355, a docking score of -4.486 kcal/mol was obtained. Compounds MMV1633968 and MMV1634391 had the lowest docking scores when docked into the putative pArg binding site of $McsB_{SA}$, -1.074 and -2.492 kcal/mol respectively.

Molecular docking studies identified ligands MMV1782355 and MMV1593539 as the best binders from the six ligands docked supported by ligand MMV1782355 obtaining the highest docking score when docked to the putative ATP $McsB_{SA}$ binding site and having the only docking score which was observed to be above the threshold of the AMP-PN negative control when docked to the putative pArg $McsB_{SA}$ binding site, whereas ligand MMV1593539 did not show favourable docking scores when docked to the pArg $McsB_{SA}$ binding site, however, a docking score of -6.518 kcal/mol was obtained when docked to the putative ATP McsBSA binding site which is similar to the docking score of the positive control AMP-PN (-7.095 kcal/mol).

3.9.4. Molecular dynamics of $McsB_{SA}$

The interactions for both ligand MMV1782355 and ligand MMV1593539 with $McsB_{SA}$ were further investigated through MD simulations in comparison with the $McsB_{SA}$ protein only or in complex with ATP (Figure 3.31. and Table 3.8.)

Table 3.8.: $McsB_{SA}$ average root mean square deviation (RMSD), radius of gyration (RoG) and root mean square fluctuation (RMSF).

	Complex			
	$McsB_{SA}$	**$McsB_{SA}$-ATP**	**$McsB_{SA}$-MMV1782355**	**$McsB_{SA}$-MMV1593539**
	Root mean square deviation (RMSD): 10-50 ns for Protein-Ligand complex (Å)			
Mean ± SD	3.024 ± 0.13	3.745 ± 0.18	3.451 ± 0.16	3.995 ± 0.18
Difference[a]	0	0.721	0.427	0.971
Min-Max Range	0.761	1.235	1.107	0.964
	RMSD: 20-50 ns for Protein-Ligand complex (Å)			
Mean ± SD	3.014 ± 0.12	3.783 ± 0.18	3.457 ± 0.17	4.069 ± 0.11
Difference[a]	0	0.769	0.443	1.055
Min-Max Range	0.720	1.07	1.106	0.668
	Radius of gyration (RoG): 10-50 ns for Protein-Ligand complex(Å)			
Mean ± SD	21.8 ± 0.09	21.8 ± 0.12	22.01 ± 0.10	22.09 ± 0.12
Min-Max Range	0.5301	0.7605	0.6399	0.8135
	RoG: 20-50 ns for Protein-Ligand complex(Å)			
Mean ± SD	21.8 ± 0.09	21.8 ± 0.13	22.0 ± 0.09	22.1 ± 0.12
Min-Max Range	0.490	0.760	0.591	0.771
		RMSD: 10-50 ns for Ligand (Å)		
		ATP	MMV1782355	MMV1593539
Mean ± SD		2.292 ± 0.29	1.022 ± 0.23	1.514 ± 0.22
Min-Max Range		2.40	1.86	1.41

[a] Difference was calculated as the difference between the observed complex mean and $McsB_{SA}$ mean

$McsB_{SA}$ and the three complexes ($McsB_{SA}$-ATP, $McsB_{SA}$-MMV1782355 and $McsB_{SA}$-MMV1593539) displayed stable structural formation from ~10 ns although the $McsB_{SA}$-MMV1593539 complex continued to show an increase in RMSD until ~20 ns. The average RMSD (10-50 ns) were 3.024 ± 0.13 Å, 3.745 ± 0.18 Å, 3.451 ± 0.16 Å and 3.995 ± 0.1814 Å

for $McsB_{SA}$ with no ligand present, $McsB_{SA}$-ATP, $McsB_{SA}$-MMV1782355 and $McsB_{SA}$-MMV1593539, respectively (Figure 3.31.A and Table 3.7.). The mean RMSD for ATP alone was 2.292 ± 0.29 Å which indicated that the ligand had a more varied conformation across the simulation of 50 ns whereas the mean RMSD observed for the novel $McsB_{SA}$ ligands MMV1782355 and MMV1593539 were 1.0 ± 0.23 Å and 1.51 ± 0.22 Å respectively which indicated a more stable configuration during the 50 ns simulation (Figure 3.31 D and Table 3.8)

The RoG for $McsB_{SA}$ with no ligand present and all three complexes had little deviation from 10-50 ns with mean RoG values of 21.8 ± 0.09 Å for $McsB_{SA}$ without a ligand present, 21.8 ± 0.12 Å for $McsB_{SA}$-ATP complex, 22.0 ± 0.10 Å for $McsB_{SA}$-MMV1782355 and 22.1 ± 0.11 Å for $McsB_{SA}$-MMV1593539 (Figure 3.31.B and Table 3.8.). The RMSF per residue was evaluated for $McsB_{SA}$ alone and all three complexes (Figure 3.31.C). The $McsB_{SA}$-ATP and $McsB_{SA}$-MMV1782355 complexes both displayed high residue fluctuations over the 50 ns simulation as observed in Figure 3.31.C which suggested that the complexes are more flexible as compared to the $McsB_{SA}$-MMV1593539 complex which displayed RMSF per residue values similar to that of $McsB_{SA}$ and suggested a more rigid complex (Figure 3.31.C).

The ligand interaction counts for both ligand MMV1782355 and ligand MMV1593539 with $McsB_{SA}$ were assessed during the 50 ns simulation by monitoring the number of hydrogen bonds, Pi-Pi stacking interactions and Pi-cation interactions (Figure 3.31.E and Figure 3.31.F respectively). Ligand MMV1782355 had substantially more interactions with $McsB_{SA}$ as compared to ligand MMV1593539 for the duration of the simulation (10-50 ns) as highlighted by the average of 5.4 hydrogen bonds formed and a consistent Pi-cation interaction between ligand MMV1782355 and $McsB_{SA}$ compared to the average of 1.8 hydrogen bonds formed and two prominent Pi-Pi stacking interactions between ligand MMV1593539 and $McsB_{SA}$ (Figure 3.31.E and F). Ligand interaction snapshots were evaluated at 10 ns intervals (starting at 0 ns and ending at 50 ns) for both ligand MMV1782355 and ligand MMV1593539 with $McsB_{SA}$ (Figure 3.32 and 3.33 respectively). Ligand MMV1782355 displayed a more rigid conformation within the binding site as reflected by the stable hydrogen bond formed with Tyr12 and the stable Pi-cation interaction with Arg26 in Figure 3.33.B-F (10-40 ns). In contrast, ligand MMV1593539 displayed changes in its positioning and its interactions within the binding site as reflected by the Pi-Pi stacking interactions which switched between the two indole rings and interacted with either Tyr12 (Figure 3.33.B and F) or His 82 (Figure 3.33.C-E). This further supported that ligand MMV1593539 should have a less stable interaction with $McsB_{SA}$ as

compared to ligand MMV1782355. The MD data supported the molecular docking data obtained and indicated that ligand MMV1782355 and MMV1593539 form stable complexes with $McsB_{SA}$ when binding to the predicted ATP $McsB_{SA}$ binding site. The MD data could be improved upon through increasing the simulation time from 50 ns to 100ns or 1000 ns to allow for a confident observation of the complexes' stability.

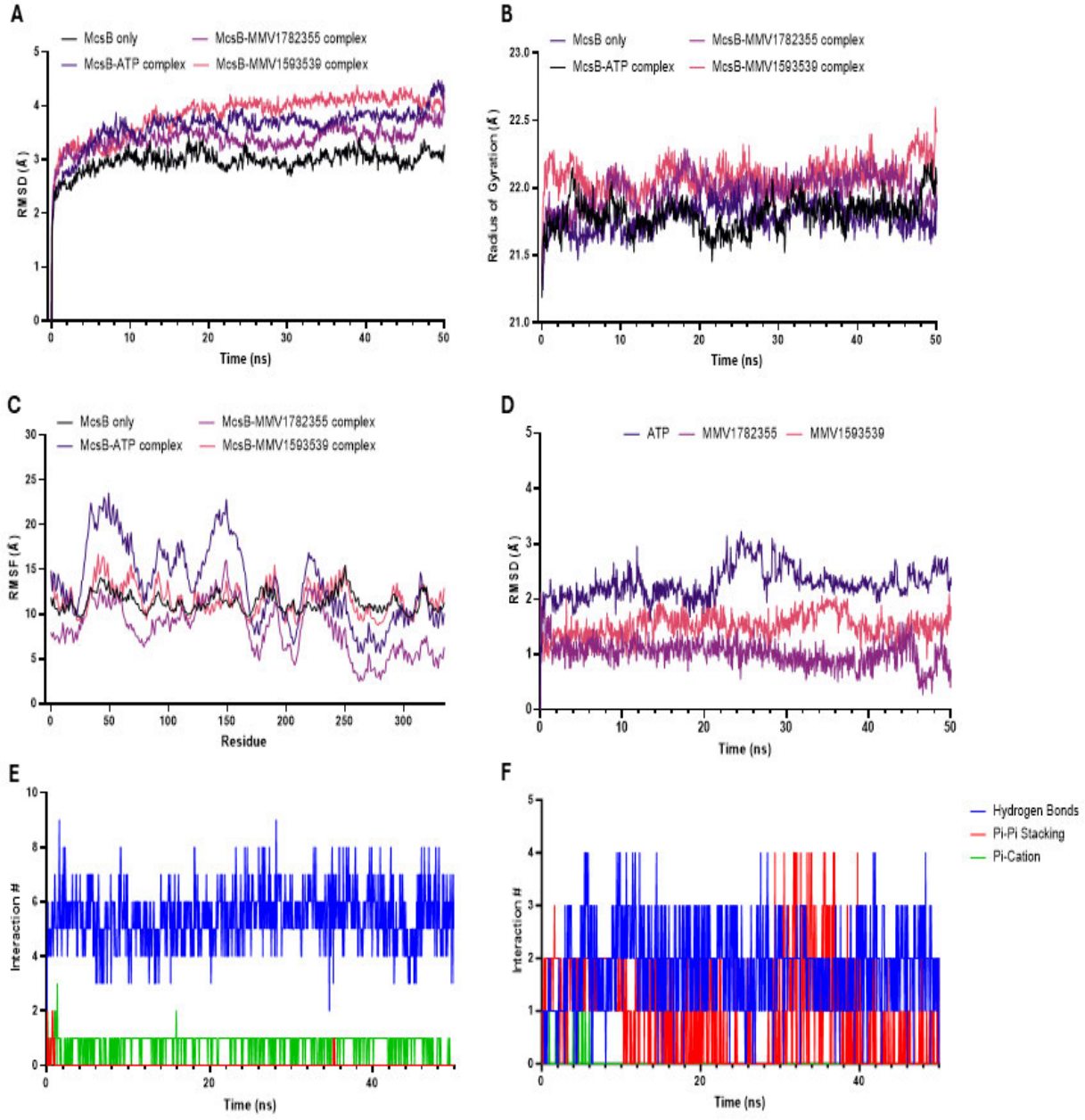

Figure 3.31. Molecular dynamic (MD) simulation of ATP, MMV1782355 and MMV1593539 in complex with $McsB_{SA}$. MD simulations were performed on the $McsB_{SA}$ monomer for 50 ns with no ligand present or in complex with ATP, MMV1782355 and MMV1593539 using Desmond. (A) Root mean square deviation (RMSD) over time. (B) Radius of gyration over time. (C) Root mean square fluctuation (RMSF) per residue. (D) RMSD of ATP, MMV1782355 and MMV1593539 only over time. (E) Ligand interaction counts for ligand MMV1782355 with $McsB_{SA}$ during the simulation. (F) Ligand interaction counts for ligand MMV1593539 with $McsB_{SA}$ during the simulation.

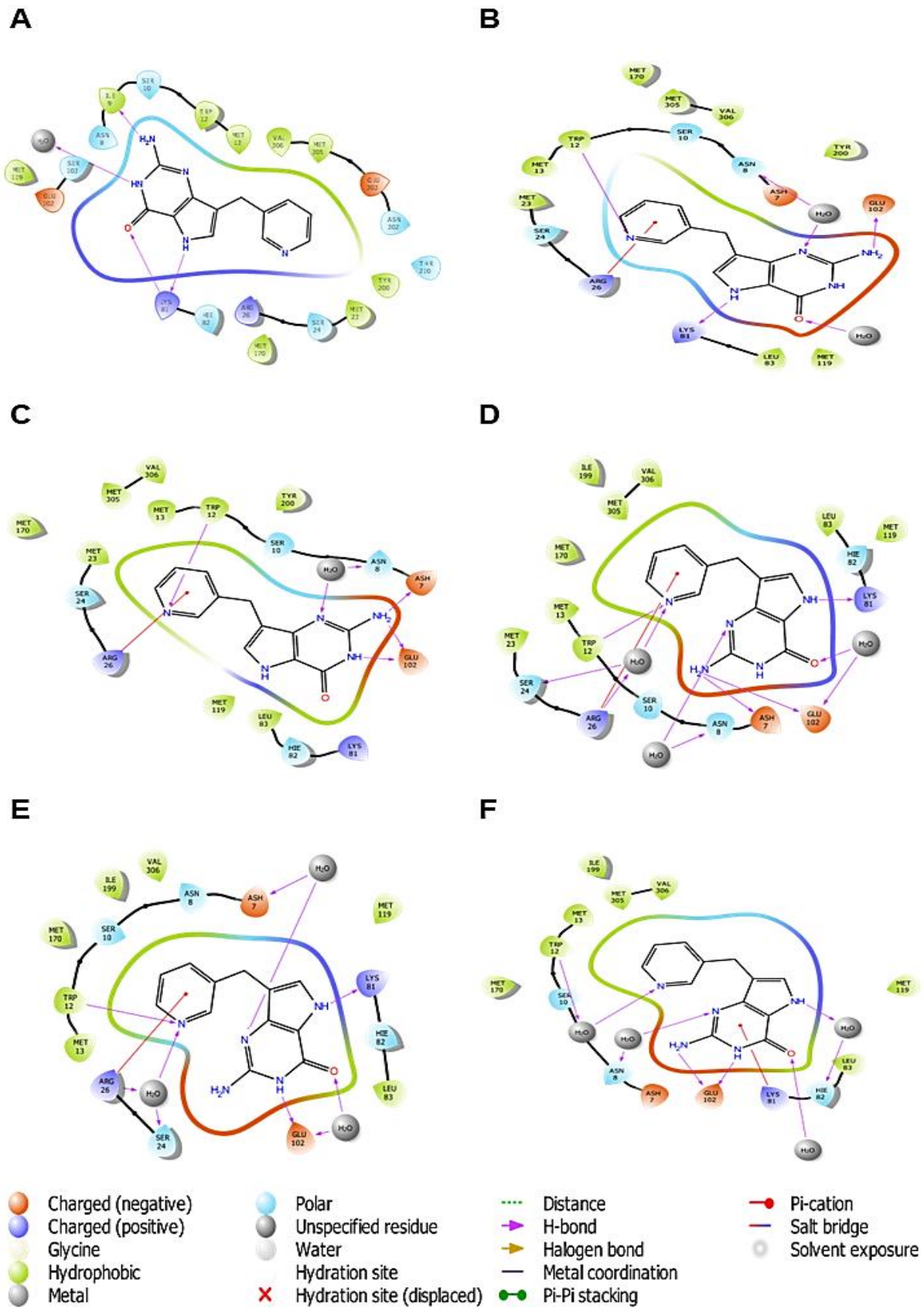

Figure 3.32. Ligand interaction diagrams for $McsB_{SA}$-MMV1782355 complexes within the ATP pocket. (A) At 0 ns. (B) At 10 ns. (C) At 20 ns. (D) At 30 ns. (E) At 40 ns. (F) At 50 ns.

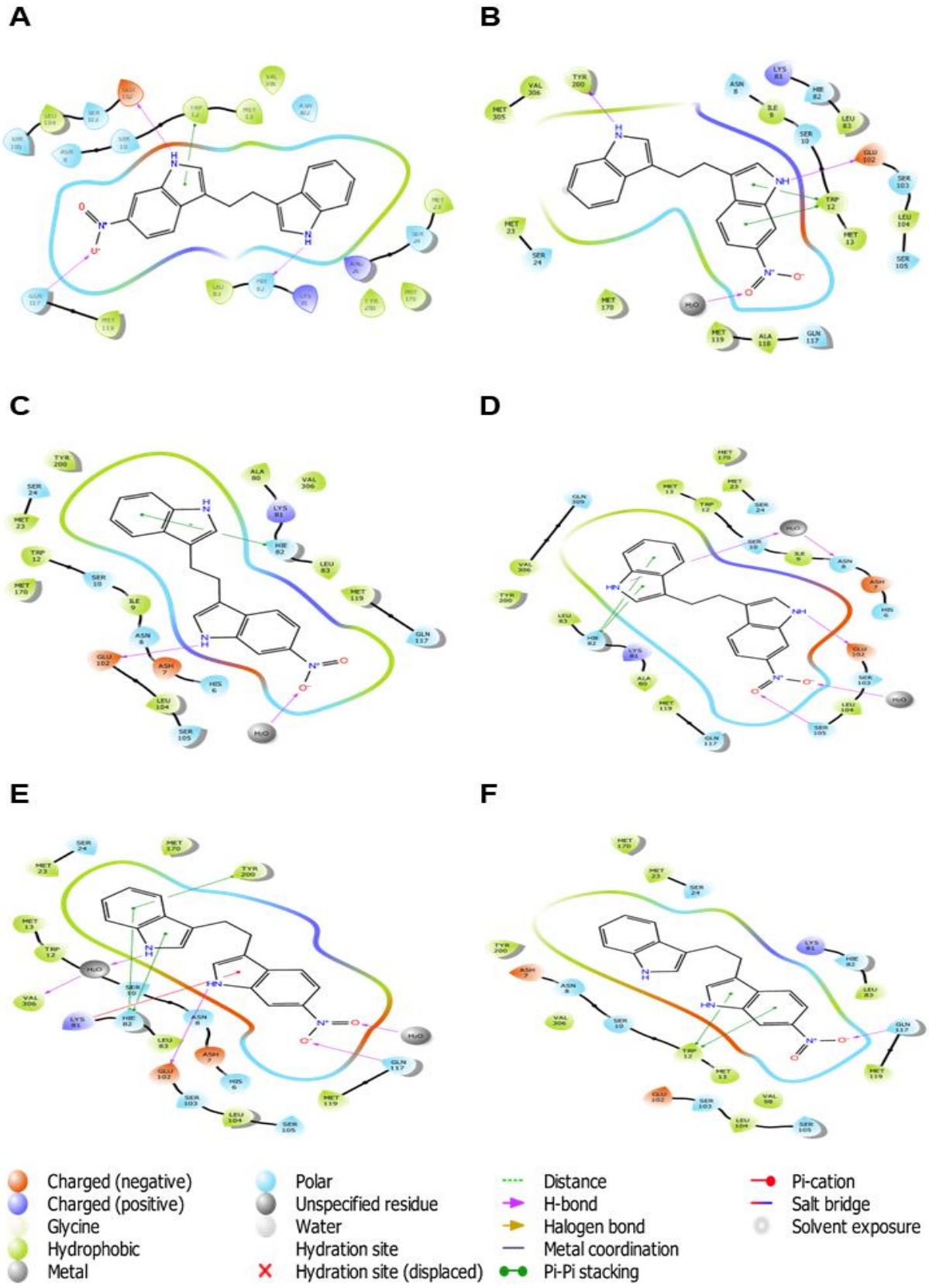

Figure 3.33. Ligand interaction diagrams for $McsB_{SA}$-MMV1593539 complexes within the ATP pocket. (A) At 0 ns. (B) At 10 ns. (C) At 20 ns. (D) At 30 ns. (E) At 40 ns. (F) At 50 ns.

CHAPTER 4: DISCUSSION

This study aimed to discover novel ligands for the protein arginine kinase $McsB_{SA}$ as the protein has been recognised as a promising drug target due to the role it plays in the stress response mechanisms of the Gram-positive pathogen *S. aureus*. To accomplish this, the protein was first recombinantly expressed in *E. coli* and purified to obtain soluble $McsB_{SA}$ protein. Secondly, the protein was assessed for its suitability to be used in thermostability assays designed to detect protein-ligand binding. $McsB_{SA}$ was then screened against the Pandemic Response Box through thermal stability assays (TSA and CETSA) and novel ligands for $McsB_{SA}$ were identified. This was followed by an in-silico study to validate the discovered novel ligands and predict the binding sites of each ligand. Finally, inhibitory / toxicity properties of the six identified ligands were examined on the Gram-positive pathogen *S. aureus.*

4.1. Soluble $McsB_{SA}$ is compatible with thermal stability assays

The full length of the *S. aureus* McsB gene was synthesised into a pET-28a (+) plasmid which was used to transform *E. coli* BL21(DE3) cells. Transformed *E. coli* cells containing the $McsB_{SA}$ gene were grown and expression of $McsB_{SA}$ was induced with the addition of IPTG. The expressed $McsB_{SA}$ protein was primarily insoluble. This was unexpected as Suskiewicz and co-workers, as well as Lu and colleagues did not report issues with solubility of $McsB_{GS}$ or $McsB_{SA}$ respectively when expressed using a recombinant expression system similar to our own, albeit a different expression plasmid (pET21-mcsB-His620 for $McsB_{GS}$ and pET47b-mcsB for $McsB_{SA}$) was used (Suskiewicz *et al.*, 2019, Lu *et al.*, 2024). The reported size of recombinantly expressed $McsB_{GS}$ is ~42 kDa whilst Lu and co-workers observed expression of the monomer at 39 kDa as they had cleaved off the HIS-tag in their study (Suskiewicz *et al.*, 2019, Lu *et al.*, 2024). In this study, the recombinantly expressed $McsB_{SA}$ (with the addition of His-tags at each terminus) was observed to be approximately 42 kDa. In addition to similar molecular weights, $McsB_{SA}$ and $McsB_{GS}$, have similar theoretical isoelectric points (pI) (5.09 and 5.37 respectively) and a similar amino acid length of 335 and 363 amino acid residues respectively. The pET-38a (+) $McsB_{SA}$ plasmid contained an N-terminal and a C-terminal His-tag whereas the pET21-mcsB-His620 plasmid constructed by Suskiewicz and co-workers contained only an N-terminal His-tag sequence (Suskiewicz *et al.*, 2019). Recombinant expression has been reported to result in proteins that are often aggregated or packaged in inclusion bodies however the precise reason has not been elucidated (Chung *et al.*, 2017). However, several factors have been recognised to contribute to protein insolubility. These

factors include the pH, presence of cofactors and folding mechanisms of the host (*S. aureus* for this study) differing to that of the transformed cell line (*E. coli* for this study)(Chung *et al.*, 2017). Expression conditions have also been evaluated and the following criteria have been previously identified to affect protein solubility: temperature, pH, salt concentration, selected media, solutes such as sugars, solvent properties and constituents (Bhatwa *et al.*, 2021, Pouresmaell and Azizi-Dargahlou, 2023) .

Two separate approaches were undertaken to obtain soluble $McsB_{SA}$. The first approach aimed to solubilise protein from the already insolubly expressed $McsB_{SA}$ (packaged in inclusion bodies) by means of sarkosyl solubilisation whilst the second approach sought to optimise expression conditions to increase the yield of soluble $McsB_{SA}$. Sarkosyl solubilisation is one of several non-denaturing approaches employed to increase the solubility of recombinant proteins and is generally preferred over denaturing methods incorporating urea or guanidine hydrochloride as this requires refolding of the protein and is more time consuming (Chung *et al.*, 2017). Both approaches led to low yields, however the first approach led to higher yields of soluble $McsB_{SA}$ when compared to the latter approach. This notwithstanding, the increased yield of $McsB_{SA}$ was ultimately unsatisfactory as the sarkosyl present in the sample brought about complications in the purification process and with the thermal shift assay, specifically, the SYPRO orange dye. Sarkosyl was removed by adding 2% Triton X-100 and 20 mM CHAPS to the lysate containing 1% sarkosyl prior to purification (Tao *et al.*, 2010, Massiah *et al.*, 2016). Triton X-100 and CHAPS are both detergents commonly used to aid in protein solubility (Massiah *et al.*, 2016). The purification yielded low levels of $McsB_{SA}$ (APPENDIX C, Figure C1) and was not always reproducible which was determined to be a consequence of incomplete sarkosyl removal as sarkosyl is known to deter efficient binding of His-tagged proteins to metal chelate affinity resins (Palmer and Wingfield, 2004). Consequently, the soluble fraction obtained from the optimised expression conditions was selected for future purification attempts. This decision was further reinforced by TSA experiments evaluating the purified $McsB_{SA}$ samples obtained after sarkosyl removal whereby a T_m could not be determined due to high initial fluorescence readings (APPENDIX C, Figure C2). Thermal shift assays containing detergents have been observed to have high background noise resulting from the dye binding non-specifically and thus hindering the assay (Errasti-Murugarren *et al.*, 2021, Gooran and Kopra, 2024). Specifically, ionic detergents such as sarkosyl interfere with the assay as they are composed of a positive/negative charged head group and a hydrophobic acyl chain tail. SYPRO orange dye has an affinity for hydrophobic regions and therefore binds to the detergent before the protein of interest can unfold (Errasti-

Murugarren *et al.*, 2021, Gooran and Kopra, 2024). Purification of $McsB_{SA}$ samples obtained through optimised expression conditions and subsequent buffer exchange using the PD-10 column resulted in a satisfactory yield of $McsB_{SA}$ which was quantified using a standard Bradford assay. Samples were analysed *via* SDS-PAGE and subsequently *via* western blot. A single protein band of approximately 42 kDa resembling the monomer of $McsB_{SA}$ was observed when evaluated under reducing conditions as previously reported (Suskiewicz *et al.*, 2019, Hajdusits *et al.*, 2021, Lu *et al.*, 2024).

Proteins need to meet certain criteria to be suitable for thermal stability assays. Specifically for the TSA, proteins are required to have low surface hydrophobicity, a hydrophobic core and a melting temperature which falls in the range of the RT-PCR instrument (>30℃ and <95℃ in this case) (Pantoliano *et al.*, 2001, Ericsson *et al.*, 2006, Niesen *et al.*, 2007). The hydrophobicity of both the control protein (papain) and $McsB_{SA}$ were evaluated through amino acid analysis and hydrophobicity plots. The analysis revealed both proteins contained hydrophobic amino acids that comprised approximately 35% of the total amino acid composition. The thermal shift assay was optimised using the control protein papain. Papain is a cysteine protease acquired from the latex of *Carica papaya* (papaya plant). The protein was analysed as per the conditions outlined by Niesen and co-workers who reported that a protein concentration of 75 µg/ml (0.075 µg/µl) is normally sufficient to accurately measure the T_m of a protein with a molecular weight of 35 kDa in conjunction with 5X SYPRO orange dye (Niesen *et al.*, 2007). We assessed papain at 0.15, 0.25, 0.35 and 0.45 µg/µl in the presence of 5X or 10X SYPRO orange dye in a final reaction volume of 20 µl. A T_m of approximately 80℃ was observed for papain which concurred with the T_m of 83℃ previously determined by DSC (Sathish *et al.*, 2007). The ratio of dye to protein concentration did not affect the T_m obtained for papain which has been reported previously for other proteins (Ericsson *et al.*, 2006, Niesen *et al.*, 2007, Lavinder *et al.*, 2009). It was observed that a higher SYPRO orange concentration yielded a higher fluorescence for each concentration of papain analysed which indicated that the 5X SYPRO orange dye was not sufficient to bind all the hydrophobic exposed residues of papain at each concentration. It was also noted that the fluorescence increased as the concentration of papain increased which was expected as this would increase the level of hydrophobic residues available for the dye to bind.

The optimised conditions derived from the papain TSA were implemented to determine the thermal stability of $McsB_{SA}$. The T_m of $McsB_{GS}$ reported by Suskiewicz and colleagues was 61.05 ± 0.1℃ which does not coincide with the T_m we detected for $McsB_{SA}$ (49.73 ± 0.21℃,

most stable form of $McsB_{SA}$ achieved without a ligand when the buffer screening was conducted) (Suskiewicz *et al.*, 2019). Sequence alignment analysis performed between $McsB_{SA}$ and $McsB_{GS}$ revealed a shared sequence identity of 43.2% which was further scrutinised to identify 30 more hydrophobic amino acids (based on the Kyte and Doolittle index) present in the sequence of $McsB_{GS}$ as compared to $McsB_{SA}$. Electrostatic interactions, van der Waals forces, disulfide bonding, hydrogen bonding and hydrophobic interactions are forces which contribute towards protein stability (Dill, 1990, Pace, 1990, Pace, 1992). Hydrophobic interactions account for majority of a protein's stability (50.8%) whilst hydrogen bonding contributes 27.1% and the remaining forces contribute 22.1% (Pace, 1990, Pace, 1992). Structural alignments, specifically between the monomers, revealed the structures to be almost identical and therefore the differences observed within the sequences of $McsB_{SA}$ and $McsB_{GS}$ - more specifically the differences in hydrophobic residues- were determined to account for the difference observed in T_m between the two McsB orthologues

A recent study by Lu and co-workers established the T_m of $McsB_{SA}$ to be 40.50 ± 0.02℃ through thermal shift analysis (Lu *et al.*, 2024). Lu and co-workers established the T_m of $McsB_{SA}$ using a gel filtration buffer [20 mM Tris-HCl, 300mM NaCl and 1 mM Tris(2-carboxyethyl)phosphine (TCEP), pH 7.5], however in this study, a T_m of 45.35 ± 0.34℃ was observed for $McsB_{SA}$ when evaluated with a Tris-HCl pH 7.5 buffer (the most similar buffer tested) (Lu *et al.*, 2024). The 300 mM NaCl, 1 mM TCEP and removal of the N-terminal HIS-tag were the only discrepancies identified (SYPRO orange dye concentration was omitted as it did not affect melting temperature between samples when pH and salt concentration are kept constant) as possible causes for the difference in melting temperature observed between studies. TCEP is a bulky reducing agent that reduces disulfide bonds and may have been a contributing factor to the reported reduced T_m by Lu and colleagues as structural disulfide bonds play an integral role in protein folding and stability (Liu *et al.*, 2016, Lu *et al.*, 2024). The increased salt concentration (300 mM NaCl) was evaluated at pH 7.5 and it was determined that a higher salt concentration could possibly increase the thermal stability of a protein or have no effect on the thermal stability as the effects are protein specific and therefore was considered as a non-contributing factor to the difference in T_m observed (Lindman *et al.*, 2006). The cleavage of the N-terminal His-tag has been evaluated to have numerous effects on protein stability (thermal stability could increase, decrease or remain unchanged) and the effects are protein specific (Booth *et al.*, 2018), thus indicating for $McsB_{SA}$ specifically, the cleavage of the N-terminal His-tag combined with the addition of the reducing agent TCEP accounted for the discrepancy in T_m attained through TSA analysis.

The CETSA is typically conducted in cells or using cell lysate (Jafari *et al.*, 2014, Weidinger *et al.*, 2024). For this study, we opted to perform the assay utilising cell lysate to account for any inconsistencies in cell lysis and / or $McsB_{SA}$ insoluble expression. A reported T_{agg} for McsB (all strains) could not be attained from literature and thus the T_{agg} of 48.28 ± 0.18℃ for $McsB_{SA}$ could not be compared. Accordingly, this study represents the first reported T_{agg} for the protein. The study could be improved through the addition of an internal reference control protein with a known T_{agg} which would serve to further validate the derived aggregation temperature of $McsB_{SA}$ in this study.

The derived T_m and the T_{agg} of $McsB_{SA}$ are two distinct measures of thermal stability whereby the first denotes the temperature at which 50% of the protein had unfolded whereas the second indicates the temperature at which 50% of the protein sample had aggregated and become insoluble. The obtained T_m for $McsB_{SA}$ was observed to be higher than the T_{agg} thus suggesting that the protein begins to aggregate prior to unfolding. A T_m is derived by exposing the protein to a temperature profile which causes the protein to unfold whereas protein aggregation may occur under normal physiological conditions, stress-induced (high temperature, oxidative stress, heavy metals, pH) protein misfolding, and protein denaturation (Weids *et al.*, 2016). These factors could account for the $T_m > T_{agg}$, specifically the contrasting conditions of the assays as the CETSA was conducted in a more native environment which was not optimal for the protein and thus resulted in aggregation whereas the melting temperature was determined using pure protein under optimised experimental conditions. The thermal shift assays were conducted using technical replicates whereas the CETSA assays were conducted using independent replicates, as such, the assays could be improved by selecting a single approach to further exemplify the reproducibility of the two thermal assays. Comparison of the TSA and CETSA have revealed a good congruence between the T_m and T_{agg} respectively which has been previously reported (Asial *et al.*, 2013, Delport and Hewer, 2019). Overall, the protein arginine kinase $McsB_{SA}$ was determined to be suitable for use within thermal stability assays, specifically the TSA and CETSA, as the T_m and T_{agg} were established.

4.2. Thermal stability assays identified novel $McsB_{SA}$ ligands

First, the Protein Thermal Shift™ Starter kit was evaluated to optimise parameters of the assay for use with the QuantStudio 5 Real-Time PCR System (Thermo Fisher Scientific, USA). The kit contained a control protein with a cognate, control, ligand, and it was observed that increasing ligand concentrations resulted in an increased T_m of the control protein while an increase in fluorescence intensity was also noted. The increase in fluorescence intensity was

not attributed to protein concentration or dye concentration as these parameters were kept constant whilst the ligand concentration increased. However, the increase in ligand concentration alone was not responsible for the increased raw fluorescence as confirmed by the LOC where it was assessed that the ligand lacked hydrophobic regions for the dye to bind (evident by the lack of fluorescence detected). The fluorescence intensity increase was only detected when the control ligand binds to the control protein resulting in a complex which stabilised the control protein and resulted in a configuration that has more hydrophobic residues exposed as the protein complex unfolds. The TSA was able to detect ligand binding by measuring the melting temperature of the control protein.

Subsequently, the binding of the N-terminally acetylated CtsR-derived sequence, Ac-KRGGGGYIKIIKV-OH peptide designed by Suskiewicz and colleagues, to $McsB_{SA}$ was evaluated *via* the CETSA (Suskiewicz *et al.*, 2019). The peptide was designed to assess the efficacy of $McsB_{GS}$ to recognise arginine residues within a peptide *via* mass spectrometry (Suskiewicz *et al.*, 2019). Although $McsB_{GS}$ was able to recognise and phosphorylate the peptide, thermal stability assays were never conducted on $McsB_{GS}$ with the designed peptide (Suskiewicz *et al.*, 2019). Thermal stability assays such as the CETSA have routinely been utilised to detect the binding of compounds that are generally much larger than a peptide, however, Tan and co-workers detected binding of a stapled peptide to both MDM2 and MDM4 proteins, which are structurally related proteins that act as key negative regulators of the tumour suppressor protein p53 (Tan *et al.*, 2015). The binding of the peptide was detected by conducting a lysate CETSA similar to the protocol implemented in this study (Tan *et al.*, 2015). The binding of the N-terminally acetylated CtsR-derived sequence, Ac-KRGGGGYIKIIKV-OH peptide to $McsB_{SA}$ was confirmed by an increased T_{agg} observed for $McsB_{SA}$ when incubated with 100 µM of the peptide. Thus, indicating that $McsB_{SA}$ could recognise the arginine present in the peptide (as observed for $McsB_{GS}$), providing insight regarding structural similarities existing between the McsB orthologues, and most importantly, the efficacy of the CETSA as a tool to detect ligand binding, specifically for $McsB_{SA}$. The experimental design could be improved upon with the inclusion of a solvent control to further validate the observed increase in T_{agg} was a result of the peptide binding and not due to the addition of the solvent (autoclaved Milli-Q water).

$McsB_{SA}$ was screened against the Pandemic Response Box of compounds. The Pandemic Response Box consisted of a collection of anti-bacterial, anti-viral and anti-fungal compounds which are currently in different phases of drug discovery or development. The Pandemic

Response Box was specifically designed to accelerate drug discovery efforts through the repositioning / repurposing of currently approved drugs (Samby *et al.*, 2022). In recent studies, the Pandemic Response Box was screened and numerous discoveries have been reported, such as the potential use of ezetimibe and benzodiazepinone as specific inhibitors of the *Plasmodium falciparum* malarial chaperone system (Singh *et al.*, 2023), the identification of a quinoline derivative with significant anthelmintic activity against *Haemonchus contrortusi* and *Caenorhabditis elegans* (Shanley *et al.*, 2022), the discovery of multistage and potent transmission-blocking antimalarial compounds (Reader *et al.*, 2021), the identification of four inhibitors of the microsporidian *Nematocida parisii* (Huang *et al.*, 2023), the efficacy of epetraborole as a novel potent *Mycobacterium abscessus* inhibitor (Kim *et al.*, 2021), the activity of Oloform and twenty three other compounds against the *Sporothrix brasiliensis* pathogen (Borba-Santos *et al.*, 2022) and numerous others which supported the utilisation of the Pandemic Response Box in this study which aimed to discover novel $McsB_{SA}$ ligands. In this study, the 400 structurally diverse compounds were grouped into cocktails as has been done previously in studies designed to screen compound or fragment libraries through the TSA (Mashalidis *et al.*, 2013, Valenti *et al.*, 2013, Elkin *et al.*, 2015, Gao *et al.*, 2020). The TSA was selected as our primary screening tool as it has been described to be medium-throughput whereas the CETSA is better suited for late stages of ligand identification as it is not amenable to medium or high-throughput screening. The cocktail screen identified four cocktails which significantly increased the T_m of $McsB_{SA}$ by ≥ 8℃. These four cocktails were further evaluated and additive/synergistic effects between compound groups were explicitly described for cocktail A1 similar to the drug combination evaluations performed by Boonyalai and colleagues (Boonyalai *et al.*, 2024). Cocktail A1 was further divided into cocktails A1.1 and A1.2 and the five compounds present in cocktail A1.1 were delineated to contribute to the induced increase in T_m of $McsB_{SA}$ that was initially observed for cocktail A1. However, a distinct pattern of stabilization could not be delineated between combinations of the five compounds. Interestingly, none of the compounds present in cocktail A1 induced any significant shifts in the T_m of $McsB_{SA}$ when screened individually at 10 µM and thus we prioritised identifying individual compounds which induced an increase in the T_m of the protein, therefore, cocktail A1, specifically the five compounds present which contributed to the induced increase in T_m were not further evaluated. The structures of compounds MMV1578560 and MMV1782223 contain fluorine in their structures which may promote binding of the compound to $McsB_{SA}$ in the unfolded state as the carbon-fluorine bond is highly lipophilic which may result in enhanced interactions with the exposed hydrophobic regions of a protein when unfolded (APPENDIX I, Figure I1).

The remaining three cocktails (B4, C3 and E3) were scrutinised, and nine compounds were delineated to have induced an increase in the T_m of $McsB_{SA}$. These nine compounds were further examined through CETSA analysis which revealed compounds MMV1593539, MMV1578899, MMV1634391, MMV1782213 and MMV1782355 to induce a significant increase ($p<0.05$) in the T_{agg} for $McsB_{SA}$. Discrepancies in the compounds identified between the two thermal shift assays were suggested to be caused by distinct differences in assay conditions. The TSA samples consisted of a purified expression product of $McsB_{SA}$ without any contaminating proteins present, whereas the CETSA was conducted in a native environment using lysate containing numerous proteins which could have interfered with the binding of compounds MMV1593531, MMV1580485, MMV1633968 and MMV658803. The solubility of the compounds was also determined to be a contributing factor as compound MMV1633968 was predicted to be poorly soluble through analysis conducted using the SwissADME in silico tool.

An $ITDRF_{CETSA}$ was conducted to further validate the binding of compound MMV1593539 (identified as out best $McsB_{SA}$ binder) and to interrogate the efficacy of compounds MMV1580485, MMV1633968 and MMV1782213 to bind to $McsB_{SA}$. Compound MMV1580485 induced non-significant decreases ($p>0.05$) in $McsB_{SA}$ levels whereas compound MMV1782213 induced significant increases in $McsB_{SA}$ levels. A significant increase in $McsB_{SA}$ levels was induced by compound MMV1634968 which was similar to that of compound MMV1782213 and thus the binding interaction of compound MMV1633968 was further evaluated. Compounds MMV658803, MMV1593531 and MMV1580485 were not further assessed due to their poor binding efficacies displayed in the CETSA and $ITDRF_{CETA}$ assays. The compounds MMV658803 and MMV1580485 contained chloride ions in their structures which would increase the negative charge of the ligand and promote binding to a positively charged metal and may account for the weak binding observed in the thermal stability assays (APPENDIX I, Figure I2). In this study, thermal stability assays conducted revealed at least nine compounds from the Pandemic Response Box of compounds as $McsB_{SA}$ ligands, however only six were selected for further evaluation which were compounds MMV1593539, MMV1578899, MMV1634391, MMV1633968, MMV1782213 and MMV1782355. Specifically, compound MMV1593539, was delineated as our best anti-bacterial $McsB_{SA}$ binder and compound MMV1782355 as our best anti-viral $McsB_{SA}$ binder.

4.3. In silico $McsB_{SA}$ ligand screening corroborates thermal stability assay discoveries

The putative ATP binding and pArg binding sites of $McsB_{SA}$ were predicted through structural comparisons between $McsB_{GS}$ and $McsB_{SA}$ implementing both SiteMap and Protein Structural Alignment tools. The six identified $McsB_{SA}$ ligands were docked in both the putative pArg and ATP sites of $McsB_{SA}$.

The compound MMV1593539, a bis-indole derivative, has been shown to act as a pyruvate kinase (PK) inhibitor (Veale *et al.*, 2015, Shanley *et al.*, 2022, Huang *et al.*, 2023). The bis-indole derivative, bisindolyl maleimide 2 (BIM2), has been shown to bind tightly in the ATP pocket of protein kinase (Gassel *et al.*, 2004). Similarly, molecular docking revealed that MMV1593539 docked better to the ATP binding site as opposed to the pArg binding site of $McsB_{SA}$ thus proposing a similar mode of action to that of BIM2 (Gassel *et al.*, 2004, Zoraghi *et al.*, 2014). Structural comparisons between MMV1593539 and other bisindolyl derivatives revealed that the compound lacks the maleimide group which may contribute to the relatively low docking score (-6.518) obtained when compared to the ATP control (-12.616). The minor groove binder (MMV1634391, MGB-BP-3) docked favourably in the ATP site of $McsB_{SA}$ corroborating CETSA analysis which determined binding of the compound to $McsB_{SA}$ through an increased T_{agg}. Phenethyl butyrate (MMV1578899) induced a significant increase in both the T_m and T_{agg} for $McsB_{SA}$, however, docked poorly to the putative pArg and ATP sites. This implied that the compound whilst still binding to $McsB_{SA}$ may occupy a space on the protein other than the known sites which were docked.

The highest docking score (-7.873) was observed for the anti-viral compound MMV1782355 (peldesine or BCX-34) when docked in the putative ATP site. Peldesine was identified as our best predicted ligand based on both thermal stability studies and molecular docking studies. Structural analysis of the peldesine compound revealed a guanine ring present which indicated the possible binding mechanism of the compound (APPENDIX H, Table H1.). The compound MMV1782213 (RDEA806) induced a significant increase in the T_{agg} of $McsB_{SA}$ and significant increases in $McsB_{SA}$ levels through the $ITDRF_{CETSA}$ was also observed, however was not corroborated through molecular docking as unfavourable docking scores were obtained which signified that this compound may be binding to the protein at a site other than the pArg or ATP binding site, as was observed for compound MMV1578899. Structural analysis of OBR-5-340 (compound MMV1633968) identified an adenine like-ring in the centre of the compound which elucidated a possible binding mechanism of the compound within the putative ATP binding site of $McsB_{SA}$ and also explains the low shifts in thermal stability and

low docking scores due to the central position of the adenine-like ring. Molecular docking predicted that compounds MMV1593539, MMV1634391, MMV1633968 and MMV1782355 bind to the ATP pocket of McsB having docked favourably in the putative ATP site as opposed to the pArg site whilst compounds MMV1578899 and MMV1782213 displayed poor docking scores in both sites.

4.4. Evaluating potency of identified $McsB_{SA}$ ligands *in vivo*

The inhibitory properties of the six identified ligands were explored through minimum inhibitory concentrations assays conducted on *S. aureus* (ATCC25923). The compound MMV1593539 a bis-indole derivative, has previously been reported to have anthelmintic activity against *H. contrortus (Shanley et al., 2022)*, to decrease spore viability in the microsporidia *N. parisii and Pancytospora epiphaga* (Huang *et al.*, 2023) and most importantly, has been shown to act as a PK inhibitor which has shown potency against MRSA (Zoraghi *et al.*, 2014, Veale *et al.*, 2015). However, the ligand had previously been reported to be inactive against *S. aureus* up to 20 µM which was the upper limit of our inhibition study (Zoraghi *et al.*, 2014). Compound MMV1634391, MGB-BP-3 is a minor groove binder which has been reported to be highly active against the tachyzoite stage of *Toxoplasma gondii* (Dos Santos *et al.*, 2023). The compound was designed to bind to *Trypanosoma brucei* nuclear and kinetoplast DNA (Dos Santos *et al.*, 2023).

Peldesine or BCX-34 (compound MMV1782355) has been described as a novel potent purine nucleoside phosphorylase (PNP) inhibitor that underwent human clinical trials for the treatment of HIV infection and T-cell cancers. The compound MMV1633968 (OBR-5-340) is a bioavailable pyrazolopyrimidine which has potent *in vivo* activity against capsid formation of rhinoviruses (Wald *et al.*, 2019). RDEA806 (MMV1782213) was identified as a novel nonnucleoside reverse transcriptase inhibitor (NNRTI) and has been shown to display potent activity against NNRTI-resistant HIV-1 (Moyle *et al.*, 2010). None of the novel $McsB_{SA}$ ligands were capable of complete inhibition of *S. aureus* growth which indicated that the compounds do not have any toxic effects on the gram-positive pathogen. Although the identified novel ligands did not reduce *S. aureus* growth under standard assay conditions where $McsB_{SA}$ is functioning primarily as a dimer, additional testing is required to assess the efficacy of the compounds to bind and inhibit *S aureus* growth under induced stress conditions where we suspect $McsB_{SA}$ to favour octamer formation.

4.5. Conclusion

A recombinant form of $McsB_{SA}$ was successfully expressed and purified under conditions which were found to effectively increase the melting temperature of $McsB_{SA}$ as we reported a melting temperature 9.23℃ higher than previously reported (Lu *et al.*, 2024). This increase was attributed to a change in buffer and pH, as it was elucidated that the protein arginine kinase was more stable when a sodium phosphate, pH 7.4 buffer was implemented as compared to a Tris-HCl, pH 7.5 buffer. The recombinantly expressed $McsB_{SA}$ in this study contained an N-terminal and a C-terminal HIS tag which differed to that of Lu and co-workers as they cleaved off the proteins' HIS tag and was thus untagged. This difference was also a contributing factor towards the increased melting temperature observed in this study. More importantly, a second thermal stability measurement was evaluated through CETSA analysis, and we derived the first reported aggregation temperature for McsB, more specifically, $McsB_{SA}$.

Thermal shift assays initially identified at least nine compounds from the MMV and DNDi Pandemic Response Box of compounds as $McsB_{SA}$ binders whilst the initial cocktail screening also emphasized the existence of additive/synergistic effects between compounds when grouped. The CETSA corroborated five of these compounds and an additional compound was verified due to induced increases in $McsB_{SA}$ levels observed through $ITDRF_{CETSA}$ analysis and thus we validated at least six compounds as novel $McsB_{SA}$ ligands. These six $McsB_{SA}$ ligands were further evaluated through in silico analysis and the anti-bacterial compound MMV1593539 and the anti-viral compound MMV1782355 were identified as our best $McsB_{SA}$ binders which were both predicted to bind to the ATP pocket of $McsB_{SA}$**.** The inhibitory effects of all six ligands were elucidated through minimum inhibitory concentration assays conducted on *S. aureus* (ATCC25923) and it was established that none of the derived novel $McsB_{SA}$ ligands were effective in inhibiting *S. aureus* growth which indicated that the identified ligands compounds do not exhibit any toxic effects up to 20 µM. This study was successful in deriving an aggregation temperature for the integral protein arginine kinase $McsB_{SA}$ and more importantly, identifying at least six novel $McsB_{SA}$ ligands from the Pandemic Response Box.

4.6. Future Studies

The additive/synergistic effects observed from the initial cocktail screening provide an opportunity to explore fragment linking for future drug discovery studies aimed to increase the binding affinities of ligands with McsB. The six identified ligands present promising candidates for future drug discovery efforts aimed at inhibiting or exploiting the protein arginine kinase $McsB_{SA}$. Inhibition of $McsB_{SA}$ could be achieved through the development of specific inhibitors

of $McsB_{SA}$ as these compounds provide a suitable platform for future drug discovery efforts. The specific exploitation of $McsB_{SA}$ could be achieved through the recruitment of the protein to aid in targeted protein degradation. This could be accomplished through the design of a heterobifunctional molecule (degrader / BacPROTAC) utilising either compounds MMV1578899 or MMV1782213 as they were proposed to bind outside of the known ATP and pArg binding sites and thus would allow $McsB_{SA}$ to retain catalytic activity and mark targeted proteins for degradation. These novel $McsB_{SA}$ ligands could possibly lay the groundwork for future development of novel BacPROTACS for specific targeted protein degradation.

REFERENCES

Ali, J., Camilleri, P., Brown, M. B., Hutt, A. J. & Kirton, S. B. 2012. Revisiting the general solubility equation: In silico prediction of aqueous solubility incorporating the effect of topographical polar surface area. *Journal of Chemical Information and Modeling*, 52, 420-428.

Aljghami, M. E., Barghash, M. M., Majaesic, E., Bhandari, V. & Houry, W. A. 2022. Cellular functions of the ClpP protease impacting bacterial virulence. *Frontiers in Microbiology*, 9, 1054408.

Arcon, J.P., Defelipe, L.A., Modenutti, C.P., López, E.D., Alvarez-Garcia, D., Barril, X., Turjanski, A.G. and Martí, M.A., 2017. Molecular dynamics in mixed solvents reveals protein–ligand interactions, improves docking, and allows accurate binding free energy predictions. *Journal of chemical information and modeling*, 57, 846-863.

Arifuzzaman, M., Kwon, E. & Kim, D. Y. 2024. Structural insights into the regulation of protein-arginine kinase McsB by McsA. *Proceedings of the National Academy of Sciences*, 121, 1-10.

Asial, I., Cheng, Y. X., Engman, H., Dollhopf, M., Wu, B., Nordlund, P. & Cornvik, T. 2013. Engineering protein thermostability using a generic activity-independent biophysical screen inside the cell. *Nature Communications*, 4, 1-8.

Avci, F. G. 2024. Unraveling bacterial stress responses: Implications for next-generation antimicrobial solutions. *World Journal of Microbiology and Biotechnology*, 40, 1-14.

Ayon, N. J. 2023. High-throughput screening of natural product and synthetic molecule libraries for antibacterial drug discovery. *Metabolics,* 13, 625.

Azvolinsky, A. 2017. Repurposing existing drugs for new indications. *The Scientist*.

Baell, J. B. & Holloway, G. A. 2010. New substructure filters for removal of pan assay interference compounds (PAINS) from screening libraries and for their exclusion in bioassays. *Journal of Medicinal Chemistry*, 53, 2719-2740.

Berdigaliyev, N. & Aljofan, M. 2020. An overview of drug discovery and development. *Future Medicinal Chemistry*, 12, 939-947.

Bhatwa, A., Wang, W., Hassan, Y. I., Abraham, N., Li, X. & Zhou, T. 2021. Challenges associated with the formation of recombinant protein inclusion bodies in *Escherichia coli* and strategies to address them for industrial applications. *Frontiers in Bioengineering and Biotechnology*, 9, 1-18.

Bittrich, S., Segura, J., Duarte, J. M., Burley, S. K. & Rose, Y. 2024. RCSB protein Data Bank: exploring 3D similarities via comprehensive structural alignments. *Bioinformatics*, 40, 1-4.

Boggon, T. J. 2019. ARGuing for a new kinase class *Nature Chemical Biology*, 15, 431-432.

Boonyalai, N., Peerapongpaisarn, D., Thamnurak, C., Oransathid, W., Wongpatcharamongkol, N., Oransathid, W., Lurchachaiwong, W., Griesenbeck, J., Waters, N. C., Demons, S. T., Ruamsap, N. & Vesely, B. A. 2024. Screening of the pandemic response box library identified promising compound candidate drug combinations against extensively drug-resistant *Acinetobacter baumannii*. *Scientific Reports*, 14, 1-14.

Booth, W. T., Schlachter, C. R., Pote, S., Ussin, N., Mank, N. J., Klapper, V., Offermann, L. R., Tang, C., Hurlburt, B. K. & Chruszcz, M. 2018. Impact of an N-terminal polyhistidine tag on protein thermal stability. *ACS Omega*, 3, 760-768.

Borba-Santos, L. P., Rollin-Pinheiro, R., Da Silva Fontes, Y., Dos Santos, G. M. P., De Sousa Araujo, G. R., Rodrigues, A. M., Guimaraes, A. J., De Souza, W., Frases, S., Ferreira-Pereira, A., Barreto-Bergter, E. & Rozental, S. 2022. Screening of pandemic response box library reveals the high activity of olorofim against pathogenic Sporothrix species. *Journal of Fungi,* 8, 1-14.

Bradford, M. M. 1976. A rapid and sensitive method for the quantitation of microgram quantities of protein utilizing the principle of protein-dye binding. *Analytical Biochemistry*, 72, 248-254.

Bruce, D., Cardew, E., Freitag-Pohl, S. & Pohl, E. 2019. How to stabilize protein: stability screens for thermal shift assays and nano differential scanning fluorimetry in the Virus-X project. *Journal of Visualized Experiments*, 144, 1-11.

Chang, A. Y., Chau, V. W., Landas, J. A. & Pang, Y. 2017. Preparation of calcium competent *Escherichia coli* and heat-shock transformation. *JEMI Methods*, 1, 22-25.

Chatterjee, I., Becker, P., Grundmeier, M., Bischoff, M., Somerville, G. A., Peters, G., Sinha, B., Harraghy, N. & Proctor, R. A. 2005. *Staphylococcus aureus* ClpC is required for stress resistance, aconitase activity, growth recovery, and death. *Journal of Bacteriology*, 187, 4488-4496.

Chatterjee, I., Schmitt, S., Batzilla, C. F., Engelmann, S., Keller, A., Ring, M. W., Kautenburger, R., Zieburh, W., Hecker, M., Lenhof, H., Somerville, G. A. & Herrmann, M. 2009. *Staphylococcus aureus* ClpC ATPase is a late growth phase effector of metabolism and persistence. *Proteomics*, 9, 1152-1176.

Chung, J. M., Lee, S. & Jung, H. S. 2017. Effective non-denaturing purification method for improving the solubility of recombinant actin-binding proteins produced by bacterial expression. *Protein Expression and Purification*, 133, 193-198.

Cimmperman, P., Baranauskiene, L., Jachimoviciute, S., Jachno, J., Torresan, J., Michailovienė, V., Matuliene, J., Sereikaite, J., Bumelis, V. & Matulis, D. 2008. A quantitative model of thermal stabilization and destabilization of proteins by ligands. *Biophysical Journal*, 95, 3222-3231.

Culp, E. & Wright, G. D. 2017. Bacterial proteases, untapped antimicrobial drug targets. *The Journal of Antibiotics*, 70, 366-377.

Daina, A., Michielin, O. & Zoete, V. 2014. iLOGP: A simple, robust, and effecient description of *n*-Octanol/water partition coefficient for drug design using the GB/SA approach. *Journal of Chemical Information and Modeling*, 54, 3284-3301.

Daina, A., Michielin, O. & Zoete, V. 2017. SwissADME: a free web tool to evaluate pharmacokinetics, drug-likeness and medicinal chemistry friendliness of small molecules. *Scientific Reports*, 7:42717.

De Oliveira, D. M. P., Forde, B. M., Kidd, T. J., Harris, P. N. A., Schembri, M. A., Beatson, S. A., Paterson, D. L. & Walker, M. J. 2020. Antimicrobial resistance in ESKAPE pathogens. *Clinical Microbiology Reviews* 33, 10-1128.

Delaney, J. S. 2004. ESOL: Estimating aqueous solubility directly from molecular structure. *Journal of Chemical Information and Computer Sciences*, 44, 1000-1005.

Delport, A. & Hewer, R. 2019. Determining the protein stability of Alzeheimer's Disease protein, amyloid precursor protein. *The Protein Journal*, 38, 419-424.

Delport, A. & Hewer, R. 2022. A superior loading control for the cellular thermal shift assay. *Scientific Reports*, 12, 1-8.

Deng, Y. and Roux, B., 2009. Computations of standard binding free energies with molecular dynamics simulations. *The Journal of Physical Chemistry B*, 113, 2234-2246.

Deore, A. B., Dhumane, J. R., Wagh, H. V. & Sonawane, R. B. 2019. The stages of drug discovery and development process. *Asian Journal of Pharmaceutical Research and Development* 7, 62-67.

Dill, K. A. 1990. Dominant forces in protein folding. *Biochemistry*, 29, 7133-1755.

Dos Santos, B. R., Ramos, A. B. D. S. B., De Menezes, R. P. B., Scotti, M. T., Colombo, F. A., Marques, J. & Reimao, J. Q. 2023. Repurposing the medicines for Malaria venture's COVID box to discover potent inhibitors of *Toxoplasma gondii,* and *in vivo* efficacy evaluation of almitrine bismesylate (MMV1804175) in chronically infected mice. *Public Library of Science One*, 18, 1-16.

Du, D., Yuan, S. & Xiong, J. 2024. Determining the *in vitro* ligand-target interaction by cellular thermal shift assay and isothermal dose-response fingerprint assay. *Bio-protocol*, 14, 1-7.

Durrant, J. D., McCammon, J. A. Molecular dynamics simulations and drug discovery. *BMC Biology*, 9, 1-9.

Duvic, M., Olsen, A., Omura, G. A., Maize, J. C., Vonderheid, E. C., Elmets, C. A., Shupack, J. I., Demierre, M., Kuzel, T. M. & Sanders, D. Y. 2001. A phase III, randomized, double-blind, placebo-controlled study of peldesine (BCX-34) cream as topical therapy for cutaneous T-cell lymphoma. *Journal of the American Academy of Dermatology*, 44, 940-947.

Elkin, L. L., Harden, D. G., Saldanha, S., Ferguson, H., Cheney, D. L., Pieniazek, S. N., Maloney, D. P., Zewinski, J., O' Connell, J. O. & Banks, M. 2015. Just-in-time compound pooling increases primary screening capacity without compromising screening quality. *Journal of Biomolecular Screening*, 20, 577-587.

Ellington, W. R. 2001. Evolution and physiological roles of phosphagen systems. *Annual Review of Physiology*, 63, 289-325.

Elsholz, A., Hempel, K., Pother, D., Becher, D., Hecker, M. & Gerth, U. 2011. CtsR inactivation during thiol-specific stress in low GC, Gram+ bacteria. *Molecular Microbiology,* 79, 772-785.

Elsholz, A. W., Turgay, K., Michalik, S., Hessling, B., Gronau, K., Oertel, D., Mader, U., Bernhardt, J., Becher, D., Hecker, M. & Gerth, U. 2012. Global impact of protein arginine phosphorylation on the physiology of *Bacillus subtilis. Proceedings of the National Academy of Sciences*, 109, 7451-7456.

Ericsson, U. B., Hallberg, B. M., Detitta, G. T., Dekker, N. & Nordlund, P. 2006. Thermofluor-based high-throughput stability optimization of proteins for structural studies. *Analytical Biochemistry,* 357, 289-298.

Errasti-Murugarren, E., Bartoccioni, P. & Palacin, M. 2021. Membrane protein solubilisation strategies for structural and functional studies. *Membranes*, 11, 1-17.

Fan, J., Fu, A. & Zhang, L. 2019. Progress in molecular docking. *Quantitative Biology*, 7, 83-89.

Frees, D., Chastanet, A., Qazi, S., Sorensen, K., Hill, P., Msadek, T. & Ingmer, H. 2004. Clp ATPases are required for stress tolerance, intracellular replication and biofilm formation in *Staphylococcus aureus. Molecular Microbiology*, 54, 1445-1462.

Frees, D., Gerth, U. & Ingmer, H. 2014. Clp chaperones and proteases are central in stress survival, virulence and antibiotic resistance of *Staphylococcus aureus. International Journal of Medical Microbiology,* 302, 142-149.

Frees, D., Savijoki, K., Varmanen, P. & Ingmer, H. 2007. Clp ATPases and ClpP proteolytic complexes regulate vital biological processes in low GC, Gram-positive bacteria. *Molecular Microbiology*, 63, 1285-1295.

Friesner, R. A., Banks, J. L., Murphy, R. B., Halgren, T. A., Klicic, J. J., Mainz, D. T., Repasky, M. P., Knoll, E. H., Shelley, M. & Perry, J. K. 2004. Glide: a new approach for rapid, accurate docking and scoring. 1. Method and assessment of docking accuracy. *Journal of Medicinal Chemistry*, 47, 1739-1749.

Fuda, C. S. S., Fisher, J. F. & Mobashery, S. 2005. B-Lactam resistance in *Staphylococcus aureus*: the adaptive resistance of a plastic genome. *Cell and Molecular Life Sciences*, 62, 2617-2633.

Fuhrmann, J., Schmidt, A., Spiess, S., Lehner, A., Turgay, K., Mechtler, K., Charpentier, E. & Clausen, T. 2009. McsB is a protein arginine kinase that phosphorylates and inhibits the heat-shock regulator CtsR. *Science*, 324, 1323-1327.

Gao, K., Oerlemans, R. & Groves, M. R. 2020. Theory and applications of differential scanning fluorimetry in early-stage drug discovery. *Biophysical Reviews*, 12, 85-104.

Gassel, M., Breitenlechner, C. B., Konig, N., Huber, R., Engh, R. A. & Bossemeyer, D. 2004. The protein kinase C inhibitor bisindolyl maleimide 2 binds with reversed orientations to different conformations of protein kinase A. *Journal of Biological Chemistry*, 279, 23679-23690.

Gooran, N. & Kopra, K. 2024. Fluorescence-based protein stability monitoring - a review. *International Journal of Molecular Sciences*, 25, 1-26.

Guo, Z., Song, T., Xue, Z., Liu, P., Zhang, M., Zhang, X. & Zhang, Z. 2020. Using CETSA assay and a mathematical model to reveal dual Bcl-2/Mcl-1 inhibition and on-target mechanism for ABT-199 and S1. *European Journal of Pharmaceutical Sciences*, 142, 105105.

Hajdusits, B., Suskiewicz, M. J., Hundt, N., Meinhart, A., Kurzbauer, R., Leodolter, J., Kukura, P. & Clausen, T. 2021. McsB forms a gated kinase chamber to mark aberrant bacterial proteins for degradation. *Elife,* 10, 1-24.

Hart, E. M., Mitchell, A. M., Konovalova, A., Grabowicz, M., Sheng, J., Han, X., Rodriguez-Rivera, F. P., Schwaid, A. G., Malinverni, J. C., Balibar, C. J., Bodea, S., Si, Q., Black, T. A., Rothman, D. M., Walker, S. S. & Silhavy, T. J. 2019. A small-molecule inhibitor

of BamA impervious to efflux and the outer membrane permeability barrier. *Proceedings of the National Academy of Sciences*, 116, 21748-21757.

Huang, K., Chandak, P., Wang, Q., Havaldar, S., Vald, A., Leskovec, J., Nadkarni, G. N., Glicksberg, B. S., Gehlenborg, N. & Zitnik, M. 2024. A foundational model for clinician-centered drug repurposing. *Nature Medicine,* 30, 3601-3613.

Huang, Q., Chen, J., Pan, G. & Reinke, A. W. 2023. Screening of the Pandemic Response Box identifies anti-microsporidia compounds. *Public Library of Science Neglected Tropical Diseases*, 17, 1-19.

Hughes, J. P., Rees, S., Kalindjin, S. B. & Philpott, K. L. 2011. Principles of early drug discovery. *British Journal of Pharmacology*, 162, 1239-1249.

Jafari, R., Almqvist, H., Axelsson, H., Ignatushchenko, M., Lundback, T., Nordlund, P. & Molina, D. M. 2014. The cellular thermal shift assay for evaluating drug target interactions in cells. *Nature Protocols*, 9, 2100-2122.

Kim, T., Hanh, B., Heo, B., Quang, N., Park, Y., Shin, J., Joen, S., Park, J., Samby, K. & Jang, J. 2021. A screening of the MMV pandemic response box reveals epetraborole as a new potent inhibitor against *Mycobacterium abscessus. International Journal of Molecular Sciences*, 22, 1-14.

Kirstein, J., Dougan, D. A., Gerth, U., Hecker, M. & Turgay, K. 2007. The tyrosine kinase McsB is a regulated adaptor protein for ClpCP. *European Molecular Biology Organization Journal*, 26, 2061-2070.

Kirstein, J., Zuhlke, D., Gerth, U., Turgay, K. & Hecker, M. 2005. A tyrosine kinase and its activator control the activity of the CtsR heat shock repressor in *B. subtilis*. *European Molecular Biology Organization Journal,* 24, 3435-3445.

Kruger, E., Zuhlke, D., Witt, E., Ludwig, H. & Hecker, M. 2001. Clp-mediated proteolysis in Gram-positive bacteria is autoregulated by the stability of a repressor. *The European Molecular Biology Organization Journal,* 20, 852-863.

Laemmli, U. K. 1970. Cleavage of structural proteins during the assembly of the head of bacteriophage T4. *Nature*, 227, 680-685.

Lavinder, J. J., Hari, S. B., Sullivan, B. J. & Magliery, T. J. 2009. High-throughput thermal scanning: a general, rapid dye-binding thermal shift screen for protein engineering. *Journal of the American Chemical Society*, 131, 3794-3795.

Lindman, S., Xue, W., Szczepankiewicz, O., Bauer, M. C., Nilsson, H. & Linse, S. 2006. Salting the charged surface: pH and salt dependence of protein G B1 stability. *Biophysical Journal*, 90, 2911-2921.

Lipinski, C. A., Lombardo, F., Dominy, B. W. & Feeney, P. J. 2012. Experimental and computational approaches to estimate solubility and permeability in drug discovery and development settings. *Advanced Drug Delivery Reviews*, 64, 4-17.

Liu, T., Wang, Y., Luo, X., Li, J., Reed, S. A., Xiao, H., Young, T. S. & Schultz, P. G. 2016. Enhancing protein stability with extended disulfide bonds. *Proceedings of the National Academy of Sciences*, 113, 5910-5915.

Lu, K., Luo, B., Tao, X., Luo, Y., Ao, M., Zheng, B., Xu, X., Ma, X., Niu, J., Li, H., Zhao, Z., Zheng, P., Wang, G., Gao, S., Wang, C., Xia, W. & Su, Z. M., Z. 2024. Complex structure and activation mechanism of arginine kinase McsB by McsA. *Nature Chemical Biology,* 1-10.

Martin, Y. C. 2005. A bioavailability score. *Journal of Medicinal Chemistry*, 48, 3164-3170.

Martinez, N. J., Asawa, R. R., Cyr, M. G., Zakharov, A., Urban, D. J., Yang, S., Hall, M. D., Marugan, J. J., Simeonov, A. & Henderson, M. J. 2018. A widely-applicable high-throughput cellualar thermal shift assay (CETSA) using split Nano Luciferase. *Scientific Reports*, 8, 1-16.

Mashalidis, E. H., Sledz, P., Lang, S. & Abell, C. 2013. A three-stage biophysical screening cascade for fragment-based drug discovery. *Nature Protocols*, 8, 2309-2324.

Massiah, M. A., Wright, K. M. & Du, H. 2016. Obtaining soluble folded proteins from inclusion bodies using sarkosyl, triton X-100, and CHAPS: Applications to LB and M9 mimimal media. *Current Protocols Protein Science*, 84, 6.13.1-6.13.24.

Mijakovic, I., Grangeasse, C. & Turgay, K. 2016. Exploring the diversity of protein modifications: Special bacterial phosphorylation systems. *FEMS Microbiology Reviews,* 40, 398-417.

Molina, D. M., Jafari, R., Ignatushchenko, M., Seki, T., Larsson, E. A., Dan, C., Sreekumar, L., Cao, Y. & Nordlund, P. 2013. Monitoring drug target engagement in cells and tissues using the cellular thermal shift assay. *Science*, 341, 84-87.

Molina, D. M. & Nordlund, P. 2016. The cellular thermal shift assay: A novel biophysical assay for in situ drug target engagement and mechanistic biomarker studies. *Annual Review of Pharmacology and Toxicology*, 56, 141-161.

Moyle, G., Boffito, M., Stoehr, A., Rieger, A., Shen, Z., Manhard, K., Sheedy, B., Hingorani, V., Raney, A. & Nguyen, M. 2010. Phase 2a randomized controlled trial of short-term activity, safety, and pharmacokinetics of a novel nonnucleoside reverse transcriptase inhibitor, RDEA806, in HIV-1-positive, antiretroviral-naive subjects. *Antimicrobial Agents and Chemotherapy*, 54, 3170-3178.

Mulani, M. S., Kamble, E. E., Kumkar, S. N., Tawre, M. S. & Pardesi, K. R. 2019 Emerging strategies to combat ESKAPE pathogens in the era of antimicrobial resistance: A review. *Frontiers in Microbiology*, 10, 1-24.

Niesen, F. H., Berglund, H. & Vedadi, M. 2007. The use of differential scanning fluorimetry to detect ligand interactions that promote protein stability. *Nature Protocols,* 2, 2212-2221.

Pace, C. N. 1990. Conformational stability of globular proteins. *Trends in Biochemical Sciences*, 15, 14-17.

Pace, C. N. 1992. Contribution of the hydrophobic effect to globular protein stability. *Journal of Molecular Biology*, 226, 29-35.

Pagadala, N. S., Syed, K. & Tuszynski, J. 2017. Software for molecular docking: a review. *Biophysical Reviews*, 9, 91-102.

Palmer, I. & Wingfield, P. T. 2004. Preparation and extraction of insoluble (inclusion body) proteins from *Escherichia coli*. *Current Protocols in Protein Science*, 1-25.

Pantoliano, M. W., Petrella, E. C., Kwasnoski, J. D., Lobanov, V. S., Myslik, J., Graf, E., Carver, T., Asel, E., Springer, B. A., Lane, P. & Salemme, F. R. 2001. High-density miniaturized thermal shift assays as a general strategy for drug discovery. *Journal of Biomolecular Screening*, 6, 429-440.

Parvekar, P., Palaskar, J., Metgud, S., Maria, R. & Dutta, S. 2020. The minimum inhibitory concentration (MIC) and minimum bactericidal concentration (MBC) of silver nanoparticles against *Staphylococcus aureus. Biomaterial Investigations in Dentistry* 7, 105-109.

Pereira, A. M., Abreu, A. C. & Simoes, M. 2012. Action of kanamycin against single and dual species biofilms of *Escherichia coli* and *Staphylococcus aureus. Journal of Microbiology Research*, 2, 84-88.

Pouresmaell, M. & Azizi-Dargahlou, S. 2023. Factors involved in heterologous expression of proteins in *E. coli* host. *Archives of Microbiology*, 205, 1-18.

Pushpakom, S., Iorio, F., Eyers, P. A., Escott, K. J., Hopper, S., Wells, A., Doig, A., Guilliams, T., Latimer, J., Mcnamee, C., Norris, A., Sanseau, P., Cavalla, D. & Pirmohamed, M. 2019. Drug repurposing: progress, challenges and recommendations. *Nature Reviews Drug Discovery*, 18, 41-58.

Queralto, C., Alvarez, R., Ortega, C., Diaz-Yanez, F., Paredes-Sabja, D. & Gil, F. 2023. Role and regulation of Clp proteases: A target against Gram-positive bacteria. *Bacteria,* 2, 21-36.

Reader, J., Van Der Watt, M. E., Taylor, D., Le Manach, C., Mittal, N., Ottilie, S., Theron, A., Moyo, P., Erlank, E., Nardini, L., Venter, N., Lauterbach, S., Bezuidenhout, B., Horatscheck, A., Van Heerden, A., Spilman, N. J., Cowell, A. N., Connacher, J., Opperman, D., Orchard, L. M., Llinas, M., Istvan, E. S., Goldberg, D. E., Boyle, G. A., Calvo, D., Mancama, D., Coetzer, T. L., Winzeler, E. A., Duffy, J., Koekmoer, L. L., Basarab, G., Chibale, K. & Birkholtz, L. 2021. Multistage and transmission-blocking targeted antimalarials discovered from the open-source MMV Pandemic Response Box. *Nature Communications*, 12, 269.

Reghunandanan, K., Akhila, T. P., Krishnan, N., Darsana, K. M., Prasad, R., Nelson-Sathi, S. & Chandramohanadas, R. 2024. Search for novel *Plasmodium falciparum* pfATP4 inhibitors from the MMV Pandemic Response Box through a virtual screening approach. *Journal of Biomolecular Structure and Dynamics*, 42, 6200-6211.

Reinhard, L., Mayerhofer, H., Geerlof, A., Muller-Dieckmmann, J. & Weiss, M. S. 2013. Optimization of protein buffer cocktails using thermofluor. *Structural Biology and Crystallization Communications*, 209-214.

Reva, B. A., Finkelstein, A. V. & Skolnick, J. 1998. What is the probability of a chance prediction of a protein structure with an rmsd of 6 Å? *Folding and Design*, 3, 141-147.

Rice, L. B. 2008. Federal funding for the study of antimicrobial resistance in nosocomial pathogens: No ESKAPE. *The Journal of Infectious Diseases,* 197, 1079-1081.

Samby, K., Besson, D., Dutta, A., Patra, B., Doy, A., Glossop, P., Mills, J., Whitlock, G., Hooft Van Huijsduijnen, R., Monaco, A., Bilbe, G., Mowbray, C., Perry, B., Adam, A., Wells, T. N. C. & Willis, P. A. 2022. The pandemic response box-accelerating drug discovery efforts after disease outbreaks. *ACS Infectious Diseases*, 8, 713-720.

Samby, K., Willis, P. A., Burrows, J. N., Laleu, B. & Webborn, P. J. H. 2021. Actives from MMV open access boxes? A suggested way forward. *PLoS Pathogens*, 17, e1009384.

Santajit, S. & Indrawattana, N. 2016. Mechanisms of antimicrobial resistance in ESKAPE pathogens. *BioMed Research International,* 2016, 1-8.

Sathish, H. A., Kumar, P. R. & Prakash, V. 2007. Mechanism of solvent induced thermal stabilzation of papain. *International Journal of Biological Macromolecules*, 41, 383-390.

Schneider, C., Rasband, W. S. & Eliceiri, K. W. 2012. NIH image to imageJ: 25 years of image analysis. *Nature Methods,* 9, 671-675.

Shanley, H. T., Taki, A. C., Byrne, J. J., Jabbar, A., C., W. T. N., Samby, K., Boag, P. R., Nguyen, N., Sleebs, B. E. & Gasser, R. B. 2022. A high-throughput phenotypic screen

of the `Pandemic Response Box' Identifies a quinoline derivative with significant anthelmintic activity. *Pharmaceuticals*, 15, 1-15.

Singh, H., Almaazmi, S. Y., Dutta, T., Keyzers, R. A. & Blatch, G. L. 2023. In silico identification of modulators of J domain protein-Hsp70 interactions in Plasmodium falciparum: a drug repurposing strategy against malaria. *Frontiers in Molecular Biosciences*, 10, 1158912.

Sinha, S. & Vohora, D. 2018. Drug discovery and development: An overview. *Pharmaceutical Medicine and Translational Clinical Research*, 19-32.

Sitthisak, S., Kitti, T., Boonyonying, K., Wozniak, D. J., Devreese, B., Mongkolsuk, S. & Jayaswal, R. K. 2012. McsA and the roles of metal binding motif in *Staphylococcus aureus*. *FEMS Microbiology Letters,* 327, 126-133.

Sivasanker, S., Premnath, M. A., Boppe, A., Grobusch, M. P. & Jeyaraj, S. 2023. Screening MMV pandemic response and pathogen box compounds against pan-drug-resistant *Klebsiella pneumoniae* to identify potent inhibitory compounds. *New Microbes and New Infections,* 55, 1-7.

Smith, S. M. & Eng, R. H. 1985. Activity of ciprofloxacin against methicillin-resistant *Staphylococcus aureus*. *Antimicrobial Agents and Chemotherapy*, 27, 688-691.

Sorrell, F. J., Greenwood, G. K., Birchall, K. & Chen, B. 2010. Development of a differential scanning fluourimetry based high throughput screening assay for the discovery of affinity binders against an anthrax protein. *Journal of Pharmaceutical and Biomedical Analysis,* 52, 802-808.

Stubbings, W. J., Bostock, J. M., Ingham, E. & Chopra, I. 2004. Assessment of a microplate method for determining the post-antibiotic effect in *Staphylococcus aureus* and *Escherichia coli. Journal of Antimicrobial Chemotherapy,* 54, 139-143.

Suskiewicz, M. J., Hajdusits, B., Beveridge, R., Heuck, A., Vu, L., D. , Kurzbauer, R., Hauer, K., Theony, V., Rumpel, K., Mechtler, K., Meinhart, A. & Clausen, T. 2019. Structure of McsB, a protein kinase for regulated arginine phosphorylation. *Nature Chemical Biology,* 15, 510-518.

Tan, B. X., Brown, C. J., Ferrer, F. J., Yuen, T. Y., Quah, S. T., Chan, B. H., Jansson, A. E., Teo, H. L., Nordlund, P. & Lane, D. P. 2015. Assesing the efficacy of Mdm2/Mdm4-Inhibiting stapled peptides using cellular thermal shift assays. *Scientific Reports*, 5, 12116.

Tao, H., Liu, W., Simmons, B. N., Harris, H., K., Cox, T. C. & Massiah, M. A. 2010. Purifying natively folded proteins from inclusion bodues using sarkosyl, Triton X-100, and CHAPS. *Biotechniques*, 48, 61-64.

Tolvanen, T. A. 2022. Current advances in CETSA. *Frontiers in Molecular Biosciences* 9, 1-8.

Treangen, T. J., Maybank, R. A., Enke, S., Friss, M. B., Diviak, L. F., Karaolis, D. K. R., Koren, S., Ondov, B., Phillippy, A. M. & Bergman, N. H. 2014. Complete genome sequence of the quality control strain *Staphylococcus aureus* subsp. *aureus* ATCC 25923. *Genome announcements*, 2, 10.1128/genomea. 01110-14.

Trentini, D. B., Suskiewicz, M. J., Heuck, A., Kurzbauer, R., Deszcz, L., Mechtler, K. & Clausen, T. 2016. Arginine phosphorylation marks proteins for degradation by a Clp protease. *Nature,* 539, 48-53.

Valenti, D., Neves, J. F., Cantrelle, F., Hristeva, S., Santo, D. L., Obsil, T., Hanoulle, X., Levy, L. M., Tzalis, D., Landrieu, I. & Ottmann, C. 2013. Set-up and screening of a fragment library targeting 14-3-3 protein interface. *MedChemComm*, 10, 1796-1802.

Veale, C. G. L., Zoraghi, R., Young, R. M., Morrison, J. P., Pretheeban, M., Lobb, K. A., Reiner, N. E., Andersen, R. J. & Davies-Coleman, M. T. 2015. Synthetic analogues of the marine bisindole deoxytopsentin: potent selective inhibitors of MRSA pyruvate kinase. *Journal of Natural Products*, 78, 355-362.

Wald, J., Pasin, M., Richter, M., Walther, C., Mathai, N., Kirchmair, J., Makarov, V. A., Goessweiner-Mohr, N., Marlovits, T. C. & Zanella, I. 2019. Cryo-EM structure of pleconaril-resistant rhinovirus-B5 complexed to the antiviral OBR-5-340 reveals unexpected binding site. *Proceedings of the National Academy of Sciences*, 116, 19109-19115.

Waldron, T. T. & Murphy, K. P. 2003. Stabilization of proteins by ligand binding: Application to drug screening and determination of unfolding energetics. *Biochemistry*, 42, 5058-5064.

Weidinger, J. D. F., Pfreundschuh, M., Zorb, D., Yee, A., Heyse, S., Barenz, F. & Steigele, S. 2024. A robust CETSA data analysis auomation workflow for routine screening. *SLAS Disovery*, 29, 1-5.

Weids, A. J., Ibstedt, S., Tamás, M. J. & Grant, C. M. 2016. Distinct stress conditions result in aggregation of proteins with similar properties. *Scientific reports*, 6, 24554.

Wiegand, I., Hilpert, K. & Hancock, R. E. W. 2008. Agar and broth dilution methods to determine the minimal inhibitory concentration (MIC) of antimicrobial substances. *Nature Protocols*, 3, 163-175.

Wildman, S. A. & Crippen, G. M. 1999. Prediction of physiochemical parameters by atomic contributions. *Journal of Chemical Information and Computer Sciences*, 39, 868-873

Wozniak, D. J., Tiwari, K. B., Soufan, R. & Jayaswal, R. K. 2012. The mcsB gene of the clpC operon is required for stress tolerance and virulence in *Staphylococcus aureus. Microbiology,* 158, 2568-2576.

Xisto, M. I. D. D. S., Rollin-Pinheiro, R., De Castro-Almeida, Y., Dos Santos-Freitas, G. M. P., Rochetti, V. P., Borba-Santos, L. P., Da Silva Fontes, Y., Ferreira-Pereira, A., Rozental, S. & Barreto-Bergter, E. 2023. Promising antifungal molecules against mucormycosis agents identified from Pandemic response box®: *in vitro* and in silico analyses. *Journal of Fungi*, 9, 187.

Yasir, M., Dutta, D. & Willcox, M. D. P. 2021. Enhancement of antibiofilm activity of ciprofloxacin against *Staphylococcus aureus* by administration of antimicrobial peptides. *Antibiotics*, 10, 1159.

Zoraghi, R., Campbell, S., Kim, C., Dullaghan, E. M., Blair, L. M., Gillard, R. M., Reiner, N. E. & Sperry, J. 2014. Discovery of a 1,2-bis(3-indolyl)ethane that selectively inhibits the pyruvate kinase of methicillin-resistant *Staphylococcus aureus* over human isoforms. *Bioorganic & Medicinal Chemistry Letters*, 24, 5059-5062.

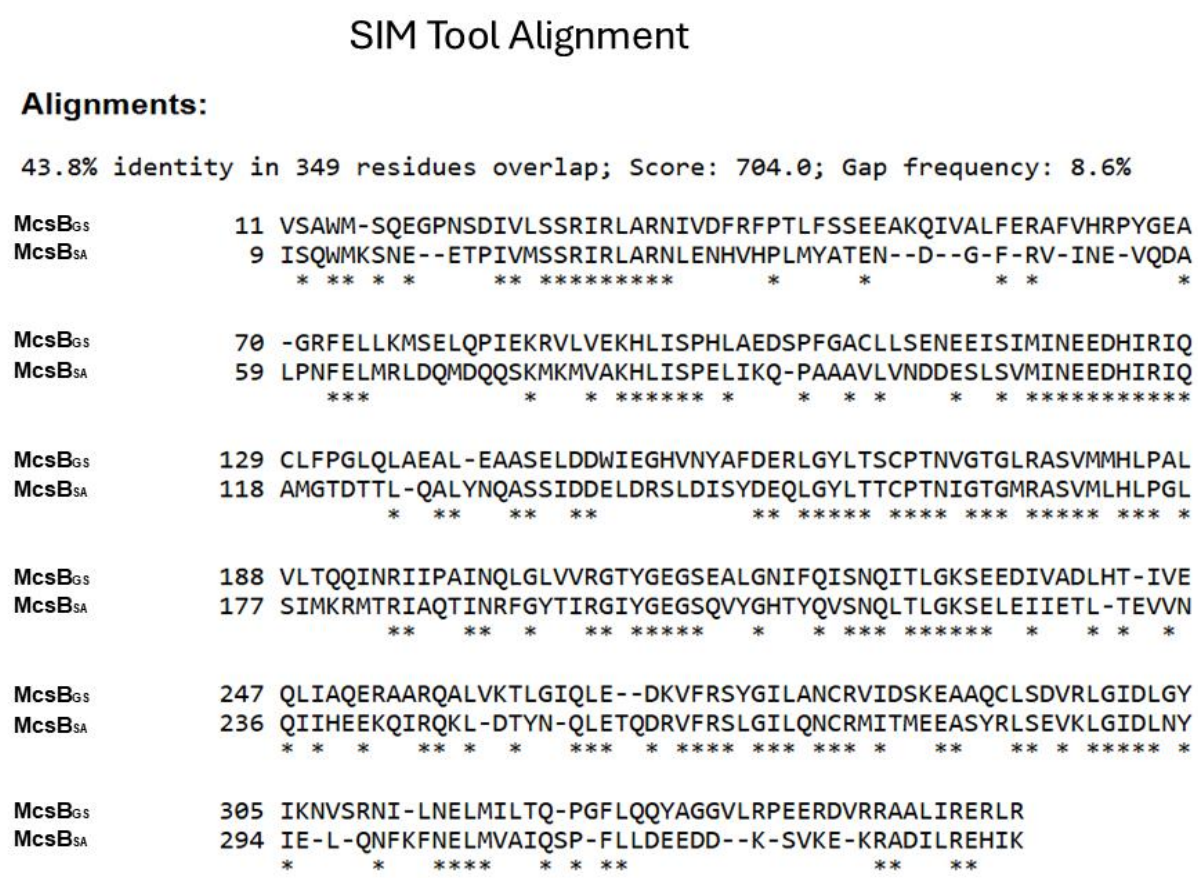

Figure A1. The SIM tool alignment output obtained for $McsB_{SA}$ (accession number: Q2G0P6) and $McsB_{GS}$ (accession number: P0DMM5). The * indicate the amino acid residues which are common to both sequences and the dashes (-) indicate gaps in the alignment, as a result of these gaps, the alignment starts at 11 for $McsB_{GS}$ and 9 for $McsB_{SA}$ due to two missing residues at the start of the sequence for $McsB_{SA}$.

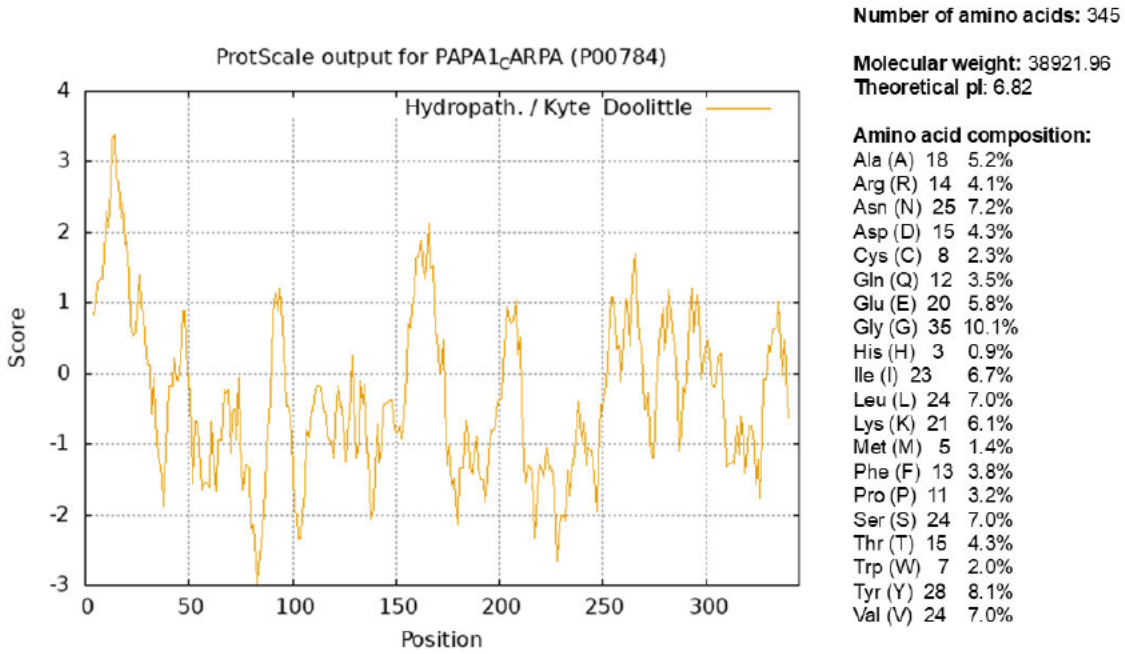

Number of amino acids: 345

Molecular weight: 38921.96
Theoretical pI: 6.82

Amino acid composition:

Ala (A)	18	5.2%
Arg (R)	14	4.1%
Asn (N)	25	7.2%
Asp (D)	15	4.3%
Cys (C)	8	2.3%
Gln (Q)	12	3.5%
Glu (E)	20	5.8%
Gly (G)	35	10.1%
His (H)	3	0.9%
Ile (I)	23	6.7%
Leu (L)	24	7.0%
Lys (K)	21	6.1%
Met (M)	5	1.4%
Phe (F)	13	3.8%
Pro (P)	11	3.2%
Ser (S)	24	7.0%
Thr (T)	15	4.3%
Trp (W)	7	2.0%
Tyr (Y)	28	8.1%
Val (V)	24	7.0%

Figure B1. Plot of the hydrophobicity score for the amino acid sequence of papain using the Kyte and Doolittle index. The blue rectangle highlights the hydrophobic portion of the sequence, and the red rectangle highlights the hydrophilic portion of the sequence.

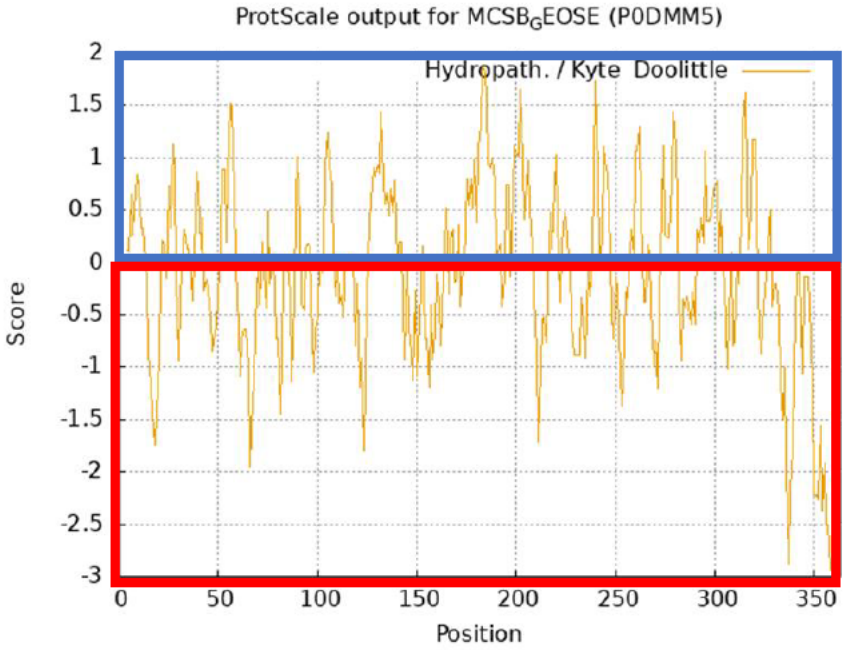

Number of amino acids: 363

Molecular weight: 40852.92
Theoretical pI: 5.37

Amino acid composition:

Ala (A)	29	8.0%
Arg (R)	29	8.0%
Asn (N)	15	4.1%
Asp (D)	15	4.1%
Cys (C)	5	1.4%
Gln (Q)	18	5.0%
Glu (E)	35	9.6%
Gly (G)	24	6.6%
His (H)	7	1.9%
Ile (I)	30	8.3%
Leu (L)	43	11.8%
Lys (K)	11	3.0%
Met (M)	9	2.5%
Phe (F)	15	4.1%
Pro (P)	12	3.3%
Ser (S)	23	6.3%
Thr (T)	12	3.3%
Trp (W)	2	0.6%
Tyr (Y)	7	1.9%
Val (V)	22	6.1%

Figure B2. Plot of the hydrophobicity score for the amino acid sequence of $McsB_{GS}$ using the Kyte and Doolittle index. The blue rectangle highlights the hydrophobic portion of the sequence, and the red rectangle highlights the hydrophilic portion of the sequence.

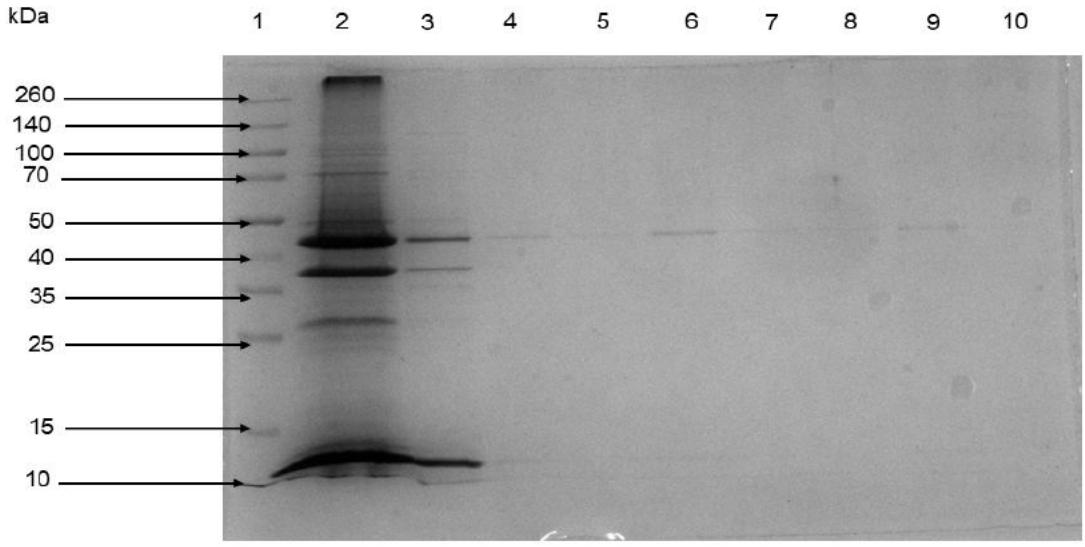

Figure C1: Analysis of a representative purification of $McsB_{SA}$ solubilised with 1% sarkosyl from *E. coli*. $McsB_{SA}$ unbound fraction, washes and eluted samples from the Ni-NTA agarose resin were analysed and separated via a 12.5% reducing SDS-PAGE. The gel was stained with standard Coomassie blue R250 stain. The gel was loaded as follows: lane 1: Spectra™ Multicolour Broad Range Protein Ladder, lane 2: unbound $McsB_{SA}$ protein, lane 3: wash waste, lane 4: $McsB_{SA}$ elution 01, lane 5: $McsB_{SA}$ elution 02, lane 6: $McsB_{SA}$ elution 03, lane 7: $McsB_{SA}$ elution 04, lane 8: $McsB_{SA}$ elution 05, lane 9: $McsB_{SA}$ elution 08 and lane 10: $McsB_{SA}$ elution 07.

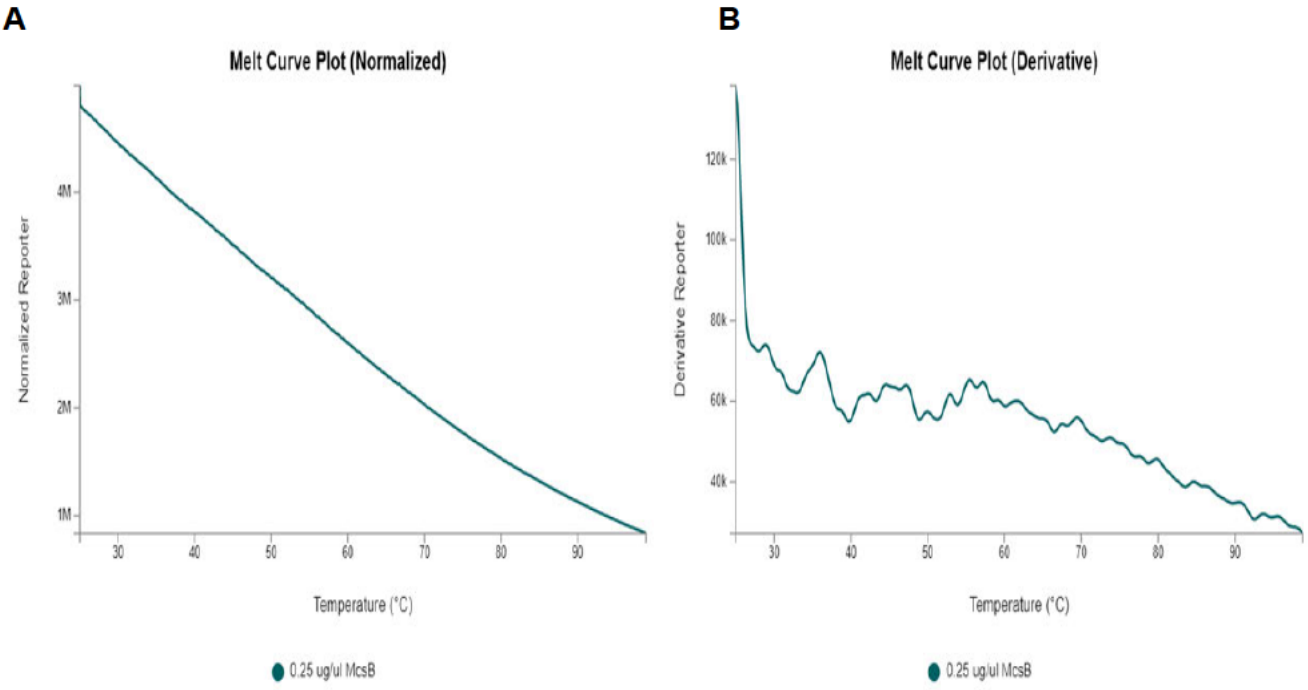

Figure C2: The thermal shift analysis for $McsB_{SA}$ solubilised with 1% sarkosyl. (A) The raw fluorescence obtained for $McsB_{SA}$ plotted against temperature. (B) The derivates (dF/dT) were calculated from the raw fluorescence and plotted against temperature (no melting temperature could be determined).

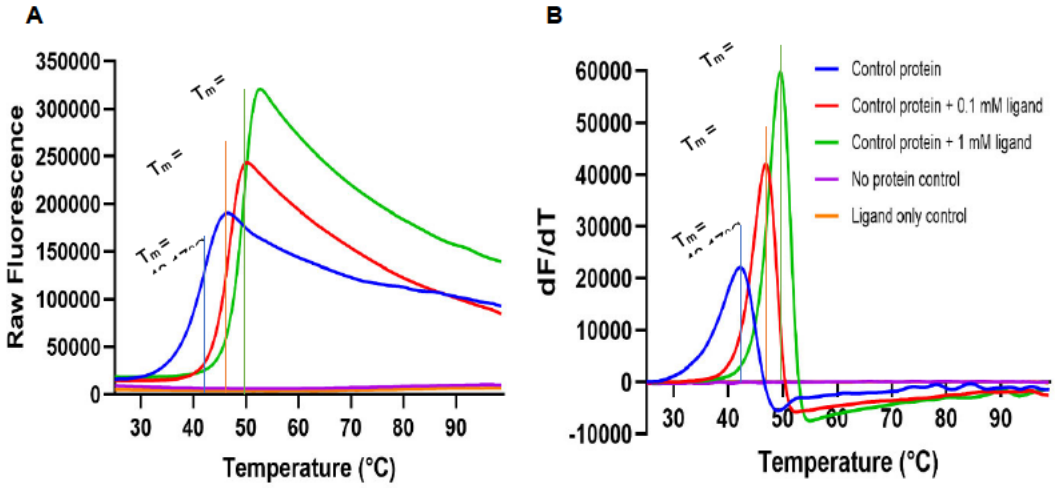

Figure D1. A representative thermal shift assay assessing the thermal shift kit. The thermal shift assay was evaluated to detect ligand binding (n≥3). (A) The real time fluorescence obtained was plotted against temperature (°C). The melting temperature (T_m) is defined as the midpoint of the slope of the curve. (B) The derivative (dF/dT) was calculated and plotted against temperature (°C). In this case, the T_m is defined as the peak of the sigmoidal curve. The derivative melting temperature for the control protein was determined to be 42.17°C and the melting temperature for the control protein with the addition of 1 mM ligand was determined to be 49.60°C, with a difference in melting temperature of 7.43°C. For both (A) and (B), the fluorescence of the control protein with no ligand present is represented in blue, followed by the control protein with 0.1 mM ligand represented in red and lastly the control protein with the ligand concentration tested at 1 mM represented in green. No fluorescence signals were observed for the NPC (represented in purple) or the LOC (represented in orange).

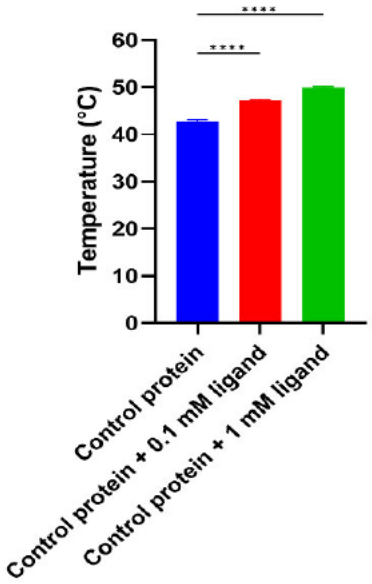

Figure D2. The thermal derivative melting temperatures obtained for the control protein when incubated with 0.1 mM and 1 mM control ligand. The melting temperature obtained for the control protein when incubated with 0.1mM control ligand and 1 mM control ligand was compared to the melting temperature obtained for the control protein (n=3). Statistical analysis was performed using a one-way ANOVA. *p<0.05, **p<0.01, ***p<0.001 and ****p<0.0001 (α=0.05, CI 95%).

APPENDIX E

Table E1: Composition of the cocktails tested against $McsB_{SA}$

Cocktail Name	Cocktail composition [10 µM (0.2 µl of each compound resulting in a total volume of 2 µl)]
Cocktail A1	MMV1634492, MMV002731, MMV003143, MMV1578560, MMV1782223, MMV1782351, MMV1593535, MMV1579783, MMV1633967, MMV1581551
Cocktail A2	MMV1782108, MMV000059, MMV002337, MMV640014, MMV1782218, MMV1782387. MMV1593533, MMV1578925, MMV1593534, MMV1580853
Cocktail A3	MMV1634494, MMV637104, MMV1634363, MMV004508, MMV1782217, MMV1782389, MMV422940, MMV1578889, MMV1582498, MMV1580841
Cocktail A4	MMV1634386, MMV637533, MMV1634359, MMV1782212, MMV1782216, MMV1782388, MMV1582497, MMV1578572, MMV1582494, MMV1579878
Cocktail A5	MMV637528, MMV1634362, MMV1782110, MMV1782227, MMV1009286, MMV1634557, MMV1581553, MMV1578568, MMV1582493, MMV1579845
Cocktail A6	MMV1782109, MMV1634360, MMV1634493, MMV1782226, MMV1782225, MMV030787, MMV1581548, MMV1580173, MMV000043, MMV1579787
Cocktail A7	MMV1645051, MMV002565, MMV344625, MMV1782221, MMV1782354, MMV000028, MMV1580850, MMV1634403, MMV003137, MMV1579786
Cocktail A8	MMV1634491, MMV396785, MMV1634358, MMV1782224, MMV689401, MMV002722, MMV002740, MMV1634390, MMV1581552, MMV1579784
Cocktail B1	MMV1483032, MMV1613560, MMV1581547, MMV1579776, MMV687273, MMV637945, MMV020752, MMV093250, MMV1581554, MMV1549626
Cocktail B2	MMV508427, MMV1230557, MMV687800, MMV1579775, MMV1634387, MMV1580854, MMV1229204, MMV1593541, MMV1581550, MMV1578559
Cocktail B3	MMV1578565, MMV1593540, MMV1580848, MMV1579354, MMV1633966, MMV1580851, MMV1578575, MMV1593537, MMV1581546, MMV1578579
Cocktail B4	MMV1578561, MMV1593539, MMV1580842, MMV1578899, MMV1505642, MMV1579849, MMV1578556, MMV1582492, MMV1580844, MMV1578578
Cocktail B5	MMV1578557, MMV1582495, MMV1580840, MMV1578890, MMV1593542, MMV1579844, MMV1663457, MMV1582491, MMV1579788, MMV1578574

Cocktail B6	MMV000725, MMV1582487, MMV046261, MMV1578886, MMV1593538, MMV141011, MMV1341773, MMV1582382, MMV1579785, MMV1578569
Cocktail B7	MMV1634384, MMV021759, MMV1579846, MMV1578573, MMV002560, MMV002516, MMV1633970, MMV002354, MMV811071, MMV1578566
Cocktail B8	MMV1634383, MMV1581555, MMV1578842, MMV1578571, MMV002459, MMV688755, MMV1633965, MMV1581557, MMV1578898, MMV1578563
Cocktail C1	MMV1578558, MMV1593532, MMV1579780, MMV1578576, MMV831201, MMV1579782, MMV1578577, MMV1582490, MMV1580849, MMV1578884
Cocktail C2	MMV1782140, MMV002224, MMV688756, MMV1578562, MMV687801, MMV1579777, MMV233495, MMV1582489, MMV1580839, MMV108465
Cocktail C3	MMV1634391, MMV637659, MMV1578897, MMV1578555, MMV1593531, MMV292173, MMV002676, MMV1582488, MMV1579779, MMV1480967
Cocktail C4	MMV1633674, MMV1580846, MMV001014, MMV1578554, MMV1581558, MMV102270, MMV1633675, MMV002665, MMV1579778, MMV1578570
Cocktail C5	MMV002169, MMV1580845, MMV1578885, MMV1634402, MMV1581556, MMV000008, MMV303733, MMV1581559, MMV099714, MMV1578564
Cocktail C6	MMV002612, MMV1579850, MMV687696, MMV1634399, MMV1581549, MMV002260, MMV003249, MMV1581545, MMV1578891, MMV1782215
Cocktail C7	MMV1613562, MMV374187, MMV011565, MMV000051, MMV1580847, MMV102833, MMV001438, MMV1580855, MMV124656, MMV1782403
Cocktail C8	MMV689758, MMV1579781, MMV452821, MMV002287, MMV1579847, MMV565773, MMV1582496, MMV1580852, MMV975972, MMV1782402
Cocktail D1	MMV1782411, MMV1593515, MMV394033, MMV690547, MMV1580794, MMV1580491, MMV1782101, MMV056052, MMV1782115, MMV1593513
Cocktail D2	MMV214956, MMV1581032, MMV1634404, MMV1165877, MMV001793, MMV1580492, MMV1633969, MMV1580504, MMV1782114, MMV1593511
Cocktail D3	MMV1634395, MMV1580799, MMV1634388, MMV1580497, MMV251679, MMV690621, MMV596723, MMV001961, MMV018362, MMV637306
Cocktail D4	MMV1634071, MMV001726, MMV180402, MMV1580495, MMV003291, MMV1782112, MMV1581378, MMV003738, MMV1634556, MMV1581377
Cocktail D5	MMV1633962, MMV690653, MMV642550, MMV1645152, MMV009948, MMV1782107, MMV1581031, MMV690540, MMV1634401, MMV002780

Cocktail D6	MMV1633678, MMV1580484, MMV1580798, MMV1633677, MMV1174026, MMV1782106, MMV1580797, MMV614278, MMV1634394, MMV1580801
Cocktail D7	MMV690480, MMV1580478, MMV1580800, MMV1593520, MMV003820, MMV1782105, MMV001761, MMV1580489, MMV1633964, MMV010036
Cocktail D8	MMV1593517, MMV1782102, MMV1580503, MMV1581029, MMV639951, MMV1782104, MMV002015, MMV1580499, MMV1593516, MMV637879
Cocktail E1	MMV617332, MMV1593519, MMV003297, MMV1634396, MMV1580482, MMV1581035, MMV638198, MMV690706, MMV1782353, MMV1580843
Cocktail E2	MMV1580480, MMV002505, MMV1580487, MMV1634385, MMV1580501, MMV1593544, MMV637413, MMV1782220, MMV1782349, MMV690555
Cocktail E3	MMV1580494, MMV1581034, MMV1580485, MMV1633968, MMV1580496, MMV1593521, MMV658803, MMV1782213, MMV1782355, MMV1613559
Cocktail E4	MMV275100, MMV1581033, MMV098836, MMV688991, MMV1580490, MMV1593514, MMV1580500, MMV1782214, MMV1782352, MMV1634361
Cocktail E5	MMV1782103, MMV1557856, MMV218827, MMV1580502, MMV1782113, MMV1581036, MMV1580498, MMV1782211, MMV1782350, MMV002350
Cocktail E6	MMV1782098, MMV1580796, MMV1782111, MMV637855, MMV1634393, MMV1581030, MMV1580488, MMV1782210, MMV1782386, MMV1580483
Cocktail E7	MMV1634397, MMV1580505, MMV1782097, MMV690467, MMV1634392, MMV247764, MMV1580486, MMV1782208, MMV1782412, MMV1782209
Cocktail E8	MMV1633963, MMV687798, MMV1634398, MMV1580493, MMV1634389, MMV019724, MMV1782222, MMV1006203, MMV1613563, MMV003069

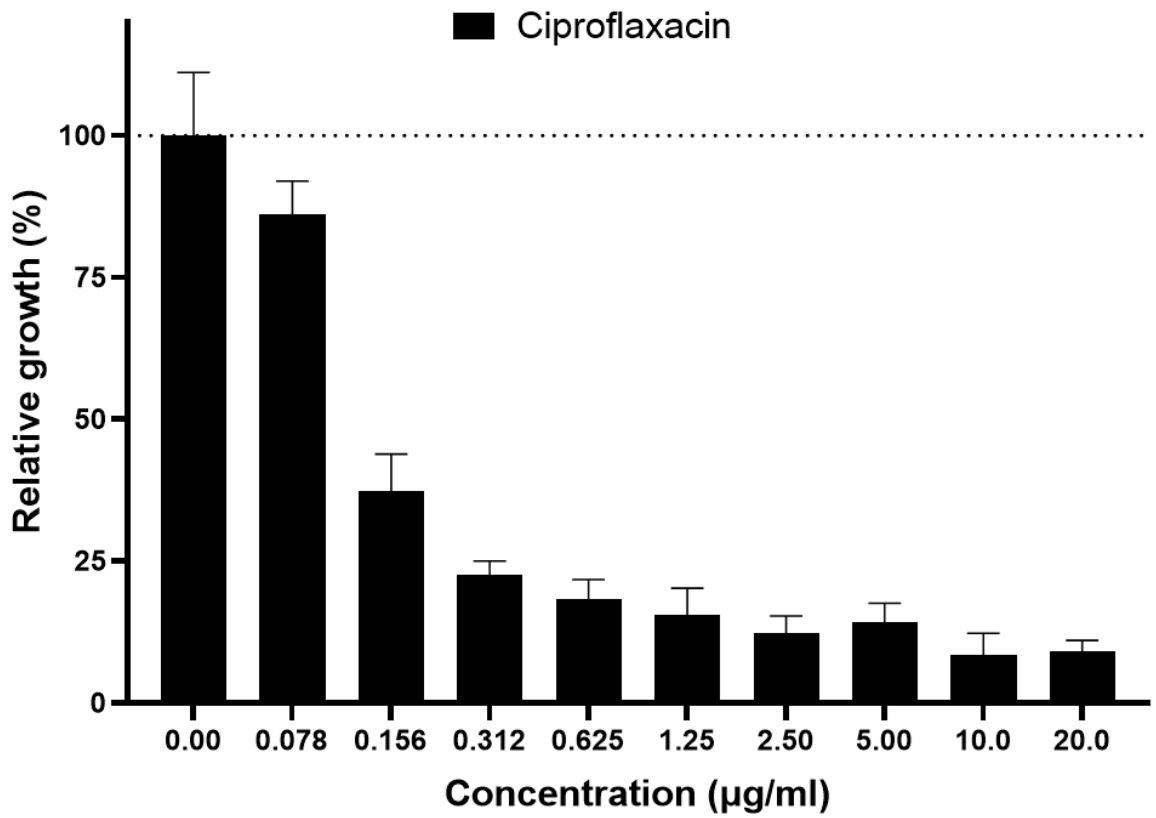

Figure F1. The effect of ciprofloxacin on *Staphylococcus aureus* growth using a minimum inhibitory concentration assay. *S. aureus* was incubated with ciprofloxacin. The compounds were tested within a range of 0.078 µg/ml – 20 µg/ml (a two-fold serial dilution was prepared from 20 µM until the concentration of 0.078 µM was reached). An OD_{600} reading was taken at 0 h and once again after a 24 h incubation period at 37℃. The relative growth of *S. aureus* was assessed by first subtracting the OD_{600} reading taken at 0 h from the 24 h reading and thereafter normalised by treating the 0 µM DMSO control as 100%.

Structural alignment:

```
                                .........+.........+.........+.........
6FH3 - Gs McsB  SSA 1610     4 -HHHHHHCCCHHHHHCCCCCCEEEEEEEEEEEEEECCCCC
8GQD - Sa McsB  SSA 1611     1 C--------------------------------------
6FH3 - Gs McsB      1610     4 -GKFFNTAVSAWMSQEGPNSDIVLSSRIRLARNIVDFRFP
8GQD - Sa McsB      1611     1 M--------------------------------------

                                .........+.........+.........+.........
6FH3 - Gs McsB  SSA 1610    43 CCCCHHHHHHHHHHHHHCCCCCCCCCCCCEEEEECCCCH
8GQD - Sa McsB  SSA 1611       ----------------------------------------
6FH3 - Gs McsB      1610    43 TLFSSEEAKQIVALFERAFVHRPYGEAGRFELLKMSELQP
8GQD - Sa McsB      1611       ----------------------------------------

                                .........+.........+.........+.........
6FH3 - Gs McsB  SSA 1610    83 HHHHHHHHHCCCCCCCCCCCCEEEEECCCEEEEECCC
8GQD - Sa McsB  SSA 1611       ----------------------------------------
6FH3 - Gs McsB      1610    83 IEKRVLVEKHLISPHLAEDSPFGACLLSENEEISIMINEE
8GQD - Sa McsB      1611       ----------------------------------------

                                .........+.........+.........+.........
6FH3 - Gs McsB  SSA 1610   123 CEEEEEEECCCCHHHHHHHHHHHHHHHHCCCCCCCCC
8GQD - Sa McsB  SSA 1611       ----------------------------------------
6FH3 - Gs McsB      1610   123 DHIRIQCLFPGLQLAEALEAASELDDWIEGHVNYAFDERL
8GQD - Sa McsB      1611       ----------------------------------------

                                .........+.........+.........+.........
6FH3 - Gs McsB  SSA 1610   163 CCCCCCCCCCECEEEEEEEECHHHHHHCHHHHHHHHHH
8GQD - Sa McsB  SSA 1611       ----------------------------------------
6FH3 - Gs McsB      1610   163 GYLTSCPTNVGTGLRASVMMHLPALVLTQQINRIIPAINQ
8GQD - Sa McsB      1611       ----------------------------------------

                                .........+.........+.........+.........
6FH3 - Gs McsB  SSA 1610   203 HCCEEECCCCCCCCCCCEEEEEECCCCCCCHHHHHHHH
8GQD - Sa McsB  SSA 1611       ----------------------------------------
```

```
6FH3 - Gs McsB      1610  203 LGLVVRGTYGEGSEALGNIFQISNQITLGKSEEDIVADLH
8GQD - Sa McsB      1611      ----------------------------------------

                              .........+.........+.........+.........
6FH3 - Gs McsB  SSA 1610  243 HHHHHHHHHHHHHHHHHHHHHCHHHHHHHHHHHHHHHCCC
8GQD - Sa McsB  SSA 1611      ----------------------------------------
6FH3 - Gs McsB      1610  243 TIVEQLIAQERAARQALVKTLGIQLEDKVFRSYGILANCR
8GQD - Sa McsB      1611      ----------------------------------------

                              .........+.........+.........+.........
6FH3 - Gs McsB  SSA 1610  283 CCCHHHHHHHHHHHHHHHHHCCCCCCCHHHHHHHHHHHHH
8GQD - Sa McsB  SSA 1611      ----------------------------------------
6FH3 - Gs McsB      1610  283 VIDSKEAAQCLSDVRLGIDLGYIKNVSRNILNELMILTQP
8GQD - Sa McsB      1611      ----------------------------------------

                              .........+.........+.........+.........
6FH3 - Gs McsB  SSA 1610  323 CHHHHHHCCCCCHHHHHHHHHHHHHHHHHHHHCCCCCCCCC
8GQD - Sa McsB  SSA 1611    2 ------------------------------------CCCCC
6FH3 - Gs McsB      1610  323 GFLQQYAGGVLRPEERDVRRAALIRERLRMETRKFFNTAV
8GQD - Sa McsB      1611    2 ------------------------------------THNIH

                              .........+.........+.........+.........
6FH3 - Gs McsB  SSA 1610   12 -CHH-HHHCC-CCCCEEEEEEEEEEEEEECCCCCCC-CH-
8GQD - Sa McsB  SSA 1611    7 CCCCHHHHHCCCC-CEEEEEEEEECEEEEC----CCCCCC
6FH3 - Gs McsB      1610   12 -SAW-MSQEG-PNSDIVLSSRIRLARNIVDFRFPTL-FS-
8GQD - Sa McsB      1611    7 DNISQWMKSNEET-PIVMSSRIRLARNLEN----HVHPLM

                              .........+.........+.........+.........
6FH3 - Gs McsB  SSA 1610   47 ---HHHHHHHHHHHHHCCCCCEEEEECCCCHHHHHHHHH
8GQD - Sa McsB  SSA 1611   42 CCCHHHHHHHHHHHHHHCCC-CEEEEECCCCHHHHHHHHH
6FH3 - Gs McsB      1610   47 ---SEEAKQIVALFERAFVGRFELLKMSELQPIEKRVLVE
8GQD - Sa McsB      1611   42 YATENDGFRVINEVQDALPN-FELMRLDQMDQQSKMKMVA

                              .........+.........+.........+.........
6FH3 - Gs McsB  SSA 1610   91 HCCCCHHHHHHCCCEEEEEECCCEEEEEECCC-CEEEEEE
```

```
8GQD - Sa McsB  SSA 1611   81 HCCCCHHHHHH-HCEEEEECCCCEEEEEECCCCC-EEEEE
6FH3 - Gs McsB      1610   91 KHLISPHLAEDSPFGACLLSENEEISIMINEE-DHIRIQC
8GQD - Sa McsB      1611   81 KHLISPELIKQ-PAAAVLVNDDESLSVMINEEDH-IRIQA

                               .........+.........+.........+.........
6FH3 - Gs McsB  SSA 1610  130 EECCCC-HHHHHHHHHHHHHHHHHCCCCCCECCCEEECCC
8GQD - Sa McsB  SSA 1611  119 EE-CCCCHHHHHHHHHHHHCCCCCCECCCCCCCCCCC-E
6FH3 - Gs McsB      1610  130 LFPGLQ-LAEALEAASELDDWIEGHVNYAFDERLGYLTSC
8GQD - Sa McsB      1611  119 MG-TDTTLQALYNQASSIDDELDRSLDISYDEQLGYLT-T

                               .........+.........+.........+.........
6FH3 - Gs McsB  SSA 1610  169 C-CCCCCEEEEEEEEECHHHHHHCCHHHHHHHHHHHHEEEE
8GQD - Sa McsB  SSA 1611  157 CCEECCCCCEEEEEEECHHHHHHCCHHHHHHHHHHHCCEE
6FH3 - Gs McsB      1610  169 P-TNVGTGLRASVMMHLPALVLTQQINRIIPAINQLGLVV
8GQD - Sa McsB      1611  157 CPTNIGTGMRASVMLHLPGLSIMKRMTRIAQTINRFGYTI

                               .........+.........+.........+.........
6FH3 - Gs McsB  SSA 1610  208 ECC-CCCCCCCCCE-EEEEEECCCCCCCHHHHHHHHHHHH
8GQD - Sa McsB  SSA 1611  197 ECCCCC-C-CCCCCCCEEEEECCCCCCCHHHHHHHHHHHH
6FH3 - Gs McsB      1610  208 RGT-YGEGSEALGN-IFQISNQITLGKSEEDIVADLHTIV
8GQD - Sa McsB      1611  197 RGIYGE-G-SQVYGHTYQVSNQLTLGKSELEIIETLTEVV

                               .........+.........+.........+.........
6FH3 - Gs McsB  SSA 1610  246 HHHHHHHHHHHHHHHHHHCHHHHHHHHHHHHHHCCCCCC
8GQD - Sa McsB  SSA 1611  235 HHHHHHHHHHHHHHHHHHCHHHHHHHHHHHHHHCCCCCH
6FH3 - Gs McsB      1610  246 EQLIAQERAARQALVKTLGIQLEDKVFRSYGILANCRVID
8GQD - Sa McsB      1611  235 NQIIHEEKQIRQKLDTYNQLETQDRVFRSLGILQNCRMIT

                               .........+.........+.........+.........
6FH3 - Gs McsB  SSA 1610  286 HHHHHHHHHHHHHHHHHCCCCCCCHHHHHHHHHHHCHHHH
8GQD - Sa McsB  SSA 1611  275 HHHHHHHHHHHHHHHHHCCCC-CCHHHHHHHHHHC---C
6FH3 - Gs McsB      1610  286 SKEAAQCLSDVRLGIDLGYIKNVSRNILNELMILTQPGFL
8GQD - Sa McsB      1611  275 MEEASYRLSEVKLGIDLNYIE-LQNFKFNELMVAIQ---S
```

```
                              .........+.........+.........+.........
6FH3 - Gs McsB  SSA 1610  326 HHHHCCCCCHHHHHHHHHHHHHHHHHHHH----------
8GQD - Sa McsB  SSA 1611  311 CCCCCC-CC---HHHHHHHHHHHHHHHHC-CCCCCCCCCC
6FH3 - Gs McsB      1610  326 QQYAGGVLRPEERDVRRAALIRERLRMETR----------
8GQD - Sa McsB      1611  311 PFLLDE-ED---DKSVKEKRADILREHIK-MTHNIHDNIS


                              .........+.........+.........+.........
6FH3 - Gs McsB  SSA 1610      ----------------------------------------
8GQD - Sa McsB  SSA 1611   11 HHHHHCCCCCEEEEEEEEECEEEECCCCCCCCCCCHHHHHH
6FH3 - Gs McsB      1610      ----------------------------------------
8GQD - Sa McsB      1611   11 QWMKSNEETPIVMSSRIRLARNLENHVHPLMYATENDGFR


                              .........+.........+.........+.........
6FH3 - Gs McsB  SSA 1610      ----------------------------------------
8GQD - Sa McsB  SSA 1611   51 HHHHHHHHCCCCEEEEECCCCHHHHHHHHHCCCCHHHHH
6FH3 - Gs McsB      1610      ----------------------------------------
8GQD - Sa McsB      1611   51 VINEVQDALPNFELMRLDQMDQQSKMKMVAKHLISPELIK


                              .........+.........+.........+.........
6FH3 - Gs McsB  SSA 1610      ----------------------------------------
8GQD - Sa McsB  SSA 1611   91 HHCEEEEECCCCEEEEEECCCCCEEEEEEECCCCHHHHHH
6FH3 - Gs McsB      1610      ----------------------------------------
8GQD - Sa McsB      1611   91 QPAAAVLVNDDESLSVMINEEDHIRIQAMGTDTTLQALYN


                              .........+.........+.........+.........
6FH3 - Gs McsB  SSA 1610      ----------------------------------------
8GQD - Sa McsB  SSA 1611  131 HHHHHHHCCCCCCECCCCCCCCCCCECCEECCCCCEEEEE
6FH3 - Gs McsB      1610      ----------------------------------------
8GQD - Sa McsB      1611  131 QASSIDDELDRSLDISYDEQLGYLTTCPTNIGTGMRASVM


                              .........+.........+.........+.........
6FH3 - Gs McsB  SSA 1610      ----------------------------------------
8GQD - Sa McsB  SSA 1611  171 EECHHHHHHCCHHHHHHHHHHHCCEEECCCCCCCCCCCCC
```

```
6FH3 - Gs McsB      1610      ----------------------------------------
8GQD - Sa McsB      1611  171 LHLPGLSIMKRMTRIAQTINRFGYTIRGIYGEGSQVYGHT

                              ..........+.........+.........+.........
6FH3 - Gs McsB  SSA 1610      ----------------------------------------
8GQD - Sa McsB  SSA 1611  211 EEEEECCCCCCCHHHHHHHHHHHHHHHHHHHHHHHHHHH
6FH3 - Gs McsB      1610      ----------------------------------------
8GQD - Sa McsB      1611  211 YQVSNQLTLGKSELEIIETLTEVVNQIIHEEKQIRQKLDT

                              ..........+.........+.........+.........
6FH3 - Gs McsB  SSA 1610      ----------------------------------------
8GQD - Sa McsB  SSA 1611  251 HHCHHHHHHHHHHHHHHCCCCCHHHHHHHHHHHHHHHHH
6FH3 - Gs McsB      1610      ----------------------------------------
8GQD - Sa McsB      1611  251 YNQLETQDRVFRSLGILQNCRMITMEEASYRLSEVKLGID

                              ..........+.........+.........+.........
6FH3 - Gs McsB  SSA 1610      ----------------------------------------
8GQD - Sa McsB  SSA 1611  291 HCCCCCCCCCHHHHHHHHHCCCCCCCCCHHHHHHHHHHH
6FH3 - Gs McsB      1610      ----------------------------------------
8GQD - Sa McsB      1611  291 LNYIELQNFKFNELMVAIQSPFLLDEEDDKSVKEKRADIL

                              ..........+.........+.........+.........
6FH3 - Gs McsB  SSA 1610      -----
8GQD - Sa McsB  SSA 1611  331 HHHHC
6FH3 - Gs McsB      1610      -----
8GQD - Sa McsB      1611  331 REHIK
```

Alignment Score: 0.336

RMSD: 2.825 Angstrom

Figure G1: Structural alignment of $McsB_{SA}$ and $McsB_{GS}$. Dimeric $McsB_{SA}$ and $McsB_{GS}$ were prepared using the protein preparation wizard with default setting in the Schrödinger drug discovering suite (Maestro, version 2022-1) and the structural alignment tool was used to align all residues from both McsB orthologues. The output generated displays the data within five lines. The first line contains . and + and outlines the reading frame. Lines 2 and 3 display structural components aligned between $McsB_{GS}$ and $McsB_{SA}$ [C = random coil, H = helix and E = sheet (Beta sheet)]. Lines 4 and 5 display the amino acid residues in single letter format for $McsB_{GS}$ and $McsB_{SA}$ respectively.

APPENDIX H

Table H1: The six identified $McsB_{SA}$ ligands identified from the Pandemic Response Box

MMV Number[a]	Structure	IUPAC Name[b]	Drug Class
MMV1593539	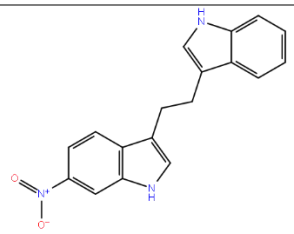	3-[2-(1H-indol-3-yl)ethyl]-6-nitro-1H-indole	Anti-bacterial
MMV1578899	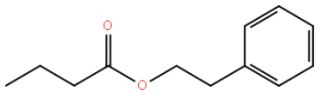	2-phenylethyl butanoate	Anti-bacterial
MMV1634391	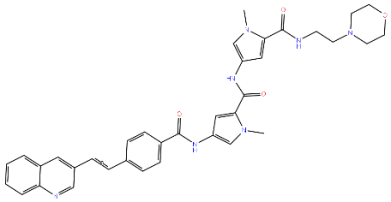	1-methyl-N-[1-methyl-5-(2-morpholin-4-ylethylcarbamoyl)pyrrol-3-yl]-4-[[4-[(E)-2-quinolin-3-ylethenyl]benzoyl]amino]pyrrole-2-carboxamide	Anti-bacterial
MMV1633968	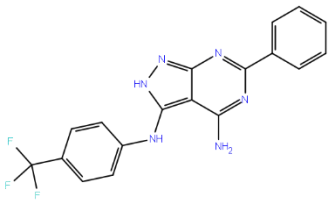	6-phenyl-3-N-[4-(trifluoromethyl)phenyl]-1H-pyrazolo[3,4-d]pyrimidine-3,4-diamine	Anti-viral
MMV1782355	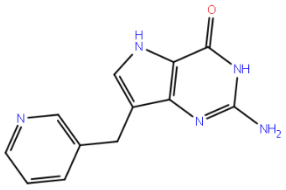	2-amino-7-(pyridin-3-ylmethyl)-3,5-dihydropyrrolo[3,2-d]pyrimidin-4-one	Anti-viral
MMV1782213	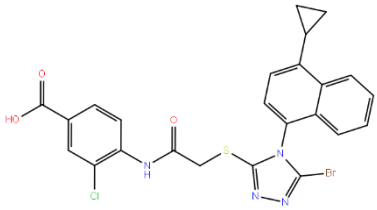	4-[[2-[[5-bromo-4-(4-cyclopropylnaphthalen-1-yl)-1,2,4-triazol-3-yl]sulfanyl]acetyl]amino]-3-chlorobenzoic acid	Anti-viral

[a] Medicines for Malaria Venture unique compound identity number

[b] International Union of Pure and Applied Chemistry nomenclature

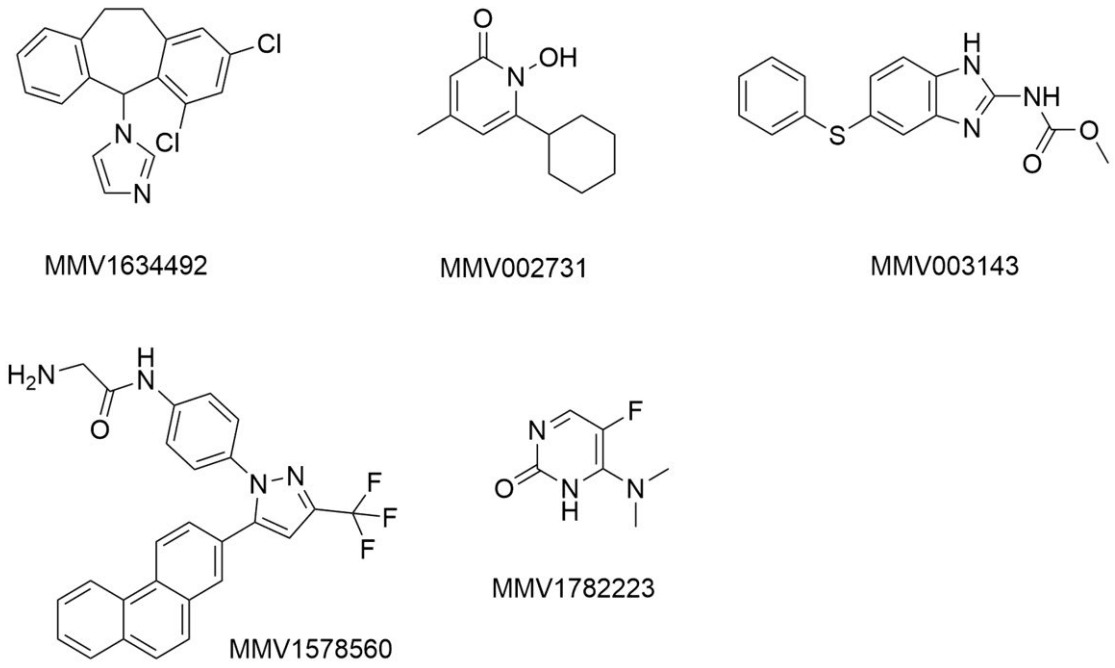

Figure I1: The five compounds from cocktail A1.1 which showed additive/synergistic effects. The structures of compounds MMV1634492, MMV002731, MMV003143, MMV1578560, MMV178223 were not evaluated further due to non-significant shifts in melting temperature obtained when evaluating each compound individually.

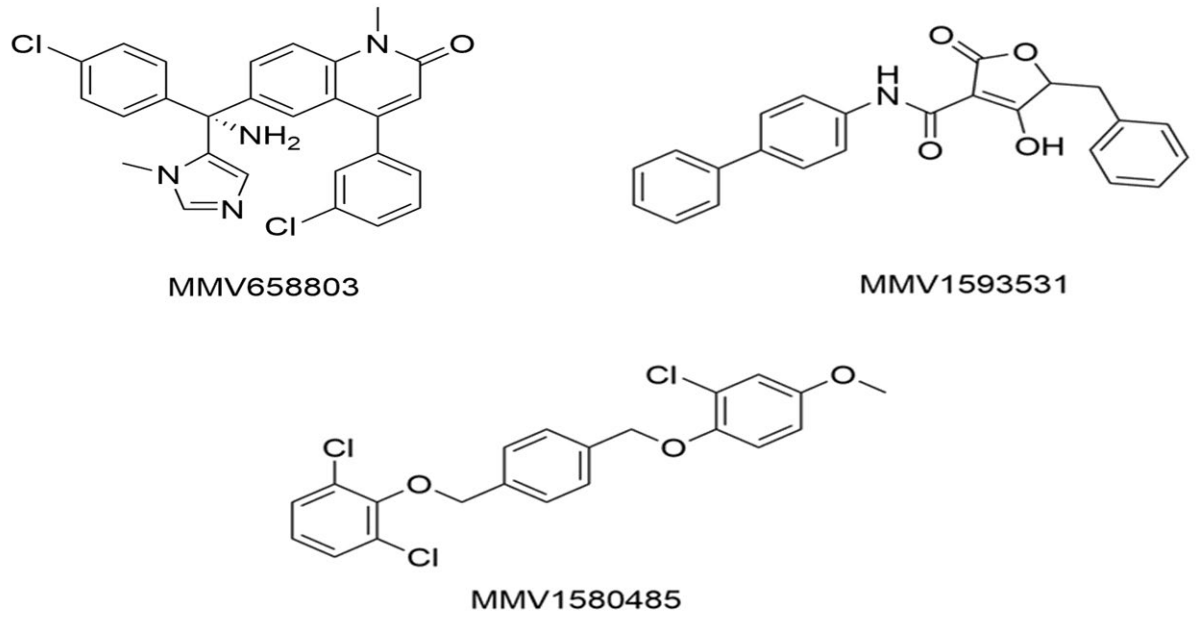

Figure I2: The three identified $McsB_{SA}$ ligands identified from the Pandemic Response Box which were not pursued. The structures of compounds MMV658803, MMV1593531 and MMV1580485 were not pursued due to non-significant shifts obtained in aggregation temperatures of $McsB_{SA}$.